UNIVERSITAT DE BARCELONA

Broadening Adenoviral Oncolysis in PDAC:
Interrogation of Patient-Derived Organoids for personalized virotherapy and modulation of miRNA content to boost adenoviral potency

Giulia Raimondi

UNIVERSITAT DE BARCELONA

FACULTAT DE FARMÀCIA I CIÈNCIES DE L'ALIMENTACIÓ

Tesi dirigida per la Dra Cristina Fillat Fonts
Grup de Teràpia Gènica i Càncer - IDIBAPS

Broadening Adenoviral Oncolysis in PDAC: *Interrogation of Patient-derived Organoids for personalized virotherapy and modulation of miRNA content to boost adenoviral potency*

Giulia Raimondi

2020

UNIVERSITAT DE BARCELONA

FACULTAT DE FARMÀCIA I CIÈNCIES DE L'ALIMENTACIÓ

Programa de doctorat en Biomedicina

Broadening adenoviral oncolysis in PDAC:

Interrogation of patients derived organoids for personalized virotherapy and modulation of miRNA content to boost adenoviral potency

Memòria presentada per

Giulia Raimondi

per optar al títol de doctor per la universitat de Barcelona

Beneficiaria del programa d'ajudes per la formació de personal investigador del Ministerio de Economia y Competitividad del govern d'Espanya

Cristina Fillat Fonts	Giulia Raimondi	Veronica Noe Mata
Directora	Autora	Tutora

Abbreviations

5-FU	5-FluoroUracil
Adwt	Adenovirus Wild Type Specie C Serotype 5
ATCC	American Type Culture Collection
BAC	Bacterial Artificial Chromosome
BiTE	Bi-specific T cell Engager
bp	Base Pair
CAF	Cancer Associated Fibroblasts
CAR	Coxsackie and Adenovirus Receptor
cDNA	copy DNA
CK19	CytoKeratin 19
CMV	CytoMegaloVirus
CPE	Cytoplasmatic Polyadenylation Element
CRC	Colorectal Cancer
CSC	Cancer Stem Cell
DAPI	4,6-DiAmidino-2-PenilIndole
DMEM	Dulbecco's Modified Eagle Medium
DMSO	DiMethyl SulfOxide
DNA	DeoxyriboNucleic Acid
dNTPs	deoxyNucleotides
DTT	DiThioThreitol
E. Coli	*Escherichia Coli*
EBV	Epstein-Barr Virus

ECM	Extra Cellular Matrix
eGFP	enhanced Green Fluorescence Protein
EMT	Epithelial Mesenchimal Transition
FC	Fold Change
FNA	Fine Needle Aspiration
Fw	Forward
G	Gauge
g	Gravity
Gem	Gemcitabine
GM-CSF	Granulocyte Macrophage Colony Stimulating Factor
h	Hours
H&E	Hematoxilyin and Eosin
HBS	HEPES Buffer Saline
HEPES	4-(2-hydroxyethyl)-1-piperazineethanesulfonic acid
HIV	Human Immunodeficiency Viruse
HSV	Herpex Simplex Virus
ID50	Infectious Dose 50
iFBS	inactivated Fetal Bovine Serum
IFU	Infectious Forming Unit
IHC	ImmunoHistoChemistry
IPMN	Intraductal Papillary Mucinous Neoplasm
ITR	Inverted Terminal Repeats
Kb	Kilobase
KO	Knock Out
KRAS	Kirsten RAt Sarcoma viral oncogene homolog
LB	Luria Broth
M	Molar
MCN	Mucinous Cystic Neoplasm
miRISC	miRNA-Induced Silencing Complex

miRNA/miR	microRNA
MLP	Major Late Promoter
MMP	Matrix MetalloProteinase
mRNA	messenger RNA
MTT	3-(4,5-Dimethylthiazol-2-Yl)-2,5-Diphenyltetrazolium Bromide
nab-paclitaxel	nanoparticle albumin-bound paclitaxel
nm	nanometer
ºC	Celsius Grade
OD	Optical Density
ORF	Open Reading Frame
OV	Oncolytic adenoVirus
PanIN	Pancreatic Intraepithelial Neoplasia
PBS	Phosphate Buffer Saline
PBS++	Phosphate Buffer Saline supplemented withCaCl2 and MgCl2
PCR	Polymerase Chain reaction
PDAC	Pancreatic Ductal AdenoCarcinoma
PDO	Patient-Derived organoid
PI	Post-Infection
Rb	Retinoblastoma
RE	Restriction Enzyme
RGD	Arginine - Glycine - Aspartic Acid
RLU	Relative Light Units
RNA	RiboNucleic Acid
rpm	revolutions per minute
Rspo	R-spondin
RT-qPCR	Real Time quantitative PCR
Rv	Reverse
SDS	Sodium Dodecyl Sulfate
SEM	Standard Error of the Mean

SPF	Specific Pathogen Free
SPS	Sequence Paired binding Sites
Taq	*Thermophilus aquaticus*
TCF	TransCription Factor
TIC	Tumor Initiating Cells
UTR	Un-Translated Region
VA-RNA	*Viral Associate RNA*
vp	viral particle
VSV	Vescicular Stomatitis Virus
Wnt	Wingless-related integration site

Presentation

Pancreatic ductal adenocarcinoma is a malignancy with a very dismal prognosis, predicted to become the second leading cancer-related death in 2030. Available treatments do not contribute to improve patients' life expectancy, with a 5 years survival lower than 10%. The enormous genetic variability, the dense desmoplastic stroma, and the immunosuppressed microenvironment make PDAC an unsolved clinical challenge.

Oncolytic virotherapy has been envisioned as a therapeutic alternative for clinical management of PDAC. Attenuated viruses, orientated to specifically eliminate cancer cells, offer multiple advantages over current treatments. The therapeutic viruses self-amplify upon tumor lysis, propagating to adjacent cells with the release of tumor associated antigens that can awake the immune system against the tumor. Nowadays, many oncolytic adenoviruses are undergoing clinical trials for the treatment of solid tumors, including PDAC.

However, patients' response to oncolytic viruses is lower than expected, and their administration as monotherapy is not sufficient to abrogate tumor mass. This can be partially attributed to the lack of relevant models of pre-clinical screening, performed in *in vitro* systems or in xenografts derived from cell lines that do not

recapitulate the genetic heterogeneity of PDAC and its complex microenvironment. PDAC organoids are 3D structures established from patient tumors that are representative of various features of PDAC, displaying inter-patient variability and characterized by an easy handling manipulation. In the current thesis we have explored the use of organoids in virotherapy for the screening of personalized adenoviral treatments, either as monotherapy or in combination with actual gold standard chemotherapy. We identified patient-specific sensitivities to adenoviruses and showed that oncolytic virus response in patient-derived organoids (PDOs) from primary tumors might predict metastases sensitivity. The results from this part of the thesis contributed to the characterization of the organoids as a feasible and personalized model for the pre-clinical study of oncolytic adenoviruses.

With the aim to generate oncolytic adenoviruses with improved tumor potency and enhanced therapeutic index, we studied the influence of the deregulated miRNome in PDAC on adenoviral replication. We identified several miRNAs that strongly impacted adenoviral propagation. Furthermore, we approached a miR-222 sponge design to inhibit miR-222 and the restoration of miR-29c as strategies to promote adenoviral replication, exploring some mechanistic insights. Studies with the novel oncolytic viruses AdNuPAR-E-miR-222-S and ICOVIR15-E-miR29c revealed their increased potency, positioning these viruses as candidates for future development.

Index

1. Introduction

1.1 The Pancreas

The pancreas is an organ located in the upper left abdominal cavity, behind the stomach, coming out from the duodenum curvature and surrounded by spleen, liver and intestines. Its dimensions range between 14 and 20 cm. It is lobulated, yellowish and anatomically divided in 3 regions: head, body and tail (Fig 1.1 A).

This organ is classified as a multicellular gland, with mixed exocrine and endocrine functions. It secretes hormones, directly into the blood flow, and digestive enzymes into the duodenum by a system of ducts.

The endocrine function is exerted in concrete globular zones inside the parenchyma of the organ, the pancreatic islets or islets of Langerhans. The islets of Langerhans comprise 4 different cellular populations, the α, β, δ and PP cells producing glucagon, insulin, somatostatin and pancreatic peptides, respectively, directly released in the blood flow.

The exocrine portion of the pancreas is responsible for the production of the pancreatic juice, containing the enzymes required for the digestion. The producers are the acinar and ductal cells, composing 85% of the pancreatic tissue. The enzymes are accurately stored in the apical portion of the acinar cells, and their secretion in the intercellular canaliculi is finely tuned by external inputs from hormones and nerves. The canaliculi are connected to small-intercalated ducts, formed by epithelial ductal cells, which end up in the interlobular duct (Fig 1.1 B). Most of pancreatic ducts

converges to the main pancreatic duct, finally entering the duodenum via the major duodenal papilla (papilla of Vater). Ductal cells release water, sodium and bicarbonate to the ductal canaliculi and flow together with the digestive enzymes, generating the pancreatic juice. The enzymes are kept in an inactive state until their reach the duodenum, where enterokinases cleave the proteins generating their active forms (Information adapted from [1,2]).

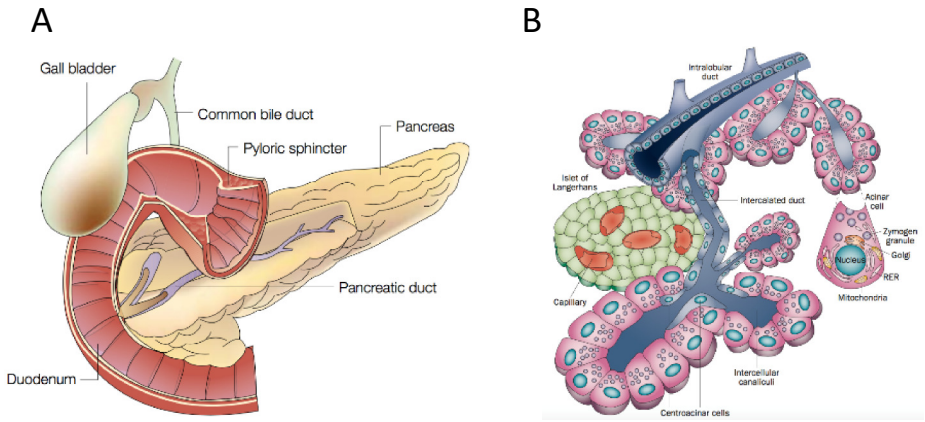

Figure 1.1. Macroscopical and microscopical organization of the pancreas. A*. Macroscopic representation of pancreas.* ***B****. System of centroacinar cells and ductal cells for secretion of digestive enzyme. Adapted from* [3].

1.2 Pancreatic cancers and Pancreatic Ductal Adenocarcinoma

The pancreatic parenchyma can give rise to a wide range of malignancies, including neuroendocrine tumors, colloid carcinomas or medullary carcinomas. However pancreatic ductal adenocarcinoma (PDAC) accounts for 90% of carcinomas arising in

the organ [4]. The preferred location for PDAC tumors is the head of the pancreas (70%), followed by body and tail (15% each) [5].
Depending on the geographical area, the incidence of PDAC can change, being environmental factors significantly responsible for the development of the pathology. Today, PDAC is considered the 7th cause of cancer-related deaths worldwide, with a 5-year survival rate lower than 10%, highlighting the need to clinically improve this very dismal prognosis [6,7].

1.2.1 Histopathological alteration in PDAC

Study of pancreatic resections identified a series of lesions in the small ducts clearly associated with the development of PDAC, named Pancreatic Intra Epithelia Neoplasia (PanINs) [8].

PanINs are pre-malignant lesions with a diameter of less than 5mm, arising from small intralobular ducts of the pancreas and with different grades of cellular and architectural atypia. PanIN-1 is a low-grade lesion, which does not present atypia yet, but can be characterized by a flat (PanIN-1A) or papillary (PanIN-1B) epithelium. Molecular characterization identifies the presence of *K-Ras* mutations and telomeres shortening in PanIN-1, classifying these alterations as PDAC initiators. PanIN-2 is characterized by moderate cytological and architectural transformation and *CDKN2A* inactivation. Mutations characterizing aggressive PDAC tumors are acquired during the PanIN-3 grade, in which the majority of cases present with loss of *TP53* and *SMAD4*. The term PanIN-3 is often interchanged with carcinoma in situ, meaning that high grade of

atypia both at cellular and architectural level is already present (Fig 1.2) [9–11].

Recent recommendations from international experts raised the consensus to classifying PanIN lesions in two groups, low-grade and high-grade, categorizing PanIN-2 as low-grade (Fig 1.2) [12].

Other pre-malignant histological alterations encountered in patients and associated to the development of pancreatic cancers are the intraductal papillary-mucinous neoplasm (IPMN) and mucinous cystic neoplasm (MCN). However, these lesions are associated to PDAC with less incidence and their characterization is not as detailed as for PanINs [8].

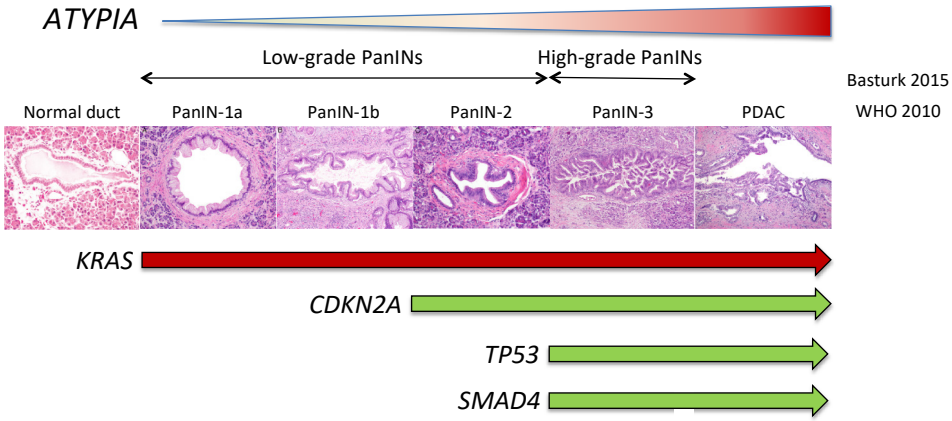

Figure 1.2. Evolution of preneoplasic PanIN lesions from normal tissue. *Image adapted from [12].*

Preneoplastic lesions can take up to 10 years to evolve to PDAC, meaning that a diagnosis at preliminary stage would be extremely helpful in the management of this malignancy. However, PDAC is generally diagnosed when the tumor is in an advanced stage,

invading circumstantial organs and thus being unresectable. Advanced PDAC is characterized by the appearance of a dense stromal component, a phenomenon called desmoplasia, proliferating ductal structures, accompanied by severe atrophy of acinar cells, inflammatory foci and surrounded by PanIN structures. These tumors acquire a plethora of extra genomic changes, permitting incredible levels of proliferation, inhibition of apoptosis, chemoresistance and ability to migrate and invade (information from Pancreatic Cancer, Methods and protocol 2008, Gloria H Su editor).

1.2.2 Molecular characterization of PDAC tumors

One of the main difficulties in PDAC management is its great molecular heterogeneity. The early driving mutations of *KRAS, TP53, CDKN2A*, and *SMAD4* are widely characterized (Fig 1.2) [13–15].

- *KRAS* is altered in more than 90% of PDAC, initiating in low grade PanIN. The most recurrent alteration is a point mutation in the 12th codon of the gene, resulting in a constitutive activation of the protein. *KRAS* belongs to the RAS superfamily, encoding a small GTPase protein regulating proliferation, differentiation, survival and migration. Once mutated, the GTPase activity is abolished, leading to constitutive activation of downstream pathways.

- *CDKN2A* is a tumor suppressor gene, encoding both p16^{INK4A} and p19^{ARF} from the same genetic locus. However,

deletions mostly affect only $p16^{INK4A}$ functions [15]. The primary function of this protein is a tight regulation of G1/S checkpoint of cell cycle, by phosphorylating CDK4 and CDK6. Loss of $p16^{INK4A}$ lets pancreatic cancer cells proliferate without control.

- *TP53* is tumor suppressor factor, present in the cell as a latent form. It is activated after damage in the genome, enabling cell cycle arrest and permitting eventual gene repair or driving cells to apoptosis. Main mutation of p53 resides in its DNA binding domain, leading to its accumulation in the nucleus. Loss of *TP53* is generally the consequence of *CDKN2A* alteration, probably induced by the accumulation of damaged DNA inducing a selective pressure for the tumor progression. It is mutated in 85% of PDAC patients.

- *SMAD4* is the co-transcription factor responsible for activation of TGF-β canonical pathway. It is lost in high grade PanINs, before the development of advanced carcinoma. It is mutated in 55% of PDAC.

Besides these common alterations, the rest of the genes harboring mutations can be encountered among PDAC patients with a frequency lower than 5%.

Recently, large scale molecular analysis provided a more detailed classification of PDAC, identifying subclasses of PDAC tumor (reviewed in [4]). PDAC tumors have been stratified according to

their mRNA expression profile, and the composition of the tumor [16,17]. A consensus nomenclature has been recently proposed [4], recognizing the following 4 subtypes:

- Quasi Mesenchymal (QM-PDA) or squamous, due to a high presence of genes overlapping with other squamous tumors
- Immunogenic progenitor: classical PDAC, characterized by decreased tumor cellularity and strong immune infiltration
- Pure classical progenitor: classical PDAC tumor
- Exocrine like or Aberrantly Differentiated Endocrine Exocrine (ADEX): characterized by a transcriptional program more similar to normal differentiated pancreas

This classification defines PDAC tumors with distinct biology and can help to identify subtype-specific therapeutic vulnerabilities.

1.2.2.1 Altered molecular pathways relevant for this study

The plethora of genetic mutations in PDAC impacts the core of many signaling pathways [18]. We briefly summarized those relevant for this study.

Notch Signaling Pathway

This embryonic signaling pathway has the control of the stem cells' niche maintenance and proliferation. Over activation of this

pathway is common to many PDACs samples. A family of 4 trans membrane proteins (Notch 1-4) acts as cellular receptor. Upon binding to its ligands Jagged 1-2 (JAG1-2) or Delta like (Delta 1,3,4), there is a conformational change in the Notch receptor that exposes the protein to intracellular proteases. A first cleavage from ADAM family protein of metalloproteinases, and a second from γ secretase complex, release the intracellular domain of Notch (NICD). Once in the nucleus, NICD interacts with RBPJ/CSL, initiating the transcription of target genes such as: HES (Hairy Enhancer of Split), HEY (HES related to YRPW), cyclin D1, p21, NFK-β, survivin or SLUG (Fig 1.3) [19–21].

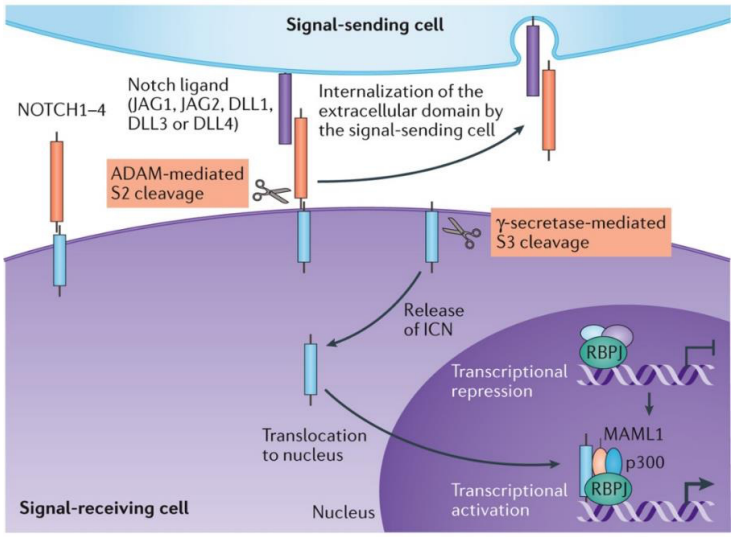

Figure 1.3. Schematic Representation of Notch Signaling Pathway. *Image from Nowell and Radtke, 2017.*

According to literature, Notch pathway is one of the major pathways responsible for chemoresistance and maintenance of cancer stem cell population inside the PDAC tumor bulk [22].

Wnt/β-catenin signaling

This pathway is physiologically related to embryonic development, with implications in morphogenesis and proliferation of many organs. However, it is also one of the early-altered pathways in PDAC.

The *Wnt* family is composed of 19 different ligands, acting in a canonical or non-canonical pathway, having as direct effector the β-catenin. The canonical pathway is regulated by an on/off system, whose activation depends on *Wnt* ligand binding to its transmembrane receptor frizzled (FRZD). In the absence of this interaction the degradation complex APC/Axin/GSK-3β tightly controls β catenin levels, and upon phosphorylation, marks the molecule for proteasomal degradation. When Wnt binds to FRZD, a series of conformational changes lead to the dishvelled protein (DSH) recruitment to the FRZD receptor, where it is required to inhibit APC/Axin/GSK-3β activity[23,24]. Then, β catenin is accumulated in the cytoplasm and migrates to the nucleus, where upon binding TCF/LEF transcription factors initiates cell fate determination programs (Fig 1.4) [25].

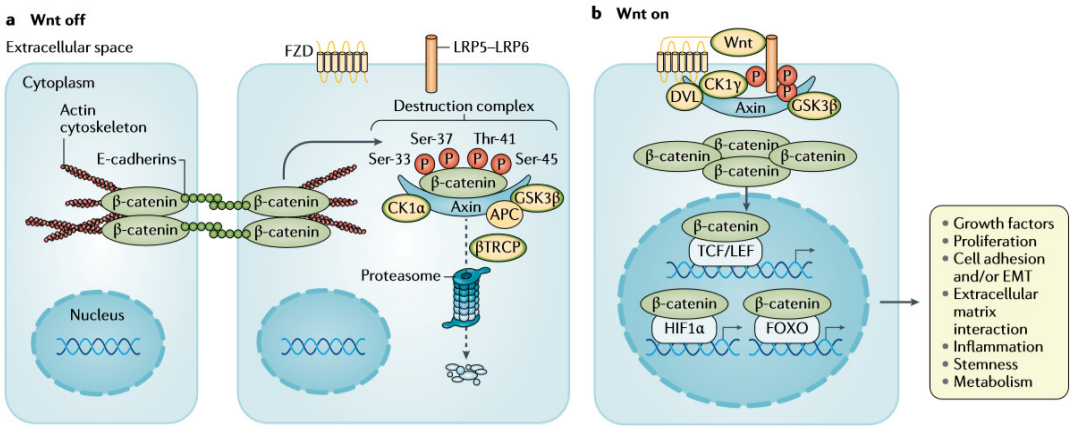

Figure 1.4. Schematic representation of Wnt/b catenin signaling pathway. *Image from* [26]

In PDAC the over activation of this pathway is considered an early event, already detected in PanINs. The main tumorigenic activity has been linked to resistance to apoptosis and maintenance of a CSC population, likely responsible for gemcitabine resistance [27].

Urokinase type plasminogen activator receptor (uPAR)

The *uPAR/uPA* system is a major regulator of the extracellular matrix (ECM) remodeling. The binding of uPA activator to the receptor uPAR leads to the cleavage of the zymogen plasminogen present in the ECM, generating the protease plasmin [28]. Plasmin removes by proteolytic cleavage ECM components and activates the metalloproteinases (MMP) for matrix remodeling (Fig 1.5). The uPA/uPAR complex is also involved in signal transduction and activation of MAPK related pathway [29–31].

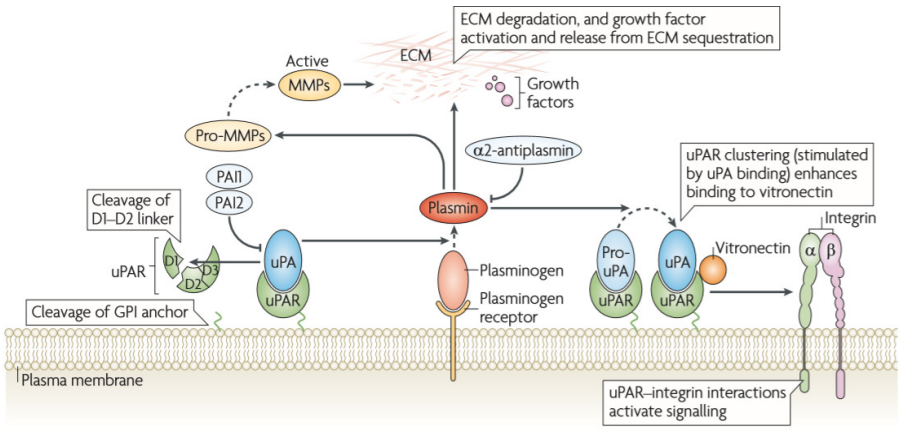

Figure 1.5. Regulation of cell signaling by uPA/uPAR. *Image from* [31]

The upregulation of uPAR gene is well described and common to many cancer types, including PDAC. High expression of this molecules has been related to dismal prognosis [32], and the main effects provoked by this upregulation are linked to EMT transformation and progression through a metastatic phenotype [29,33]. Many studies linked the upregulation of these molecules to the acquisition of a CSC phenotype.

1.2.3 PDAC microenvironment

PDAC is one of the most stroma-enriched cancers, where stromal cells outstand tumor cells number, ranging from 50 to 80% of tumor population [34]. Widespread fibrotic desmoplasia, composes the PDAC tumor microenvironment (TME) [35].

The desmoplastic reaction is characterized by the recruitment and activation of cancer associated fibroblasts (CAFs), remodeling of the extracellular matrix via deposition of hyaluronic acid, collagen

and fibronectin, and recruitment of regulatory immune cells, conferring an immunosuppressed environment [36,37].

CAFs were first thought to be originated from pancreatic stellate cells, mesenchymal-like cells resident in normal pancreas; however, their origin from mesenchymal stem cells, bone marrow derived stem cells and endothelial cells have been well documented (reviewed in [37]). In the last years, their role in PDAC progression has been better understood, defining subtypes of CAFs inside tumors, with different aggressive phenotypes. The first characterization of a normal and activated stromal subtypes was performed by Moffit and collaborators [38]. The discovery of two different subpopulations of CAFs, defined as inflammatory CAFs (iCAFs) and myofibroblast (myCAFs), endowed with pro-tumorigenic and tumor-restraining properties, respectively[39], identified these cells as a key factor for PDAC evolution and treatment (Fig 1.6).

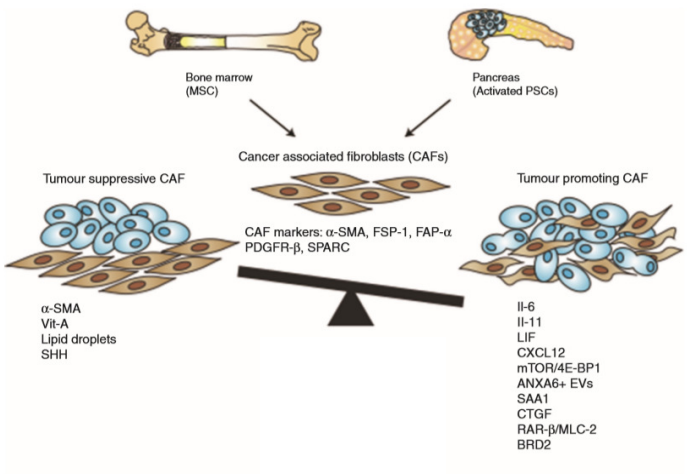

Figure 1.6. Different Populations of Cancer Associated Fibroblasts existing in PDAC tumors. *Image from* [40]

Besides CAFs, more factors must be taken into account in TME. PDAC is considered a non-immunogenic tumor, due to the ability to mask its own tumor antigens from the immune system. This is related to the secretion of immunosuppressive cytokines and other molecules, transmitting inhibitory signals to immune cells. Several studies highlight how PDAC TME is mainly populated by immunosuppressive cell types, such as regulatory T cells or myeloid-derived suppressor cells, with very low infiltration of Cytotoxic T Lymphocytes (CTL) [34,36] (Fig 1.7).

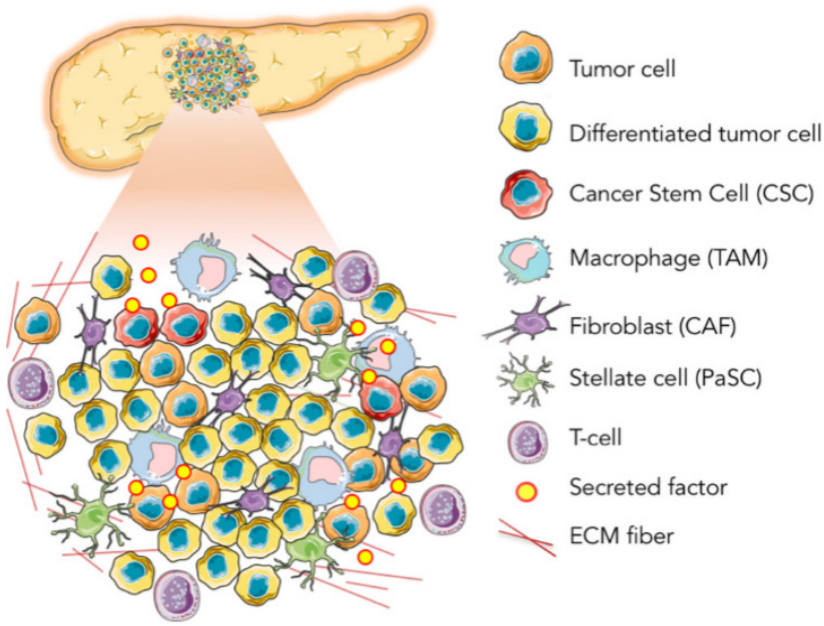

Figure 1.7. Composition of the PDAC tumor microenvironment. *Image from* [41]

1.2.3.1 Pancreatic cancer stem cells

Similarly to normal tissues, preserving a reservoir of adult stem cells, in the last decade a population of cancer stem cells (CSCs), or

tumor initiating cells (TICs), has been described as a part of the cellular component in a variety of tumors [42]. This small percentage of cells is endowed with tumor initiating potential, self-renewal and ability to reconstitute the tumor [43]. This low-differentiated subpopulation has been associated with increased resistance to cytotoxic agents, such as gemcitabine, due to the overexpression of efflux pumps (ABC transporter), antioxidative agents and antiapoptotic proteins (Fig 1.8) [44].

A strong reactivation of the embryonic signaling pathway, such as hedgehog, Notch and Wnt, is a common feature of CSC. However, the molecular characterization of this subpopulation is still highly incomplete [45]. The divergence of molecular markers encountered is variable, stressing the probability of the existence of more than one population with plasticity within the pool of CSCs (Fig1.8) [43].

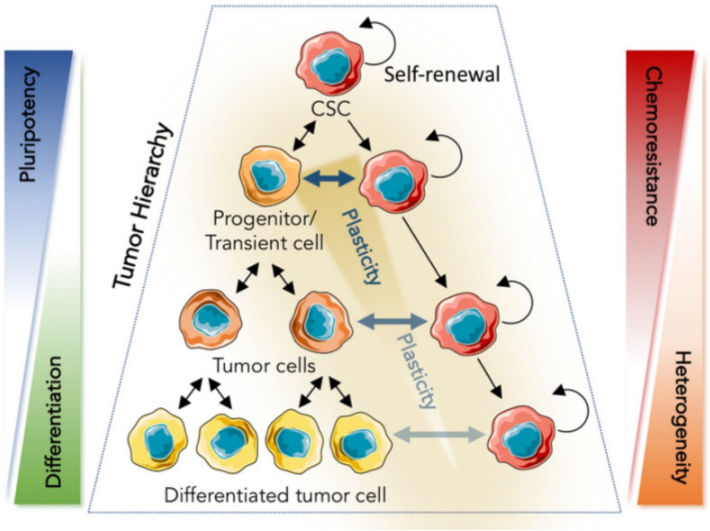

Figure 1.8. The cancer stem cell model. Image from [41].

Remarkably, the PCSC population establishes strong communication with the desmoplastic TME of PDAC. The interaction between CAFs and PCSC has started to be characterized, revealing the presence of a tight crosstalk with the secretion of pro-tumorigenic cytokines (IL-6, IL-8…) and chemokines stimulating CSCs properties [46]. Intervening in this crosstalk can provide novel development for future therapies.

1.2.4 PDAC treatment

PDAC is a complex malignancy, highlighting the importance of a multidisciplinary team in patients' management [47]. Surgery still remains the only cure for patients affected by this malignancy. However, the number of patients arriving at diagnosis with a resectable PDAC is of 10-20%. Instead, the number of individuals diagnosed with a borderline resectable (BRPC) or locally advanced pancreatic cancer (LAPC) ranges around 30-40% of cases. Remaining patients (50-60%) already present metastatic or systemic disease at diagnosis [14].

Surgery alone is not sufficient, since the number of relapses within the year after surgery is around 90% of operated patients. Then, the best strategy consist on the administration of adjuvant therapies based on gemcitabine + capecitabine, following surgery, resulting in a 5 years-survival of 30% [48]. An emerging strategy for BRPC or LAPC is the administration of neoadjuvant therapies that can reduce the tumor mass from a local advanced stage to a resectable tumor. In this scenario, the mixed regimen of FOLFIRINOX (Oxaliplatin, Irinotecan, leucovorin and fluorouracil) or the double combination

of gemcitabine + albumin bounded paclitaxel (nab-Paclitaxel) are the chemotherapies of choice (reviewed in [49]).

In advanced non operable PDAC, depending of the physical status of the patient, either FOLFIRINOX, for those with a general good health status, or gemcitabine + nab-Paclitaxel, for the rest, are administered [50–52]. Overall survivals of 9,9 and 7,9 months, respectively, were reported in a recent study gathering clinical routine data across Europe [53].

PDAC patients' life expectancy is still very low. Despite the good knowledge about the molecular and pathological alterations, the targeted therapies against PDAC have not led to results comparable to actual standard of care. Nowadays, immunotherapies are promising and are giving good results in many cancers. However, the immunosuppressed environment of PDAC is probably the reason why any clinical success has been reported yet for this neoplasia (reviewed in ([54])).

1.3 microRNAs

MicroRNAs are a huge class of single strand RNA molecules composed of 22-23 nucleotides, able to regulate gene expression at post-transcriptional level. Described for the first time in *C. Elegans* [55], their presence in many eukaryotic organisms has been documented. These small RNA molecules are involved in all plethora of processes balancing the correct cellular homeostasis, and

thus having a key role in the evolution towards pathological status, such as cancer[56,57]. In 2010, the number of miRNAs claimed in the human genome was 700[58]; nowadays, thanks to high throughput sequencing techniques and analysis, miRBase release 22.1 accounts for 4719 known human miRNAs.

1.3.1 microRNAs biogenesis and regulation

The process of miRNA production is tightly regulated, involving huge number of factors, responsible either for miRNA processing or modulation. Mature miRNAs come from different sources; the most abundant ones, and the first to be discovered, localize in intronic regions. They are processed co-transcriptionally, before splicing, from RNA polymerase II [56,59]. Intronic miRNAs are usually processed following the canonical pathway of miRNA biogenesis.

The canonical pathway involves a first transcriptional step inside the nucleus, followed by molecule exportation and processing in the cytoplasm. Intronic miRNAs are processed by RNA polymerase II, which generate a pri-miRNA, characterized by one or more stem loop structures with 3' and 5' tails, reaching more than 1 Kb length. A single stem loop is composed of an upper stem of 22 nt long, in which the future mature miRNA is localized, and a lower stem of 11 nt long, ending in overhang 3' and 5' extremities [59]. As a distinctive feature of RNA polymerase II transcription, pri-miRNAs are capped and polyadenylated, like mRNAs, and from the same transcriptional unit more than one microRNAs can originate [58,60]. A dual protein complex called the microprocessor captures pri-mRNAs. The principal proteins of the complex are Drosha, an

RNAse III enzyme, and DGCR8 (DiGeorge Critical Region 8), its cofactor.

Briefly, the pri-miRNA structure ending in a loop is recognized by DGCR8, whose binding will permit the cleavage performed by Drosha. After that, a 65-70 nt stem loop is released, known as the pre-miRNA. The cut performed by Drosha leaves a signature of a 2-nucleotide overhang at the 3' end of the pre-miRNA [60]. Additional proteins finely tune the process, either acting over the efficiency of the process (helicases) or modulating the activity of the microprocessor via post-transcriptional modification (phosphorylation, sumoylation, ubiquitination) [57,61].

The pre-miRNA is exported to the cytoplasm with the help of the GTP dependent Exportin 5 (XPO5). GTP to GDP hydrolyzation mediated by XPO5 releases the dsRNA structure (Winter et al., 2009). Once in the nucleus, the nuclease Dicer, with the help of double stranded RNA binding proteins TRBP and PACT, recognize the 3' overhang of the pre-miRNA and generates a cut 22-25 nt downstream, resulting in the removal of the stem loop and the generation of a dsRNA duplex [56].

The formation of this small duplex is determinant for the assembly of the RNA-induced silencing complex (miRISC), formed by the union of the duplex with the AGO proteins. In humans, 4 AGO proteins have been discovered, showing preferences for RNA duplexes characterized by mismatches in the nucleotides through the positions 8-11. Dicer is essential for the duplex charging on the Ago protein, generating the pre-miRISC complex [59,61]. The less

thermodynamically stable of the two strands is selected to form the mature miRISC complex, and it will receive the name of the guide strand. This complex is the responsible for the binding to target mRNA, which is recognized by base-pair complementarity to the guide strand of the miRNA previously charged in the AGO protein. The other strand, known as passenger strand, is unwound and released with the help of endonucleases and ATP hydrolyzing proteins (Process resumed in fig 1.9) [59,60].

Besides canonical pathway, other routes independent from Drosha have been listed for miRNAs. MiRNAs having origins from small introns spontaneously assume a structure resembling pre-miRNA and are directly recognized by XPO5 and transferred to the cytosolic compartment. In other cases, pre-miRNAs can originate from short hairpins directly transcribed by RNA pol II, or from non-coding-RNAs, such as t-RNAs and snoRNAs (Fig 1.9). These are Drosha independent, but their processing still depends on Dicer activity to be functional [59,61].

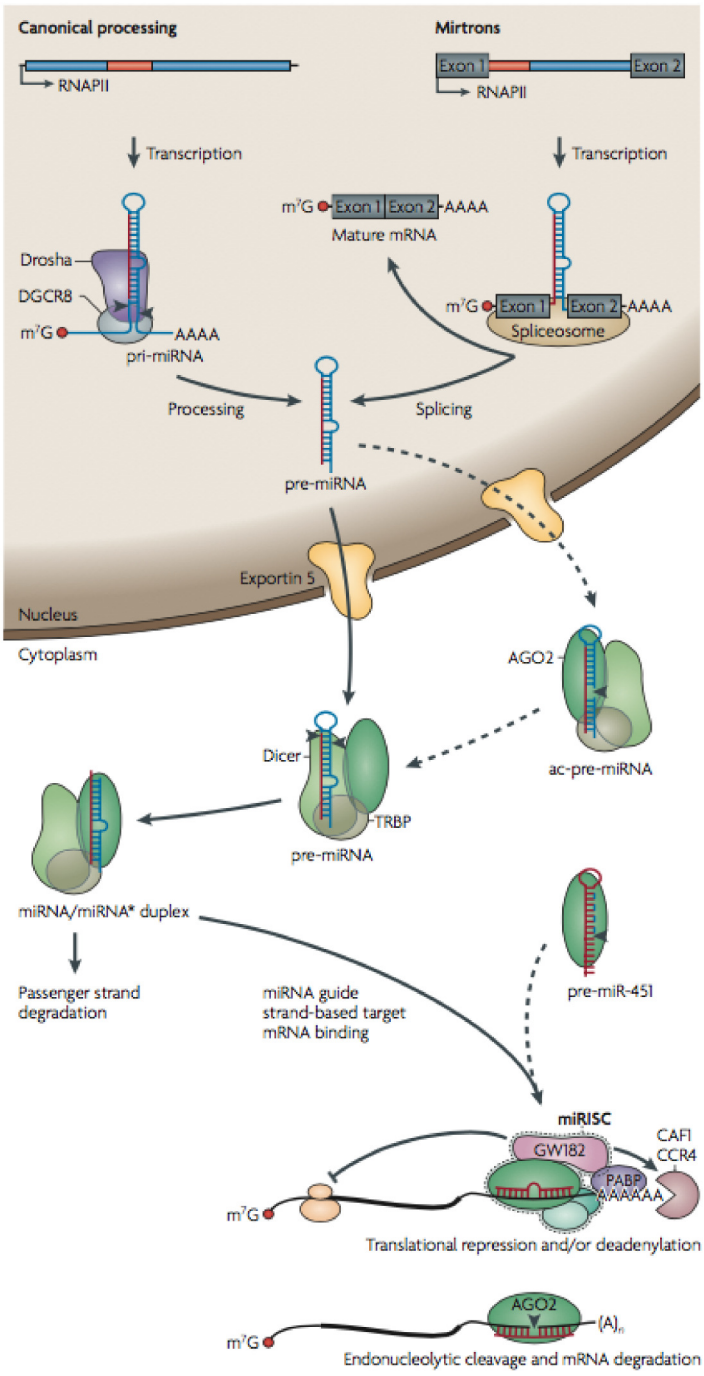

Figure 1.9. Canonical and non-canonical biogenesis of miRNAs and formation of silencing complex. *Image from* [57].

1.3.2 Target recognition

Study of the pairing of miRNAs with their target genes led to the identification of principles useful for target recognition or prediction. It is well established that the most determinant region for target recognition is the seed sequence, a 6 nt long sequence located at the 5' of the miRNAs, including nucleotide from 2 to 7 [62]. The seed sites on the mRNA and the seed sequence on miRNA pair via Watson Crick complementarity, determining an interaction called canonical. Besides canonical interaction, extra nucleotides pairings can take place, depending if the 1st and 8th nucleotide preceding and following the seed, respectively, are involved in the target recognition [63]. Pairings admitting wobbling or bulged sites inside the seed sequence have been described, especially in mammals. This results in a less strong inhibitory interaction, and it is often helped by the presence of extended complementarity at the 3' end of the miRNA seed sequence [64,65].

The preferred region for these interactions is identified in the 3'UTR of an mRNA, although binding sites inside the codifying sequence or regulatory motifs have also been encountered. Within the 3'UTR, the miRNA interacts with a variety of RNA Binding Proteins (RBPs), whose interactions and abundance will determine the post-transcriptional regulation of the mRNA. In general, genes with stable expression are characterized by very short 3'UTR, limiting the interaction with inhibiting miRNAs and RBP, whereas short-living genes have longer 3'UTR, permitting tight and precise expression [66,67]. In long 3'UTR, majority of seed sites are located

towards its end, whereas in the short one seed sites have been encountered 15-20 nt away from stop codons [68]. In general, the presence of more than one seed sites enhances the strength of interaction, leading to best target inhibitions.

1.3.3 Regulation of mRNA translation

The recognition of the miRISC complex and the seed site on a target mRNA leads to a destabilization of mRNA, first inhibiting translation and then causing target degradation.

Secondary structure of mRNA is fundamental to understand the process of miRNA silencing. It is well established that 5' end of the mRNA is immediately capped during transcription, whereas the 3' end of the sequence is formed by a long polyA tail, bound to the PolyA binding protein (PABP). The cap and the PABP interact via a molecular bridge composed by the proteins eIF4E, directly recognizing the cap, eIF4G, a scaffold protein, and eIF4A, a RNA helicase. All these proteins organize the mRNA in a circular structure promoting ribosome binding and translation [68].

MiRISC complex disrupts this organization through sequential steps. The miRNA resides inside the AGO protein in a stretched conformation, where only the seed sequence is exposed for mRNA target identification [66]. Upon recognition, the protein GW182 mediates the disruption of mRNA structure. The molecular bridge between PABP and eIF4E is interrupted and mRNA linearized. The polyA tail is now exposed to cellular nucleases, recruited by the AGO-GW182 complex. CAF1/CCR4/NOT and PAN2/3 complexes

digest the exposed polyA of the mRNA, which is in turn submitted to a decapping process by exonuclease XRN1 and finally degraded (Fig 1.10).

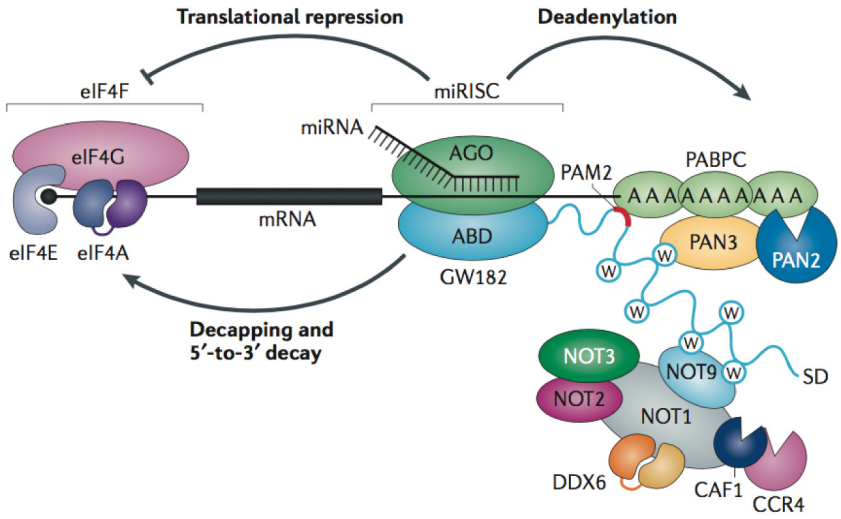

Figure 1.10. Translational repression induced by the action of the miRISC complex. Image from [69].

1.3.4 miRNAs and cancer

Considering their regulatory properties, since the very beginning of their discovery miRNAs were studied for participation in carcinogenesis. The first evidences arrived with the discovery of miR-15/miR-16 deregulation in chronic lymphocytic leukemia. The loss of these miRNAs was associated to a frequent deletion in chromosome 13, present in about 70% of cases [70].

Successive studies classified chromosomal loss or amplification as one of the driving events for miRNA downregulation or upregulation, respectively (reviewed in [71–73]). Another important

cause for miRNA deregulation came from studies demonstrating that the pro-tumorigenic MYC and TP53 genes acted as important regulators of miRNAs expression. MYC has been demonstrated to activate miR-17-92 pro-tumorigenic cluster [74], responsible for E2F regulation and progression through cell cycle. On the other hand, MYC negatively regulates tumor suppressive miRNAs, such as miR-26, miR-29 and let-7 family, favoring tumorigenesis [75].

TP53 acts by regulating miRNAs involved in cell cycle and apoptosis, processes that become misbalanced as a consequence of TP53 mutation [73]. Other mechanisms of miRNA deregulation are linked to epigenetic silencing or activation, and defects in miRNA biogenesis machinery. Deletion in Dicer and Drosha has been linked to an accelerated tumor progression *in vivo*, and mutations along the pathway of miRNA biogenesis are related to enhance risk of cancer [72,73].Accumulation studies on cancers' miRNome defined lists of miRNAs whose expression changes in malignancies. A widespread underexpression of miRNAs in tumor tissue is observed, although upregulation of certain miRNAs is also detected. Whereas the location of the tumor and its stage are the main determinants of the deregulation, some miRNAs are permanently altered in many cancers [76–78].

1.3.4.1 miRNAs and PDAC

The first description of the PDAC-associated miRNome is from 2007. Szafranska and collaborators gathered miRNA-related data from normal pancreas, chronic pancreatitis, PDAC tumors and cell lines and listed 26 miRNAs that were differentially deregulated

between normal and transformed tissues [79]. Nowadays, there are plenty of studies integrating data and listing miRNAs associated to PDAC malignancies. Discrepancies between studies are mainly due to different type of samples and analysis. However, there are miRNAs whose role has been well studied and constitute part of the PDAC deregulated miRNome [80–82].

Downregulated miRNAs of interest in this study: miR-29c.

The miR-29c belongs to a family of miRNAs composed of three mature members, miR-29a, miR-29b and miR-29c encoded in two genetic clusters. MiR-29c is located in the chromosome 1, in a cluster with miR-29b. The expression of this family is widespread down-regulated among cancers exerting a control over ECM deposition[83]. In PDAC, a deregulation of the whole family is observed, linking this loss to the progressive accumulation of fibrosis in $KRAS^{G12V}$ pancreata of KC mice and human PDAC tumors, stressing the importance of miR-29s in remodeling tumor stroma [84]. Specific studies on the role of miR-29c showed that the re-introduction of this miRNA led to an enhanced gemcitabine-induced apoptosis in PDAC pre-clinical models [85]. Furthermore, miR-29c avoids β catenin accumulation into the nucleus leading to inhibition of Wnt/β catenin signaling. This phenomenon demonstrated to revert self-renewal ability and CSC-like properties of PDAC cells [86].

Moreover, miR-29c may have an active role in regulating host-pathogens interactions, especially in response to viral infections by modulating the innate immune response [87].

Upregulated miRNAs of interest in this study: miR-222

The overexpression of miR-222 has been described among gastric cancers[88]. Specifically, the upregulation of the whole cluster comprising miR-221 and miR-222 has been reported, and related to poorer survival in PDAC patients[89]. These miRNAs are located in the X Chromosome, sharing an identical seed sequence and with extremely high sequence complementarity. MiR-221 and miR-222 are separated by 727 bp, transcribed by the same promoter and thus presenting comparable expression profiles [90]. MiR-221 and miR-222 regulate p27 and p57, respectively, favoring progression through G1/S phase of cell cycle. The upregulation of these miRNAs in PDAC cells induces resistance to apoptosis [91] and confers tumor-remodeling properties by inducing MMP, favoring tumor dissemination and spread of metastases [92].

The interaction of this cluster with adenoviral infections demonstrated to be important. Zhao and collaborators described a constant diminution of miR-221 in adenovirus-infected lung fibroblast [93]. Similarly, downregulation of miR-222 showed increased adenoviral oncolysis in prostate cancer cells, revealing an inhibitory role of this miRNA on adenoviral fitness [94].

1.4 Patient-derived organoids (PDOs)

Recent advances in cell culture technologies permitted the introduction of a 3D model recapitulating human physiological and pathological conditions: the organoids. These are 3D-multicellular structures derived from organ-specific cells with stem-like

characteristics, which can self-organize and divide in a manner similar to *in vivo*, simulating the architecture and functionality of native organs [95–97].

Organoids were introduced for the first time in 2009 by Dr. Clever's group, with the discovery that intestinal cells expressing Leucine-reach repeat containing G-protein coupled receptor 5 (*Lgr5*), a marker of adult stem cells (aSC), formed organized 3D structures when cultured in Matrigel under specific stimuli [98].Organoids have been then introduced in many research fields, to model human development and diseases "in a dish".

These 3D structures can be developed either from pluripotent stem cells (PSC), and more interestingly from adult stem cells (aSCs) of many tissues, including colon, intestine, pancreas, stomach, liver, prostate and kidney (reviewed in [95,99]). Interestingly, the presence of a subpopulation of cancer stem cells residing in tumors enabled the generation of organoids from transformed tissue of different tumor types, opening novel insights in cancer research [100–102].

1.4.1 Organoids and cancer

The generation of tumor-derived organoids opened a new field in cancer research, uncovering clues in cancer development and biology, together with accelerating the discovery of new compounds and introducing personalized therapies [103].

Tumor-derived organoids overcome many limitations presented by current pre-clinical models. Actual knowledge on cancer is mainly

based on the use of classical 2D cell lines, Genetically Engineered Mouse Models (GEMMs) and patient-derived xenograft (PDX) [104,105]. Although 2D cell lines are easy to propagate in culture, they are submitted to strong *in vitro* selection, leading to the loss of tumor molecular characteristics. GEMMs and PDXs better recapitulate tumor histo-architecture, mutational landscape and phenotypic diversity, serving as more reliable models for the study of tumor biology and therapeutic testing. However, they are expensive and time consuming, limiting preliminary drug screening [95,106].

Instead, organoids have the intrinsic ability to represent individual patient's characteristics, resembling histo-architecture of tumor of origin. Interestingly, tumor-derived organoids can be cryopreserved and propagated for many passages, and unlike cell lines, remain genetically stable. The establishment of a culture is easy and briefly accomplished [101,107,108]. With an intermediate cost between cell lines and PDX, it is likely that organoids will become the preferred tool in preclinical screenings (Resume on fig 1.11).

	CLs	PDXs	PDOs
Wild Type Culture	-	-	+
Pre-invasive Cancer Models	-	-	+
Invasive Cancer Models	+	+	+
Metastatic Cancer Models	+	+	+
Cost	$	$$	$$
Time	+	++++	++
Success Rate	Medium	Medium	Medium
Throughput Therapies	High	Low	Medium
Predictable Value	Low	Medium	High

Figure 1.11. Advantages and disadvantages of actual PDAC pre-clinical models.

Considering all these benefits, organoids are nowadays applied in cancer research to deep insight cancer biology and novel therapeutic approaches. Their main applications will be described as follows.

Organoids for cancer modeling

Cancer is a pathological state induced by a progressive accumulation of mutations. The possibility to genetically manipulate healthy organoids by CRISPR/Cas9 technology permits the study of single mutation-contribution to the development of malignancies (reviewed in [104,108]). Colorectal cancer (CRC) is the best case of accumulating alterations; studies managed to recreate in vitro single cell-gene mutations, identifying additive effects in organoids transformation and acquisition of aggressive phenotypes

[109]. Following these pivotal studies in CRC, analogous experiments were performed in esophagus[110], gut[111] and pancreas[112], generating stepwise progression of malignant organoids from non-transformed tissues (reviewed in[104]).

Mutational processes behind cancer can be further studied with tumor-organoids biobanks. Organoids can be generated from resected tumors at different stages, including metastasis, broadening inside the role of mutations in cancer development and exploring different genomic landscapes (Fig 1.12). Moreover, organoids can help to elucidate the heterogeneity among sub-clonal populations within the same tumor mass. Roerink and collaborators individuated parallel mutational processes co-existing inside a CRC tumor, describing subpopulations resistant to treatment, likely responsible for therapies failure[113].

Considering the emerging role of organoids in the study of genetic landscapes of cancer, their unique generation from resected tumors can be limiting. For cancers such as PDAC, where only 10-20% of patients undergo surgery, the introduction of organoids from different cancer stages is required. Recently, the derivation of organoids from fine needle biopsies permitted the study of more preliminary or more advanced stages of tumors, generating novel insight in cancer evolution[114,115].

Organoids for personalized drug screening

The high structural and genetic analogies presented by tumor-derived organoids with their tumor of origins make them a superior model in the identification of novel anti-cancer therapies and personalized treatment (fig 1.12).

Although organoids have not been directly implied in drug development yet, small scale drug screening suggested promising results [104]. Organoids biobank have been explored for the discovery of novel druggable targets, favoring the identification of new altered molecules for pharmacological inhibition [100]. Moreover, the possibility to derive organoids from healthy livers can help in the management of drug-associate toxicity, responsible for failure of a big number of treatments starting clinical trials [104].

The use of organoids for personalized drug screening have been introduced since their very beginning, identifying different grade of sensitivity among PDOs [100,116]. However, until recently, the cytotoxicity observed in organoids *in vitro* was not compared to patients' response in the clinic. In the last two years, studies in CRC and PDAC demonstrated matching sensitivities between patients and their derived organoids, suggesting the predictive value of this system in terms of drug response[115,117,118]. Interestingly, the possibility to derive organoids from patient's metastasis can help to identify specific treatments for different tumor grades, and in a short

time frame determine the most adequate approach for patients with advanced diseases [117,118].

Considering the validity and predictivity of the system, it is likely that in the following years organoids will become a determinant tool for prompt clinical decision making.

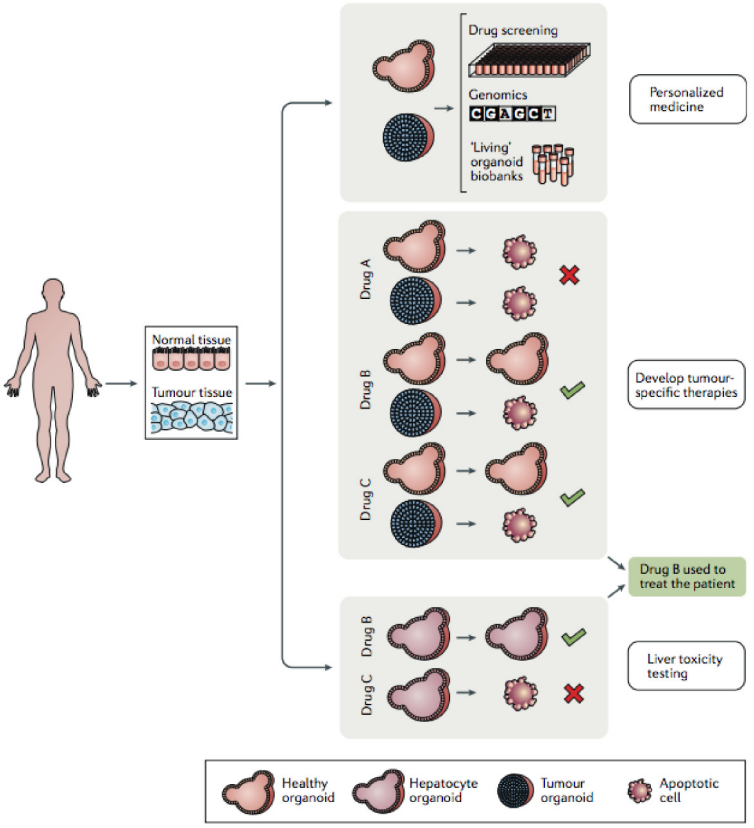

Figure 1.12. Possible applications for organoids in cancer research. *Image from* [104]

1.4.1.1 PDAC-derived organoids

The introduction of organoids in cancer research has been particularly beneficial for those malignancies characterized by high mortality rate, such as PDAC. With a 5 years survival lower than 10%, and widespread resistance to existing therapies, PDAC is a

major clinical problems[7]. The great genetic diversity among patients, not represented in cell lines, but strongly respected in organoids, stimulated the interest on this tool for PDAC research.

Huch and collaborators generated organoids from pancreatic tissue for the first time in 2013. Like for intestinal organoids, they demonstrated that upon pancreatic injury, ductal cells were activated with a concomitant expression of *Lgr5* marker and upregulation of *Wnt* signaling[119], required for tissue remodeling[120,121].

Information gathered with the organoid model in PDAC has demonstrated the structural and genetic features shared between primary PDAC tumor and its derived PDOs[107,122,123]. Others have proved the value of PDAC organoids to identify the contribution of specific genetic mutations towards the development of the malignancy [112].

The unmet clinical need to identify efficacious treatments for PDAC patients resulted in the generation of a biobank of 69 PDOs, derived from surgeries, fine needle biopsies and post-mortem autopsies, with primary tumors and PDAC metastasis to screen for therapies[115]. Whole genome sequencing identified common mutations between primary tumor and PDO, and transcriptomic analysis permitted the classification of PDAC tumors in classic and basal-like subtypes, according to the actual nomenclature [4]. In this work, the concept of "pharmacotyping" was introduced for the first time, meaning the characterization of organoids according to the

observed drug sensitivity. Interestingly, when treated with actual gold standards, organoids derived from tumors with high cellularity mirrored the outcome observed in their corresponding patients, dividing individuals in responders and non-responders.

The publication of this study in 2018 pointed towards organoids as a novel rationale to guide personalized therapeutic regimens in PDAC. However, there are also some limitations to current organoids technology, being the most relevant the lack of stromal elements in PDOs cultures. Since the PDAC organoids community is highly aware of this limitation, efforts to establish conditions for cultures of organoids with CAFs and/or T-cells have been described[39,124].

However, considering the importance of the desmoplastic reaction in PDAC tumors, further investigation is needed to the establishment of 3D cultures involving PDOs, and recapitulating the tumor microenvironment. This would evolve in the generation of more predictive screening models.

1.5 Oncolytic Virotherapy

Oncolytic virotherapy is an emerging cancer therapy that takes advantage of replication-competent viruses to selectively destroy cancer cells (Fig 1.13). The interest of viruses as possible agents for tumor destruction originates in early 1900s, with the observation of tumor regression in patients who contracted viral infections. With

the birth of cell culture in 1950s, many studies evaluated the activity of different viruses on tumor cells, resulting in clinical trials. However, since the use of wild type viruses showed systemic toxicities in many patients and transitory clinical benefits, the interest of viruses as cancer weapons was abandoned (reviewed in [125–127]). The idea of introducing tumor selectivity to a virus was first explored in 1991 by Martuza and collaborators for the treatment of gliomas [128].

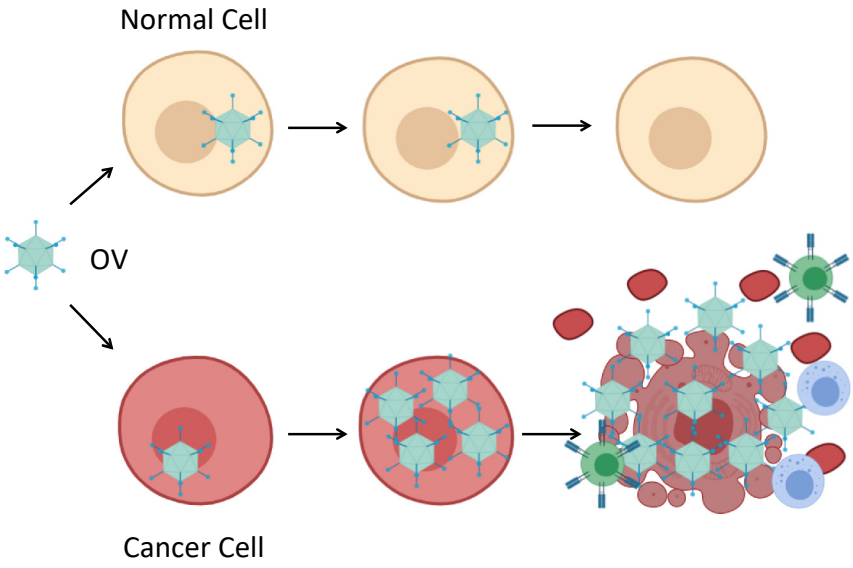

Figure 1.13. Schematic Representation of the concept of oncolytic virotherapy.

Since then, both RNA and DNA viruses have been genetically modified to obtain tumor selectivity and higher potency [129–131]. Oncolytic viruses (OV) are now designed to replicate and kill tumor cells, leaving normal cells unharmed. Lysis induced by viral replication leads to the release of new virions, that can in turn infect

new cancer cells, and liberate tumor-associated antigens, that can be recognized by T cells, engaging the immune system against the tumor (Fig 1.13)[132,133].

An attenuated adenovirus serotype 5, Oncorine (H101) has been authorized since 2005 in China for head and neck carcinomas [134]. However, the first virus worldwide approved as virotherapy from both the Food and Drug Administration (FDA) in the USA and the European Medical Agency (EMA) in Europe was the T-VEC in 2015 [135–137]. T-VEC is an attenuated herpes simplex virus (HSV-1) modified for the expression of granulocyte-macrophage colony stimulating factor (GM-CSF) transgene, promoting antitumor immunity [138]. It is nowadays used in clinic as monotherapy for advanced stages melanomas.

Following T-VEC approval, a big number of oncolytic viruses have been armed with transgenes with characteristics that can complement viral activity. Herpes viruses, vaccinia viruses, picornaviruses, retroviruses and adenoviruses are undergoing phase I/II clinical trials, alone or in combination with drugs, bringing new horizons in the treatment of incurable tumors [132,136,139].

1.6 Oncolytic adenoviruses

Following its discovery in 1953 [140], studies of adenoviruses elucidated intrinsic characteristics making them attractive therapeutic agents. Adenoviruses are not associated to serious pathologies (i), their genome is well known and easy to manipulate (ii), can infect both quiescent and actively dividing cells (iii), do not

integrate inside the genome (iv), can be produced at high titers (v) and are able to activate immune responses upon cell lyses (vi) [141–143]. The sum of these properties makes this virus largely explored in clinic, being nowadays in 51 clinical trials for cancer treatment (source: https://clinicaltrials.gov).

1.6.1 Adenoviral Biology

Adenoviruses belongs to the *adenoviridae* family, infecting eukaryote cells and classified in 7 different groups, from A to G. Nowadays, 57 different serotypes of adenovirus have been described [144,145]. Among the human adenovirus, the group C, especially serotype 2 and 5 are the best studied and mostly applied for therapies.

1.6.1.1 Adenoviral genome structure and dynamics of expression

Adenovirus C serotype 2 and 5 present a dsDNA genome of 35-36 KB length, encoding more than 40 proteins. Given its limited dimensions, adenoviral genes are efficiently organized in polycistronic transcription units, with overlapping genes (Fig 1.14 A). The perfect temporal organization of the adenovirus permits a sequential expression of its genes to gradually take over host cells, permitting viral DNA replication and maturation [146,147].

Depending on when they are expressed during the life cycle, adenoviral genes are classified in:

- **Immediate early**: E1A. Existing in 4 different splicing isoforms, it is determinant for the manipulation of host cell environment and the expression of the early genes. The conserved regions (CR) 1-4 of E1A establish more than 4000 protein interactions, suppressing cellular innate immunity and forcing host cell to enter the S phase of cell cycle. E1A CR3 trans-activates E1B, E2, E3 and E4 early genes [147,148].
- **Early**: E1B, E2, E3 and E4 continue with the remodeling of the cellular environment and induce adenoviral DNA transcription. E1B interferes with cellular mRNAs accumulation and protein degradation, repressing interferon-stimulating genes (ISG) and favouring viral RNA transcription and splicing [149]. E2 encodes for the viral replication machinery, composed by the DNA binding protein (DBP, E2A), adenoviral polymerase (AdPol, E2B), and pre terminal protein (pTP – E2B) [146,147]. E3 produces multiple spliced proteins contributing to the suppression of the anti-viral response. E4 encodes at least 7 proteins with functions involved in DNA replication and host-cell manipulation [150,151].
- **Intermediate**: the small genes IX and IVa are transcribed at intermediate point of infection, independently of late transcripts expression. They have a role in DNA packaging into mature virions and facilitate the activation of the major late promoter (MLP) [146,151].
- **Late**: the activation of these genes defines the second phase of adenoviral infections and takes place after viral DNA replication has started. The late genes (L1-L5) are alternatively spliced and polyadenylated from the same 28000 Kb transcript under the control of the MLP. Late genes codify for viral capsid and

packaging proteins, permitting the encapsidation of viral DNA and consecutive formation of mature virions [146,151].

Besides these genes, two smalls non-coding RNAs have been described: small virus-associated RNA (VA-RNA) I and II, located inside MLP transcription unit, but independently transcribed by cellular RNA polymerase III. They can interfere with cellular miRNA processing and stimulate viral genome replication al late time of infections (Fig 1.14 A)[151,152]

1.6.1.2 Virion Structure

X-ray crystallography, and later electron microscopy, unveiled the adenoviral structure, consisting of a non-enveloped icosahedral capsid (Fig 1.14 B). The hexon (a trimer of polypeptide II) forms the 20 facets of the structure, and in each vertex the penton-base protein (pentamers of polypeptide III) stabilizes the structure. The penton works as base for the fiber (trimmers of protein IV), which protrudes from the vertex and determines attachment to cell surfaces. The viral capsid is further cemented by the presence of minority protein (IIIa, VI, VIII, and IX), stabilizing the facets[153–155].

To fit in this 900 A diameter-structure, the 36KB genome of the adenovirus is tightly packed with viral DNA binding proteins[156], the basic proteins VII, V, μ Iva2 and terminal protein μ. The adenoviral genome is wrapped around protamine-like protein VII, main responsible for DNA condensation within the physical dimension of the capsid[151,153,157]. The process of genome packaging inside the capsid generates young virions, that need to be proteolytically activated to generate infective adenoviruses[155].

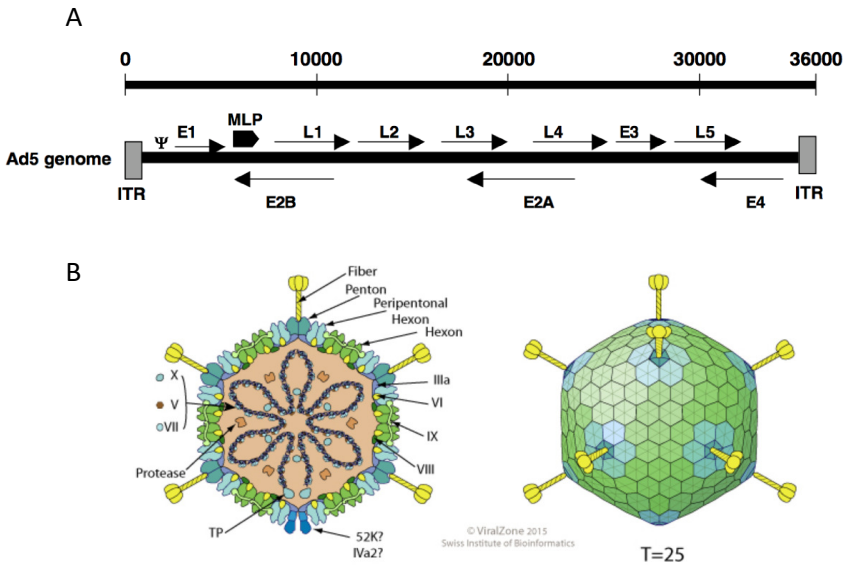

Figure 1.14.Concepts of basic adenoviral biology. ***A****. Schematic representation of Ad5 genome structure.* ***B****. Schematic representation of Adwt virion structure. Image adapted from* [158].

1.6.1.3 Adenoviral infectious cycle

An adenoviral infection begins when the fiber terminal domain, termed knob, interacts with the epithelial receptor CAR (Coxsackie-Adenovirus Receptor). Following this first attachment, the penton base recognizes cellular integrins, mainly avβ3/avβ5, thanks to the presence of an RGD motif [145,152]. This determines the virion internalization in cellular endosomes, with a clathrin-dependent mechanism. The acid pH present inside the endocytic compartments triggers modification in the adenoviral capsid that leads to disassembly of the more external structural proteins, resulting in endosome lyses and adenoviral escape to the cytosol [159,160]. Capsid interactions with cytosolic molecular motors (dynein) permit

adenoviral trafficking through cellular microtubules until reaching the nucleus. At the nuclear pore complex, viral DNA is released from the virion and imported in the cellular nucleus with the help of the nuclear pore complex. Once in the nucleus, the host transcriptional machinery starts to produce early viral mRNAs, followed by viral genome replication, expression of structural proteins and virions assembly. In 36 hours, the adenoviral life cycle is completed, leading to yields of hundreds of thousands of virions, which will lyse the cell and propagate to adjacent cells (Fig 1.15).

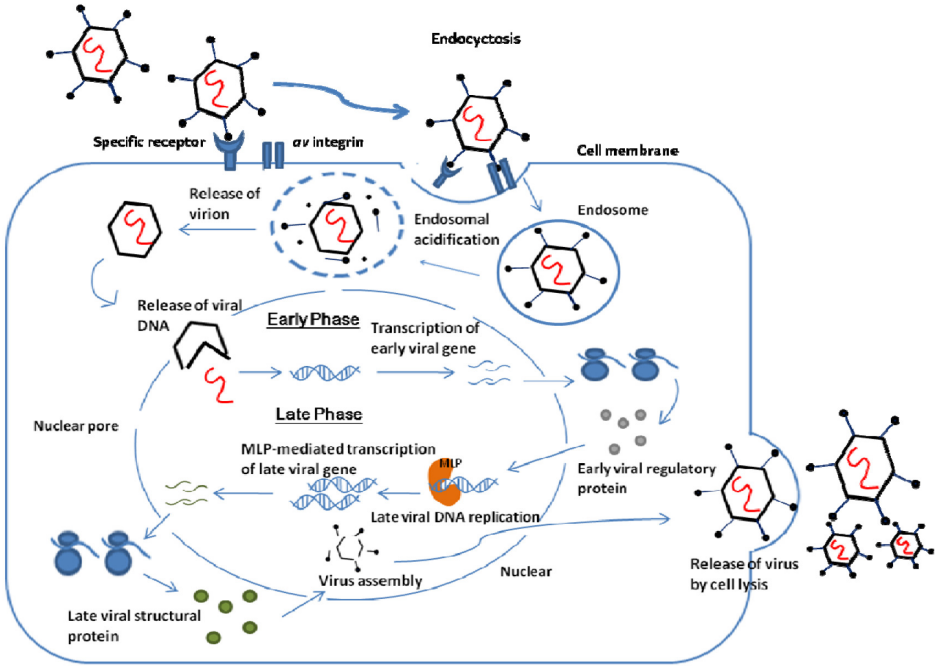

Figure 1.15. Schematic representation of adenovirus lytic cycle. Image from [161]

1.6.1.4 miRNAs and viral infection

There is increasing evidence that miRNAs play important roles in virus-host interactions. The host cell miRNAs might exert specific

pro-viral or anti-viral activities. Moreover, viral infections can modulate the cellular miRNome with changes induced either by the virus, to promote a proviral environment, or by the antiviral cellular response, to limit the viral life cycle (reviewed in [162,163]).

Initial studies analysing miRNA expression in response to adenovirus infection were carried out in human laryngeal epithelial cells (Hep2) with Ad3 [164]. The authors described a total of 36 upregulated and 44-downregulated microRNAs in infected cells, compared to the control condition. They observed a group of miRNAs upregulated at 6h PI, which gradually diminished with propagation of infection. Studies from Zhao and collaborators, in lung fibroblast cells defined fluctuating microRNA levels at different steps of Ad2 infection [93]. At early phase of infection (0 to 12 h PI), upregulation of miRNAs that favor cell growth arrest and an antiviral signaling were detected, suggesting that in the early onset of the infection, the miRNAs amount is modulated by the cell, trying to counteract the virus infection[93,162–164]. With the start of adenoviral DNA replication, from 12 hours PI, many miRNAs started to be downregulated, favoring the expression of molecules inducing progression through cell cycle, mainly transcription factors. At 24h PI the virus has the complete control of the cell, and by 36h PI a large majority of miRNAs are downregulated, inducing sustained viral replication escaping any control exerted by the cell.

1.6.2 Design of oncolytic adenoviruses

Adenoviruses do not present a natural tropism for replication in cancer cells, requiring genetic modifications of its dsDNA to

provide tumor selectivity. Nowadays, oncolytic adenovirus design is oriented to obtain tumor specificity and augment their potency.

1.6.2.1 Strategies to enhance tumor-targeting

Three major different strategies can be exploited to specifically direct adenovirus towards tumor cells, involving transcriptional and post-transcriptional processes.

1.6.2.1.1 Tropism alteration

The main receptor responsible for adenoviral attachment on cell surface is the CAR receptor. However, its downregulation is common among cancers[165], and a re-direction of the fiber-host surface interaction towards more common receptors can improve tumor-targeting. Adenovirus 5 fiber tropism can be switched to Ad3 or Ad35 fiber, that recognize DSG2 and CD46 receptors, respectively, upregulated in many cancers [166,167]. An alternative is the introduction in the capsid of targeting peptides recognizing other molecules than CAR. The insertion of an RGD motif in the fiber knob permits adenoviral recognition through cellular integrins, highly expressed in cancer cells, broadening tumor transduction [168].

1.6.2.1.2 Control of viral gene expression

A widely explored strategy to control viral gene expression is the insertion of a tumor-specific promoter regulating E1A expression. Different oncolytic adenoviruses have been generated using promoters of upregulated genes in cancer, including cyclooxygenase 2 (*COX2*), human telomerase (*hTERT*) and *uPAR*

[169–171]. Some of these regulatory elements have been further modified to be chimeric promoters with sequences responding to deregulated signaling in cancer. In this line, our group generated an oncolytic adenovirus with the uPAR promoter and three SPS sequences that respond to Notch activation signals, enhancing the tumor-specific regulation of E1A [172]. Others, have modified the natural adenoviral E1A promoter by the introduction of binding sites for the E2F transcription factor, altered in many tumors [173].

Viral gene expression in tumors has also been post-transcriptionally regulated by miRNAs [174]. MiRNAs differential expression between transformed and normal tissue has been used to improve tumor-targeting by insertion of miRNA-complementary sequences in the 3'UTR of viral genes, resulting with detargeting activity of the virus in normal cells [175–177]. The insertion of a multiple miRNAs - controlled circuit in an oncolytic virus permitted the tight expression of viral genes and immune effectors, leading to high selective viruses with superior tumor-killing efficacy [178].

Recently, the insertion of CPE (cytoplasmatic polyadenylation elements) regulatory sequences at the 3' UTR of E1A permitted the selective activation of viral genes transcription in transformed cells. The differential expression and activity of the CPE binding proteins between normal and cancer cells provided a new paradigm of oncoselectivity to adenoviruses [179].

1.6.2.1.3 Manipulation of viral genes

Viral genes can induce progression through G1/S phase bypassing the molecular control exerted by p53 and pRb. Mutations of both molecules in cancers have been exploited as a mean to increase adenoviral tumor selectivity.

E1B, together with E4Orf6, binds and re-localizes p53, favoring adenoviral genome replication [149]. ONYX-15 and H101 oncolytic adenoviruses have been engineered with a mutation in the E1B-55K gene, avoiding p53 sequestration in normal cells, but favoring adenoviral genes transcription in cancer cells where p53 is inactive [180].

E1A CR2 region recognizes and binds pRb, leading to the release of E2F and favoring cell cycle progression. The 24bp deletion in this E1A region restricts viral replication to cells that have constitutively active the retinoblastoma pathway, avoiding pRb binding in non-transformed cells [181].

1.6.2.2 Strategies to enhance adenoviral potency

Adenoviruses can be armed with transgenes to augment their potency. Engineered transgenes can provide additional functions, such as improving viral spread through the stroma or facilitating the activation of the immune system. The introduction of ECM remodeling factors, including hyaluronidase [182], DNAseI [183] or metalloproteinases [184] demonstrated higher grade of adenoviral diffusion in desmoplasic PDAC tumors. VCN-01, an attenuated adenovirus encoding for a hyaluronidase [185] is now in clinical trials

in combination with gemcitabine and nab-paclitaxel for the treatment of advanced PDAC [185,186].

To stimulate patients' immune system against the tumor, oncolytic adenoviruses are being modified to express cytokines, chemokines [187], tumor associated antigens [188] or bi-specific t-cell engagers (BiTE), inducing T-cell recognition of the tumor [189].

1.6.2.2.1 miRNAs modulation to boost adenoviral potency

Recently, mechanistic insights among adenoviral infection, cancer and microRNAs identified these ssRNA molecules as an easy handling tool to enhance adenovirus potency [94,190].

Overexpression of miR-26b triggered stronger adenoviral-related cell death and spreading to adjacent cells in prostate cancer cells, suggesting miR-26b as a sensitizer of oncolysis in this cancer [94]. In PDAC, our group has recently shown that miR-99b and miR-485 act as enhancers of adenoviral oncolysis through increased adenoviral fitness leading to improved antitumoral activity *in vivo* [190].

Despite the recent findings of miRNA sensitizers, the impact of over-expressed miRNAs in cancers on adenoviral oncolysis has not yet been explored. In the current work we have addressed this point and studied the oncolytic effects of sequestering candidate endogenous miRNAs by miRNA-sponges engineered adenoviruses.

2. Objectives

The general goal of this thesis has been to progress oncolytic adenovirus therapy for PDAC, by the incorporation of novel preclinical models to test for patient-specific responses and the generation of oncolytic adenoviruses with enhanced therapeutic index.

The two main objectives have been the following:

i) Evaluate patients-derived organoids (PDOs) technology as a platform to screen for personalized virotherapy *in vitro*

1) Establishment of a battery of PDOs from PDAC and normal pancreatic tissues, and evaluation of their applicability in the study of adenoviral infection;

2) Screening of a battery of PDOs to identify individual sensitivities to virotherapies, and the effects derived from the combination with chemotherapy;

3) Study virotherapy-responses in metastasis originated from PDOs xenografted in mice;

(ii) Improve oncolytic adenovirus potency by modulation of miRNAs deregulated in PDAC

4) Screening of aberrantly expressed miRNAs sensitizing viral oncolysis in PDAC via CRISPR/Cas9 system;

5) Generation of a miRNA sponge-adenovirus and evaluation of its oncolytic effects *in vitro* and *in vivo;*

6) Modulation of miRNA levels with the THZ1 transcriptional inhibitor, and assessment of the effects of its combination with oncolytic adenoviruses.

.

3. Materials and Methods

3.1 DNA Manipulation

3.1.1 Plasmid DNA isolation from prokaryotic cells

Bacteria can be used as a vector to amplify DNA exogenously inserted in the form of a plasmid. This process is called transformation and permits the plasmid replication together with bacterial DNA. In this way, great quantity of vector can be produced.

3.1.1.1 Small scale isolation of plasmid DNA

Minipreparations (miniprep) were used to obtain small amount of plasmid DNA (30-50 µg) from liquid bacterial culture. This purification was based on DNA precipitation in the presence of salts and isopropanol.

Transformed bacteria containing the DNA of interest were grown in Luria Broth's (LB) medium with the appropriate antibiotic overnight at 32ºC or 37ºC. An aliquot of 1.5 mL of cells was then centrifuged and the cellular pellet homogenized in an isotonic buffer containing RNAse A (buffer P1), and further lysed with an alkaline solution containing SDS (buffer P2). The reaction was stopped by the addition of an acid buffer (buffer P3), then incubated on ice for 20 min and centrifuged (15000 rpm, 10 min) to remove cellular debris. Supernatant phase was harvested, and the plasmid DNA easily precipitated by the addition of isopropanol and finally collected after a second centrifugation. The pellet containing DNA was further cleaned up with 70% ethanol. When ethanol was

completely evaporated, plasmid DNA was re-suspended in 30 µL of Nuclease-free water and stored at -20ºC.

3.1.1.2 Large Scale isolation of plasmid DNA

To get larger amount of DNA, an analogous process as the one for minipreps was followed. MAXIpreparations (MAXIpreps) were used to produce large amounts of high-quality plasmid DNA with the help of a commercial kit (Plasmid Maxi Kit – Quiagen).
Depending on the number of plasmid copies/bacteria (high copies or low copies plasmid), 250 mL or 500 mL of LB were required. After incubation overnight at 32ºC or 37ºC, LB containing the bacteria was pelleted at 6000 g for 15 minutes. Cell lysis was then performed following manufacturer's protocol.

3.1.2 Isolation of genomic and viral DNA from cells

Genomic DNA from cultured cells or organoids was isolated with the help of a commercial kit (Blood DNA Isolation Mini Kit – Norgen Biotek), following manufacturer's protocol. When cells were infected with adenovirus, the viral DNA was obtained together with the chromosomal DNA of infected cells.

3.1.3 DNA quantification

The amount of DNA in a sample and its purity was determined by spectrophotometer absorbance (Nanodrop -Thermo Scientific). Nucleic acids absorb at 260 nm, and this wavelength was used to trace their concentration according to the Lambert-Beer Law.

Besides concentration, following absorption ratios have to be taken into account:

- **260/280**: values around 1.8 were considered optimal, meaning purity of nucleic acids. Values lower than 1.8 indicated strong contamination from proteins or phenols that absorb at 280nm.
- **260/230**: ratio used as additional measurement of purity, assessing for salts contaminant. Pure nucleic acids values used to range from 2 to 2.2.

3.1.4 DNA digestion

Pure DNA can be digested with bacterial endonucleases, also known as restriction enzymes (RE) that recognize specific sequence on endogenous DNA and introduce a cut in these loci. Digestion with RE in this study was used for two different aims:

- **Cloning strategies**: RE helped to cut a specific DNA fragment from a vector (e.g. a plasmid), to locate it in a new backbone previously cut with the same RE. Products of digestions were generally analyzed by agarose gel electrophoresis, and the desired band purified for further cloning. Purification was performed after agarose dissolution with a commercial extraction kit (QIAquick Gel Extraction Kit – QUIAGEN).
- **Plasmid DNA pattern recognition**: once a new plasmid was obtained, or commercially purchased, the fidelity of the sequence was tested by RE digestion.

3.1.5 DNA amplification via Polymerase Chain reaction (PCR)

PCR allows for the specific amplification of DNA fragments by the activity of the DNA polymerase of *Thermophilus aquaticus* (Taq Polymerase), working at high temperatures (72ºC). To amplify, specific oligonucleotides (primers) matching sense and antisense strand of target DNA sequences are required. Primers are 20-25 nucleotides sequences that hybridize to target sequences and facilitate the DNA fragment elongation in the presence of deoxynucleotides (dNTPs) by the DNA polymerase. To define the conditions of the PCR reaction two main factors were considered: 1) each pair of primers works at a hybridization temperature (Th), 2) the length of a target sequence influences the duration of the elongation phase (Te), amplifying Taq Polymerase at 1Kb/minute.

PCR phases are summarized as follows:

Initial denaturation	95ºC - 5 minutes	1X
Denaturation	95ºC - 30/45 s	30-40X
Hybridization	Th (variable) – 30/45s	30-40X
Elongation	72ºC - Te (variable)	30-40X
Stabilizingfinal elongation	72ºC - 5 minutes	1X

A list of primers used in the study for PCR amplification is available in Table 3.1.

PCR reactions were conducted with the commercial kit Dream Taq™ Hot Start DNA Polymerase (Thermofisher Scientific) and dNTPs from 100mM dNTP Set (Invitrogen). When DNA fragments were amplified for cloning in plasmids, a DNA-polymerase with high-fidelity activity was used (Expand High Fidelity PCR System - Roche*)*, in order not to introduce random changes in the nucleotide sequence.

3.1.6 DNA sequencing

DNA fragments amplified via PCR were sequenced via Sanger's Method. This is based on the incorporation of fluorescently marked chain terminating dNTPs to a DNA fragment being elongated *in vitro.*

Beckman Coulter Genomics and Eurofins Genomics performed sequencing reactions, upon delivering template DNA and specific primers. The set of primers used for sequencing is listed in Table 3.1.

3.2 DNA constructs generation

3.2.1 Plasmids expressing miRNA sponges

The plasmid backbone used for miR sponge insertion was the miRVec. This is a commercially available plasmid, previously modified in the lab by Estela Nuñez to express an eGFP under the control of a CMV promoter. The eGFP was completely functional, due to the presence of a promoter (CMV), three STOP codons, a short 3' UTR and a polyA tail to permit translation of the protein.

This construct was further modified to have an *EcoRI* restriction site at the 3' end of the eGFP.
The clonings of the miRNA sponge repetitions were performed in this backbone, forming part of the 3' UTR of the eGFP, by insertion in the *EcoRI* site.

3.2.1.1 miRNA sponge design

Sponges were generated with the help of the software miRNA-song (http://www.med.muni.cz/histology/miRNAsong/index.php)[191]. We provided to the software the desired miRNA sequence to target, and specified the number of sponge repetitions. The software generated a combination of sequences working as sponges. We designed 4 tandem sequences, separated by a different spacer, and with a budge between nucleotides 9-12. This was described to increase the efficiency of the sponges [192–194].

For miR-222 sponge, we selected the combination with the lowest free energy of duplex (-130 kcal/mol) and the highest number of "on-target" sites. For the miR-Scramble sponge, we selected the sequence with the highest free energy of duplex (maximum value obtained was -30 Kcal/mol) and the lowest number of recognizing target sites. We also analyzed the off-targets recognized by both miR-222 and Scramble Sponges and we found miRNAs very poorly expressed in PDAC.

To assure the termination of the transcription of the eGFP after the sponges, the sequence was terminated with two extra stop codons (TAA-TGA) at the 5`of the sequence corresponding to forward

primer. Both forward and reverse primers were also endowed with sticky ends containing *EcoRI* recognition sequence to re-establish the presence of this RS after cloning. The sponge sequences selected were ordered as ssDNA in the sense and reverse orientation and are listed in Table 3.2.

3.2.1.2 miRNA sponge annealing and phosphorylation.

To anneal ssDNA fragments, they were re-suspended in duplex buffer (IDT) at a final concentration of 100µM. Oligos were mixed in equal amounts and heated at 94 ºC for 4 min. Then, switching off the heat block gradually ramped the temperature down.

Annealed oligos were then phosphorylated with T4 PNK enzyme, in a mix containing T4 ligase buffer enriched with ATP. Reagents reacted for 40 min and the phosphorylated annealed products were further purified via PCR, and quantified.

3.2.1.3 Cloning miRNA sponges in the miRVec backbone

miRVec backbone was digested O/N with *EcoRI*. The day after, the product was run on agarose gel, and the band of the digested vector purified. After purification, digested miRVec was submitted to dephosphorylation with alkaline phosphatase enzyme (Fast AP), for 10 min, to avoid re-ligation of extremities.

Sponges were ligated with miRVec (*EcoRI*) with the help of T4 ligase ON. Different molar ratios were used to enhance the chance of ligation.

Ligated constructs were introduced in DH5α bacterial via heat-shock transformation, and then plated on LB+Agar+Ampicillin. Next morning, colonies were tested for insertion of miR-Scramble or miR-222-S sponges by PCR. Three positive clones were sequenced and a correct colony was chosen. A schematic representation of the cloning process is represented in Fig 3.1.

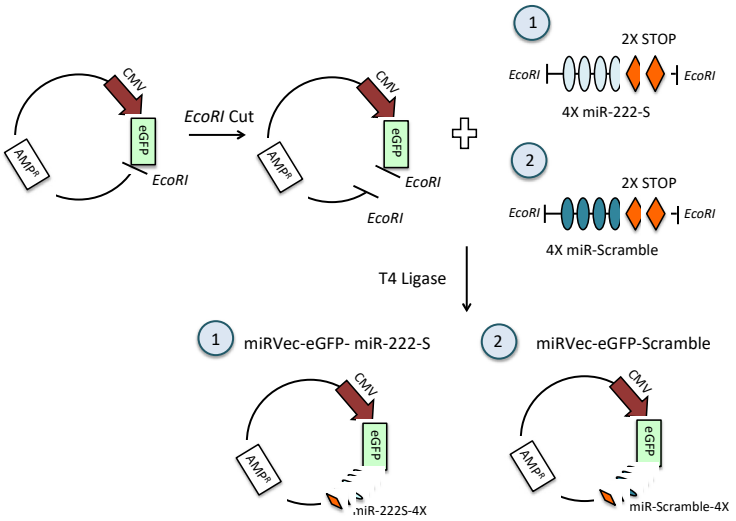

Figure 3.16. Cloning strategy for the generation of miRVec-eGFP-miR-222-S and miRVec-eGFP-Scramble.

3.2.2 Generation of plasmid vectors with sgRNAs for miRNA KO

To express the Cas9 protein and sgRNAs in eukaryotic cells, we used the lentiviral vector system lentiCRISPRv2 (Addgene catalogue #52961). The different steps needed to clone the sgRNAs in the *BsmBI* restriction site of the lentiviral vector are described as follows.

3.2.2.1 Single guide RNA design (sgRNA)

sgRNAs are responsible for the specificity of the CRISPR/Cas9 system. The sgRNAs are composed by a single strand RNA (ssRNA), complementary to the target sequence, and a trans-activating crRNA (tracrRNA) that binds to the Cas9 nuclease. The sgRNA guides the Cas9 to the region of complementarity where target recognition and DNA cut will occur. Since the tracrRNA is common to all the sgRNA, for simplicity the specific ssRNA sequences are referred as sgRNAs.

sgRNAs were bioinformatically designed with the help of different softwares:

- MIT Software (http://crispr.mit.edu/);
- Benchling (https://benchling.com/);
- Breaking Cas(http://bioinfogp.cnb.csic.es/tools/breakingcas/)Oliveros et al., 2016)

Candidate sgRNAs were tested by two or three programs. The selected sgRNAs were chosen based on high on-target activity and specificity, and low off targets score. The sgRNAs were designed as blunted-end sequences to permit ligation in the *BsmBI* site. Two pairs of ssRNAs, close to a PAM sequence, were designed for each target, since the theoretical design does not always lead to functional guides. The sgRNAs were ordered as ssDNA oligos from IDT and further annealed in the laboratory. A list of the sgRNAs used in the study is available in Table 3.3.

3.2.2.2 ssDNA oligos annealing and phosphorylation

ssDNA for sgRNA strands were re-suspended in the amount of ddH_2O recommended by the supplier. ssDNA strands were paired together due to their complementarity, with the help of a thermocycler. The mixture was first stabilized at 37ºC for 30 min, then heated up at 95ºC for 5 min to separate eventual dsDNA formed, and gradually ramped down to 25 ºC to favor specific base-pair recognition (5ºC/min). T4 PolyNucleotide Kinase (T4 PNK – New England Biolabs) was added to the mixture to favor dsDNA phosphorylation and permit further ligation with the unphosphorylated lentiCRISPRv2.

After reaction, sgRNA Fw and Rv were diluted 1:500 and 1:1000 in ddH_2O. For a stoichiometric reason the sgRNA was present in lower quantity than the plasmid in the reaction to permit a productive ligation (the plasmid was 600 times the length of the duplex of sgRNAs).

1 µL	sgRNA Fw 100µM
1 µL	sgRNA Rv 100µM
1 µL	10X T4 Ligation Buffer (with ATP)
6.5 µL	ddH_2O
0.5 µL	T4 PNK

3.2.2.3 LENTICRISPRv2 digestion and dephosphorylation

The plasmid was incubated for 3 h with the enzyme *Esp3I* (*BsmBI*, ThermoFisher Scientific) together with FastAP (Thermo sensitive Alkaline Phosphatase – ThermoFisher Scientific), to dephosphorylate the vector and avoid re-ligation. These enzymes could be used in the same master mix, since they worked well together using the buffer from *Esp3I*.

5 µg	lentiCRISPRv2
3 µL	*Esp3I*
3 µL	FastAP
6 µL	10X *Esp3I* buffer
0.6 µL	DTT 100 mM
Up to 60 µL	H20

When the digestion was completed, the product was run on a 0.8% agarose gel, and a band of approximately 12000Kb and one of 2000 Kb were visible. The 12000Kb band was isolated and purified using QIAquick gel extraction KIT (QIAGEN).

3.2.2.4 sgRNA ligation into lentiCRISPRv2 and selection of positive colonies

Two different ligation mixtures were set up at two sgRNA dilutions. The ligation reaction was incubated O/N at 4ºC with T4 ligase (Roche). A control ligation reaction, containing ddH_2O instead of annealed sgRNA was performed in parallel.

X µL	Digested lentiCRISPRv2 (50ng)
1 µL	Oligo Duplex (1:500/1:1000)
1 µL	10 X Ligase Buffer
Up to 11 µL	ddH_2O
1 µL	T4 Ligase

The products of ligation were transformed in DH5α bacteria strain via heat-shock transformation. After recovery, bacteria were seeded in LB+AGAR+Ampicillin plates, and the day after grown colonies were selected for plasmid DNA extraction with miniprep protocol. First, a PCR with lentiCRISPRv2 hybridizing primers was performed, and positive bands sequenced. A colony with the correct sequence was selected. A schematic representation of the process can be found in Fig 3.2.

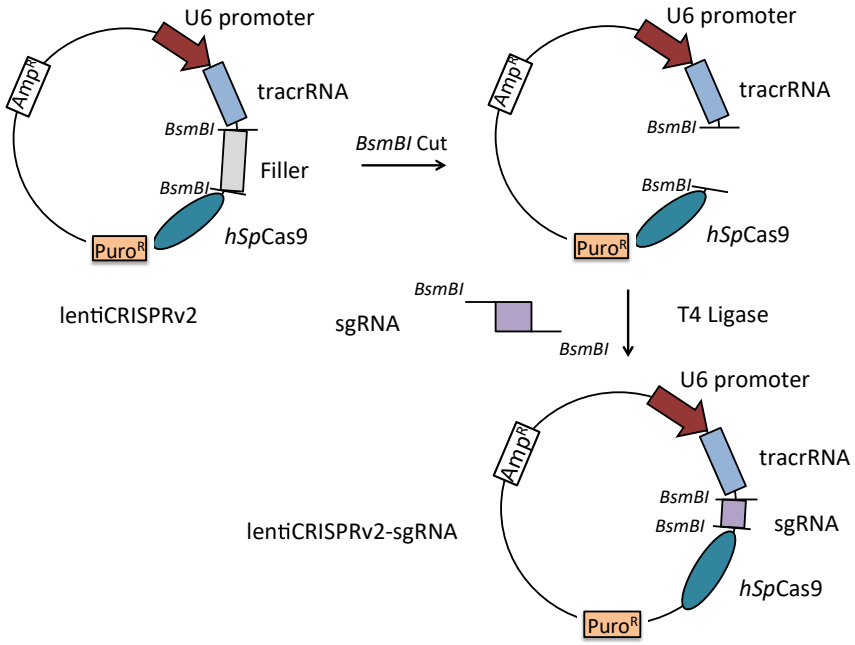

Figure 3.17. Schematic representation of sgRNAs cloning in lentiCRISPRv2 vector

3.3 RNA manipulation

3.3.1 RNA extraction and retro transcription to cDNA

Total RNA was isolated from adherent cell lines, organoids and patient's tissues using miRNeasy mini Kit ®(QUIAGEN), which permits obtaining both mRNAs and small RNAs, such as miRNAs. Cells were disrupted with the help of QIAzol lysis reagent and RNA was purified following manufacturer's protocol. In the case of tissues, disruption and homogenization were facilitated by the use of a 20G needle.

To avoid contamination of genomic DNA, purified RNA was treated with DNAse, DNA-free ™ DNA removal kit (Invitrogen),

as described by manufacturer. Quality and quantity of extracted RNA were measured with Nanodrop.

- For mRNA, 500 µg of total RNA was used for complementary DNA (cDNA) synthesis with polyA primers by Primescript ™ RT Reagent KIT (Takara) in a final volume of 20µL, following manufacturer's protocol.
- For miRNAs, due to their smaller size, the use of specific probes was required. These are stem loops that, upon melting at high temperature, recognize the miRNA to which they are complementary to and permit retro transcription to cDNA. The resulting cDNA fragment is then long enough to permit adhesion of primers for qRT-PCR. MiRNA retro-transcription was performed on the amount of 3 µg of total RNA, and the reverse transcriptase and stem-loop primers used are commercially available from Applied Biosystem (TaqMan MicroRNA Reverse Transcription Kit, TaqMan MicroRNA assay).

3.3.2 RNA Expression

Expression of mRNAs and miRNAs were quantified via qRT-PCR in a Viia7 Real time PCR system (Applied Biosystem), using specific primers for mRNAs and TaqMan probe for miRNAs.

3.3.2.1 Gene expression analysis

To analyze gene expression, abundance of cDNA was quantified via qRT-PCR. cDNA is directly proportional to the amount of mRNA for a gene of interest in the sample analyzed, giving a direct

measurement of its expression. An un-specific dye commercially available (the LightCycler® 480 SYBR Green I Master Mix – Roche Applied Science) intercalates into double strand DNA during the amplification with specific primers. This reaction was performed in a 384 well plates in a thermocycler capable to detect fluorescence from samples (Viia7 Real Time PCR System – Applied Biosystems). Evolution of fluorescence across the PCR cycles allowed for the calculation of the initial amount of cDNA of the gene of interest. This was quantified via ΔCt method and always relativized to a housekeeping gene, which expression did not change within the different conditions. The hypoxanthine phosphoribosyltransferase 1(*HPRT*) was used in most of the analysis as housekeeping gene. The reaction mixture was prepared mixing 5µL of Master Mix 2X, 0.3 µL of specific primers (10µM) and 3.7 µL of H2O. To the mixture, 1 µL of cDNA was added for each well. Reactions were performed in triplicates. Primers are listed in Table 3.4.

3.3.2.2 miRNAs expression analysis

MiRNAs expression was quantified via qRT-PCR based on TaqMan assays, in a Viia7 thermocycler. TaqMan assays (TaqMan MicroRNA Assay – ThermoFisher) combine primers and hydrolysis probes that recognize the miRNA's cDNA and emit fluorescence when the fluorophore is cleaved and thus separated from the quencher by the exonuclease activity of the polymerase. TaqMan probes permit quantitative measurement of the fluorescent product during the cycles of the PCR. Reaction mixture was prepared as

follows and performed in triplicate for each sample: 5 µL Master MIX 2X, 0.5 µL TaqMan miRNA assay 20X, 1.5 µL of reverse transcription product and 3µL of Nuclease-free-water. MiRNAs expression was quantified using the ΔCt method, relativizing to the ribonuclear RNA (rRNA) RNU6B. A list of the commercial probes used is available in Table 3.5.

3.4 Eukaryotic cell lines manipulation

3.4.1 Cell lines. Maintenance and culture conditions.

All the cell lines used in this study were adherent and grew as 2D cultures. They were maintained in a humidified incubator at 37 ºC with 5% of CO_2. All the cell lines were grown in DMEM (Dulbecco's Modified Eagle Medium), supplemented with 10% of inactivated fetal bovine serum (iFBS), 100 U/mL penicillin, 100 µg/mL streptomycin, and 2mM L-glutamine. All the cell lines were split twice a week to assure their wellness and avoid cell overgrowth.

A-549: human cell line derived from a lung adenocarcinoma. Mainly used for recombinant adenoviral production due to their high efficiency in amplification of this virus. Cells kindly provided by Dr. Ramon Alemany (IDIBELL - Institut Català d'Oncologia, Barcelona).

HEK-293 ICO: Human Embryonic Kidney 293 cells, derived from embryonic kidney cells immortalized via introduction of 5' of

adenoviral genome including E1A. Due to their easiness in transfection, this cell line is used in the first step of recombinant adenovirus production, as well as for the generation of replication-deficient adenoviruses. Cells kindly provided by Dr. Ramon Alemany (IDIBELL - Institut Català d'Oncologia, Barcelona).

HEK-293 T/17: highly transfectable cell lines derived from parental HEK293 with the introduction of SV40 antigen. Due to this characteristic, they were mainly used for transient transfection and for lentiviral generation. Purchased from ATCC (CRL-11268).

ASPC-1: pancreatic cancer adenocarcinoma cell line derived from a xenograft in nude mice generated from cells from an ascites of a patient with pancreatic cancer. Purchased from ATCC (CRL-1682). Used in Dr. Goel's laboratory, Baylor Charles A Sammons Cancer Center, Dallas (TX).

Capan-1: pancreatic cancer cell line derived from a liver metastasis obtained from a patient affected from PDAC. Purchased from ATCC (HTB-79). Used in Dr. Goel's laboratory, Baylor Charles A Sammons Cancer Center, Dallas (TX).

CP-15 Luc: human cell line expressing firefly luciferase. The parental line came from a human pancreatic ductal adenocarcinoma xenografted in athymic mouse [196] then stably transduced with a retrovirus expressing firefly luciferase. Cells were then selected with hygromycin, and after the generation of clones, tested for luciferase expression. This line was generated in our laboratory.

MIA PaCa-2: human cell line derived from a pancreatic ductal adenocarcinoma. Acquired from ATCC (CRL-1420).

PANC-1: human cell line derived from a pancreatic ductal adenocarcinoma. Acquired from ATCC (CRL-1469).

3.4.2. Transient Transfection

Transfection is the process that permits non-permanent introduction of genetic material inside eukaryotic cells. It is a fast and easy way to have a primary assessment of plasmid constructions.

Cells were transfected by DNA co-precipitation with calcium phosphate (CalPhos Mammalian Transfection Kit- Clontech).

HEK-293T cells were seeded the day before transfection at a density of 300.000 cells/well in a MW6 plate. Depending on the construct, a different amount of plasmid DNA was transfected, following manufacturer's protocol (from 0.2 to 1 μg). The DNA was mixed with $CaCl_2$ in a Vortex and a phosphate buffer HBS solution was added drop by drop. After 15 minutes of incubation, the solution containing the DNA/phosphate crystals was added to cells. The day after, transfection media was replaced with fresh one to remove the precipitates, due to their long-term toxicity.

3.4.3 Lentiviral transduction

3.4.3.1 Generation of stable KO/KD in PDAC cells via lentiCRISPRv2 transduction.

To generate PDAC cells with specific miRNA KO we used the lentiCRISPRv2 (Dr. Feng Zhang – purchased from Addgene) vector containing Cas9 and engineered with sgRNAs [197]targeting miRNAs.

Lentiviruses are RNA viruses requiring a series of genes (*Gag, Pol, Rev, Env, Tat*) to be produced. Once lentivirus enters the cells, its RNA genome is retrotranscribed to dsDNA and this can integrate randomly inside the genome. We used 2nd generation lentiviruses to generate infective particle transfected to HEK-293T cells [198].

The three plasmids were:

- **Envelope Plasmid**: containing *env*, codifying for the viral glycoprotein of the capsid of the *Vesicular Stomatitis Virus* (VSV)
- **Packaging Plasmid**: containing *gag, pol, rev* and *tat* genes, responsible for retrotranscription of viral RNA, incorporation in the host genome and production of structural proteins;
- **Transfer Plasmid**: containing the transfer DNA: lentiCRISPRv2 + sgRNA. LentiCRISPRv2 also contains the Cas9 protein and the LTR and PSI packaging sequences at its extremities, to permit final viral particles formation.

Semi-confluent (60-70%) p100 plate of HEK-293T cells were transfected with the three plasmids:

Envelope plasmid (pVSV-G)	3.4 µg
Transfer plasmid (lentiCRISPRv2)	9.8 µg
Packaging plasmid (p8.91)	6.3 µg
$Cacl_2$ 2 M	86.8 µL
ddH_2O	Up to 700µL

The transfection method was performed with the calcium phosphate technique. Transfection medium was replaced with fresh one the morning after. Two days following change of medium, the supernatant containing viral particles was filtered to remove cell debris, and transferred to PDAC cells. PDAC cells were incubated with the virus for two days and then puromycin selection was added (4-8 µg/mL, depending on the cell line). After selection, cells were checked for genome editing in the desired genomic locus. All the miRNAs targeting were verified by sequencing (primers used for sequencing listed in table 3.1; sequencing on appendix 8.1). TaqMan probe assays were used to evaluate target miRNA expression. A scheme of the process is shown in fig 3.3.

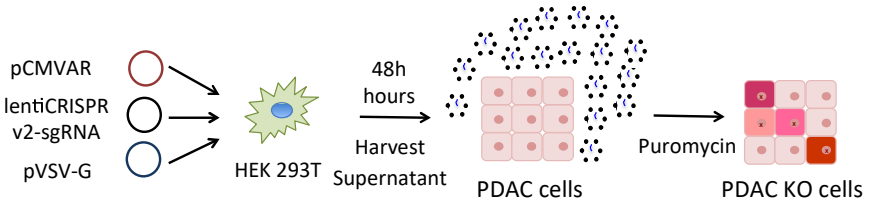

Figure 3.18. Schematic Representation of lentiviral transduction of PDAC cells for the generation of CRISPR/Cas9 KOs.

3.4.3.2 Selection of KO clones for candidate miRNAs

To generate individual cell clones, the initial pool was diluted up to 1 cell/well in a 96MW plate. For this, 100 cells were diluted in 10 mL of medium, and 100 µL were added to each well. Cells were grown for at least 10 days, and then visible colonies were trypsinized, and transferred to a bigger plate (p60) for further analysis.

3.5. Patient-derived pancreatic organoids (PDOs)

Between 2015 and 2019 tumor and healthy pancreatic samples from PDAC patients undergoing surgery in the Hospital Clinic were collected, upon signed informed consent. The Hospital Clinic Ethical Committee approved the study.

3.5.1 Organoids generation from human pancreatic tissues

After surgical operation, the tissue was immediately collected and submitted to anatomo-pathological evaluation by a qualified medical doctor. Fragments from both healthy and transformed pancreatic tissues were preserved at 4ºC in advanced DMEM/F12 (Gibco), supplemented with 100 U/mL penicillin, 100 µg/mL streptomycin, 2mM L-glutamine and 1 M HEPES. Tissue was immediately processed or within the next 24h. A list of materials required to initiate the protocol is listed in Table 3.6.

The procedure to obtain organoids is summarized as follows (adapted from [101,199]):

1. The tissue was placed under the tissue-culture hood in a sterile p60 plate and minced to small pieces with a surgical knife;
2. When fragments reached dimensions around 1-2mm, 2mL of digestion solution were added (see Table 3.6) and everything transferred to 15 mL falcon tube. The tube was filled up to 7 mL with digestion media and incubated at 37ºC, 450 rpm shaking with 30º of inclination.
3. Tissue digestion was checked every 30 min. When the digestion media become turbid, we moved to culture hood.
4. The digestion medium was pipetted up and down with a 5 mL serological pipette, to let the undigested tissue precipitate. The medium with digested cells was transferred to a p100 plate containing 10mL of wash medium, in order to dilute digestion medium (Wash 1).
5. Extra fresh digestion medium was placed with not digested pancreatic tissue and returned to the shaker at 37ºC.

By placing the p100 plates containing wash 1 under the microscope we checked for ducts, resembling stalks of grape. If great majority of cells has a round-shaped form, the solution was generally discarded. If a considerable number of ducts was observed, we moved to next steps from **a** to **e**. For normal pancreatic tissues, ducts would be picked after 2^{nd}-3^{rd} wash, whereas for tumor tissues they were obtained after longer digestions, generally discarding the

first washes. This was due to the different stiffness of the tumor compared to the normal tissue, which was always easier to digest.

a. For higher success rate, ducts could be picked to enrich the culture in ductal cells rather than acinar cells. Plate was located under microscope at 10-20X magnifications and with the help of pipette manually picked one by one.
b. When 100 ducts or more were picked, and collected in 15mL falcon tube, wash medium was added on the top and centrifuged at 300g for 5 minutes.
c. The medium was aspirated and cleaned again with wash medium by centrifuging. The pellet obtained, in this case P1, could be either directly seeded or placed on ice waiting for more ducts from following digestions. We generally preferred to seed directly after pelleting, to avoid too long wait that could affect cell viability.
d. To properly seed ducts, a mixture 20%: 80% of cells with medium: Matrigel was prepared. Wash medium in the tube containing the pellet was aspirated and only the amount required for seeding was left in the tube (eg to seed 6 wells in a 24MW plates 60 µL of wash media were maintained in the falcon). Matrigel was then added (for 6 wells, 240 µL of Matrigel were required), mixed to obtain a homogeneous solution and seeded in 24MW plates.

e. We incubated at 37ºC for 20 min, on the top of a pre-warmed flask, and when Matrigel was solid, 500 µL of complete culture medium were added.

6. Remaining tissue incubated with digestion medium was checked every 30 minutes - 1 hour and when cells were liberated in the solution, it was processed as P1 to obtain Pellets P2, P3, P4 …).
7. The digestion process was ideally stopped when no more tissue was seen by naked eye or when sufficient cells were obtained. Tumors highly resistant to dissociation were submitted to an extra round of digestion with Tryple trypsin (not requiring inactivation with FBS). Tissue was incubated with 3-4 mL of Tryple for a maximum of 15 min at 37ºC, diluted with wash media to stop the Tryple and centrifuged at 300g for 5 minutes.
8. Pellet was processed and seed as described in d.

3.5.2. Organoids follow up after seeding

Two days after seeding, the organoids started budding. They were maintained in culture by changing medium every 3 days. When they reached confluence (70-80%), generally after 7-10 days, they were passaged. Before the first passage cultures, medium was supplemented with a Rho Kinase inhibitor (to avoid single cell death for anoikis, due to the lack of adherence to an external matrix). All the organoids generated from tumor tissues survived for more than 20 passages. Healthy tissue derived organoids could be maintained up to 10 passages.

3.5.3. Organoids culture routine

Organoids were split once a week at a 1:4 or higher dilutions, depending on the confluence, and seeded in 24MW plates with matrigel (see 3.5.2). The passage Medium was DMEM F12 (Gibco), supplemented with 100U/mL penicillin, 100 µg/mL streptomycin, 2mM L-glutamine and 1 mM HEPES. After seeding, fresh growth medium was added, and replaced 4 days later.

3.5.3.1 List of organoids used in the study

IDIT1: PDAC organoids directly derived from patient's fresh tissue. Kindly provided by Dr. Hans Clevers (Hubrecht Institute, the Netherlands).

IDIT2: PDAC organoids directly derived from patient's fresh tissue sample. Kindly provided by Dr. Hans Clevers (Hubrecht Institute, the Netherlands).

IDIT3: PDAC organoids directly derived from patient's fresh tissue sample. Kindly provided by Dr. Hans Clevers (Hubrecht Institute, the Netherlands).

IDIT4: pancreatic tumor organoids derived from CP-15 pancreatic adenocarcinoma tumor. A biopsy from the original tumor was propagated in nude mice; afterwards organoids were generated from these orthotopic xenografts.

IDIT5: PDAC organoids derived from patient's fresh tissue after surgical operation in Hospital Clinic, Barcelona.

IDIT6: PDAC organoids derived from patient's fresh tissue after surgical operation in Hospital Clinic, Barcelona.

IDIT7: PDAC organoids derived from patient's fresh tissue after surgical operation in Hospital Clinic, Barcelona.

IDIS0: healthy pancreas derived organoids, generated from digested pancreatic tissue. The tissue was kindly provided by Dr. Meritxell Rovira (CMRB Barcelona).

IDIS6: healthy pancreas organoids derived from patient's fresh tissue after surgical operation in Hospital Clinic, Barcelona (healthy portion of pancreas from IDIT6 patient).

IDIS7: healthy pancreas organoids derived from patient's fresh tissue after surgical operation in Hospital Clinic, Barcelona (healthy portion of pancreas from IDIT7 patient).

3.5.3.2. Preparation of organoids growth medium

3.5.3.2.1. Organoids growth medium formulation

Organoids need a medium enriched in many growth factors, to recapitulate gastro-intestinal niche and its stimuli. The components required to obtain 50 mL of medium are listed in table 3.7. This medium was prepared in the amount of 50 or 100 mL and stored at -20 ºC for less than one month.

3.5.3.2.2. Conditioned media production

Wnt3a, Rspondin-1 and Noggin conditioned media were obtained from stably transfected cell lines expressing the different genes codifying for each of the recombinant proteins. The three cell lines were kindly provided by Hans Clevers' laboratory, Utrecht, the Netherlands.

- ***L-Wnt-3a***: murine cell lines engineered to produce *Wnt-3a* at high concentration (Willert K et al, Nature 2003). Zeocin at 125 µg/mL was used for selection after thawing.
- **HA-*R-Spondin1*-Fc 293T**: HEK-293 stably transfected to express murine *R-Spondin* protein. Zeocin at 300 µg/mL was used for selection after thawing.
- **m-*Noggin*-Fc 293T**: HEK-293 stably transfected to express murine *Noggin*. Geneticin G418 at 500 µg/ml was used for selection after thawing.

3.5.2.2.3 TOP/FOP Assay for WNT and Rspo activity

This assay is based on exploiting molecular mechanisms of *Wnt* signaling, characterized by an ON/OFF state. Briefly, in the ON state of the pathway, a ligand member of *Wnt* family (in this case *Wnt-3a*), binds to its receptor named frizzled (FZD) and to its coupled lipoprotein receptor-related protein 5 or 6 (LRP5/6). This trimeric complex intracellularly recruits Dishevelled (DSH) and Axin, inhibiting β-catenin degradation. Thus, β-catenin migrates to nucleus where it recognized TCF / LEF transcription factors for the activation of the *Wnt*-related genes. When the system is OFF, meaning no *Wnt* signaling is transduced, β-catenin is constitutively phosphorylated by the kinases GSK and CKIa with the help of the scaffold proteins Adenomatous Polyposis Coli (APC) and Axin. This amino-terminal phosphorylation of the protein leads to proteasomal degradation, and transcriptional activity in the nucleus is not observed [24,200].

On the bases, the TOP/FOP assay consists on the transfection of 2 different plasmids, containing TCF motifs [201] :

- **TOP Flash Plasmid**: this plasmid contains a minimal HSV thymidine kinase (TK) promoter, whose activity is helped by the presence of 3 binding sites for TCF. Together, they control the transcription of the *firefly luciferase* (reporter gene). When *Wnt-3a* molecule is enriched in the conditioned medium, it binds to TCF binding sites permitting luciferase transcription and translation (inducible expression).
- **FOP Flash Plasmid**: it is the same construct as FOP flash, but the TCF binding sites are mutated. In this way, the signal obtained when transfecting this plasmid is the same in presence or not of *Wnt-3a* molecules. It works as an internal control for the experiment.
- **pRL-TK vector**: this vector contains the *Renilla luciferase* under the control as HSV-TK promoter. It provides low to medium levels of *Renilla* in co-transfected mammalian cells (constitutively expressed). It will be the control of transfection of the assay (information available on Promega.com).

With this assay both *L-Wnt-3a* and *Rspo* conditioned medium activity could be tested. Indeed, *Rspo* can augment the induction of transcription of *firefly luciferase* acting on the promoter containing TCF binding sites.

Procedure:

- **Day 1**: 30.000 cells/well were seeded in triplicate in a 24 MW plate.
- **Day 2**: the combination of plasmids TOP Flash/*Renilla* or FOP Flash/*Renilla* were transfected by CalPhos mammalian transfection kit (Takara).
- **Day 3**: normal DMEM 10% was replaced with conditioned media or control media to both TOP and FOP conditions and incubated for 24 hours (See Table 3.8 for further details on media preparation).

Transfection Mix	**1 X**
Flash / FOP-Flash plasmid (400 ng/µL)	0.25 µL
p-RL TK (100ng/µL)	0.1 µL
$CaCl_2$	3.1 µL
H2O	21.55 µL
Total / well	25 µL

- **Day 4**: medium was replaced with 100 µL of passive lysis buffer from dual luciferase reporter assay kit (Promega), diluted 1:5 in water. The plate was frozen for 1 h at -80ºC, and then the *luciferase* signal was detected with the help of the kit.
- **Reading the assay**: 10 µL of the lysate were transferred to the 96MW white plate together with 30µL of Luciferase Activation Reagent (LARII) and the reaction was analyzed in a luminometer (Synergy - Biotek). After the first read,

luciferase was stopped and *renilla* activated by the addition of the buffer STOP and GLO.

For each well, we calculated the ratio *luciferase/renilla* *1000, called relative luminescence unit (RLU). It is a direct measurement of the luminescence recorded during the assay. The RLU ratio of TOP/FOP transfected conditions needed to be higher that 30-fold to be used for the production for organoids growth (see fig 3.4).

	Media Composition	RLUs			Mean	TOP/FOP Ratio
TOP Assay	50% WNT 50% DMEM	39.832	44.862	48.871	44.522	46.83
	50% WNT 10% Rspo 40% DMEM	193.225	198.81	178.77	190.268	270.06
	Control Medium (DMEM)	2.263	2.095	2.2514	2.291	3.59
FOP Assay	50% WNT 50% DMEM	1.169	0.907	0.777	0.951	
	50% WNT 10% Rspo 40% DMEM	0.833	0.676	0.605	0.705	
	Control Medium (DMEM)	0.566	0.481	0.866	0.638	

Figure 3.19. Example of the output of a TOP/FOP assay for the evaluation of WNT and Rspo conditioned media activity.

3.6. Drug treatments

Drugs used in this study alone or in combination with the adenovirus are listed below:

- **Gemcitabine** (Gemzar, Lilly CO) this chemotherapeutic agent was used in combination with AdNuPARmE1A at 2.5

ng/mL. We prepared a stock at 10µg/mL by diluting purchased gemcitabine in saline solution. Stock was maintained up to 2 months at room temperature. Work solution was prepared fresh every day in DMEM 10%.

- **Nab-Paclitaxel** (Abraxane – Cell gene): used in combination with AdNuPARmE1A at 100 nM. This drug was purchased as powder stable at RT and prepared fresh at every use, due to its fast degradation once resuspended. A 10mM stock in saline solution was prepared on the day of the experiment. Then, working concentration was prepared in DMEM 10%.
- **THZ1**: CDK7 inhibitor, purchased as a powder from MedChem Express. It was reconstituted in DMSO to obtain a 1 mM stock. For every experiment, serial dilutions were prepared starting from this stock, diluting in fresh DMEM 10%.

3.6.1 Evaluation of Synergism

Eventual existing synergisms between the treatments analyzed were calculated with the following formula:

$$\mathbf{CI = (C_{A,X}/IC_{X,A}) + (C_{B,X}/IC_{X,B})}$$

$C_{A,X}$ and $C_{B,X}$ are the concentration of one of the treatment required to induce 50% of mortality in combination. $IC_{X,A}$ and $IC_{X,B}$ are the combination for a single agent to achieve the same effects when administered alone [202]. If the value of the Combination Index

calculated for the two treatments was lower than 0.8, the combination treatment was considered synergistic.

3.7. Adenovirus manipulation

3.7.1 List of adenoviruses in this study

In this study, both replication-deficient (lacking E1A) and replication-competent adenoviruses have been used. All the adenoviruses backbone described were previously generated in the laboratory, except for AdNuPAR-E-miR222-S and AdNuPAR-E-Scramble that have been generated during this thesis.

- **AdGFP-LUC**: reporter adenoviruses, lacking functional replicative genome. It includes an enhanced GFP (eGFP) gene under a cytomegalovirus (CMV) promoter in sense strand, and a CMV-leaded *firefly luciferase* gene in antisense. This virus was kindly provided by Dr Alemany's laboratory [203].
- **Ad5wt**: normal adenovirus serotype 5 with no modifications.
- **Adwt-E**: replication competent Ad5wt, modified by the insertion of an eGFP gene after the fiber unit (L5) as an extra splicing acceptor for mayor late promoter (MLP). M. Rovira previously generated this virus in the lab.
- **ICOVIR15**: Oncolytic adenovirus kindly provided by Dr Alemany's lab [173] . In this adenovirus, E1A transcription is under a double system control: an E1A modified promoter with 8 E2F binding sequences and a SP1 binding sequence

plus a 24bp deletion in the E1A gene to redirect E1A transcription towards Rb/p16 altered pathway. Moreover, it bears an RGD motif inserted in the fiber gene [204].

- **ICOVIR15-E**: ICOVIR15 backbone, with an eGFP gene introduced in late after the fiber unit (L5) as an extra splicing acceptor of MLP. Previously generated in the lab by M. Rovira.
- **ICOVIR15-E-miR29c**: ICOVIR15 backbone modified by the insertion of a sequence codifying for the pre-miR-29c, including both 5p and 3p of the mature miRNA. The fragment, including the premiR sequence leaded by a cytomegalovirus (CMV) promoter, was inserted in a region between E4 and right ITR, in which viral genes would not be affected.
- **AdNuPARmE1A**:Oncolytic adenovirus previously generated in the lab by Ana Mato [172] . In this adenovirus, E1A transcription is kept under control of a promoter consisting of the fusion of an uPAR minimal promoter with Notch Responding sequences (SPS elements). Both pathways are over activated in PDAC cells, comparing to normal cells. In this way, E1A will be expressed only the cells having highly active Notch signaling and high uPAR transcriptional activity.
- **AdNuPARmE1A-E**: AdNuPARmE1A parental backbone endowed with an eGFP gene inserted in late, as another splice site of MLP. Previously generated in the lab by Carlos Lopez.

- **AdNuPAR-E-Scramble**: AdNuPARmE1A backbone, modified with a CMV driven eGFP containing in the 3'UTR 4 target sites for a scramble sequence of a mixture of putative miRNAs. This construct has been inserted between E4 and right ITR of the virus.
- **AdNuPAR-E-miR222S**: AdNuPARmE1A backbone, modified with a CMV driven eGFP containing in the 3'UTR 4 target sites for hsa-miR-221/222.

3.7.2 Generation of AdNuPAR-E-miR-222-S / Scramble genomes

3.7.2.1 pAdZ system

These viruses were generated with the pAdZ system, developed in 2008 by Richard J. Stanton [205], and further modified by R. Alemany [206]. They provided a rapid, high-throughput method for genetic engineering of adenoviral genomes, only requiring a one-step recombination.

This is possible thanks to a particular *E.Coli* strain, SW102, which contains a bacterial artificial chromosome (BAC) with the adenoviral genome in which the RpsL-Neo cassette is inserted. This BAC contains basic resistance to the antibiotic chloramphenicol.

Briefly, the system is based on two principles:

1) SW102 strain is endowed with phage λ recombination genes. These are silent at 32ºC but are activated by shifting

the bacteria at 42ºC for 15 min. These genes permit recombination between sequences having 40bp of identity.

2) Presence of RpsL-Neo Cassette: by homologous recombination, the RpsL-Neo cassette can be inserted in the adenoviral genome amplifying, its sequence with 40bp of homology arms for the adenoviral region of interest. The RpsL-Neo cassette confers sensitivity to streptomycin and resistance to kanamycin, and upon its insertion, the bacteria will grow in kanamycin + chloramphenicol. Once this fragment is inserted in the adenoviral genome, this can be further replaced by a gene or sequence of interest, by a second homologous recombination. When RpsL-Neo is replaced, SW102s will grow in streptomycin and chloramphenicol.

3.7.2.2. Generation of fragments containing CMV-eGFP-miR-Scramble/ miR-222-S and homologous recombination in pAdNuPARmE1A-RpslNeo E4

CMV-eGFP-miR-Scramble and CMV-eGFP-miR-222-S were amplified with primers hybridizing at the 5' and 3' of the plasmid sequence (primers miRNA cua, listed in table 3.1). Besides recognizing miRVec sequence, those primers were characterized by overhanging sequence homology with the adenoviral genome, in the region between E4 and R-ITR. In this way, PCR amplification of miRVEC-CMV-eGFP-miR-Scramble/miR-222-S with the described primers would generate a 1600bp fragment having 40 bp

extremities homologous the adenoviral genome. Thus, according to pAdZ system, this short homology should permit recombination between the RpsL-Neo cassette contained in the adenoviral backbone and our fragment. The primers were designed to clone the fragment in an antisense direction in the adenoviral genome pAdNuPARmE1A-RpslNeo E4.

Following recombination, colonies growing on LB + Agar + Chloramphenicol (12.5 µg/mL) + streptomycin (5mg/mL) were picked and cultured in liquid medium containing the indicated antibiotics. Colonies were further tested by PCR and restriction analysis and finally confirmed by Sanger sequencing.

3.7.3. Amplification of adenovirus in eukaryotic cell lines

3 µg of pAdZ plasmids pAdNuPARmE1A-E-Scramble and pAdNuPAR-E-miR222-S were transfected with SuperFect reagent (QUIAGEN) to a p60 plate of HEK293 ICO cells. pAdZ plasmids codify for *Sce-I* endonuclease, which permits genome linearization inside the cells.

Five to 10 days after transfection the cytopathic effect was observed and cells and media were collected and homogenized by 3 x freeze/thaw cycles to release viral particles. Solution was centrifuged at 600g -10 min to eliminate cellular debris. This supernatant containing virus was called P1 homogenate.

1/10 of P1 was added to a p100 plate of A549, growing in DMEM 10%. Again, when cytopathic effect was observed, both cells and medium were collected and submitted to freeze/thaw cycles to

generate P2. With 1/10 of P2 2 p150 plates of A549 cells were infected, and collected when evident cytopathic effect was observed, about 3-4 days later and generate P3. Before performing the final infection (P4), a preliminary trial was performed on 3 p150 a549 plates to determine the optimal dose of infection, with 250, 500, 750 µL of P3. Then, 500 µL of P3 (established dose after trials) was used to infect the final production of 15 p150 A549 plates for the viral stock. This step was performed growing cells in a 2% FBSi supplemented DMEM. When cells appeared cytopathic, they were harvested for final purification. Cells were centrifuged 300 g for 5 min and their pellet was submitted to freeze/thaw cycles before purification. P4 Freeze/thaw cycles were operated by the resuspension of the pellet in a 5 mL volume of PBS ++ (PBS containing $CaCl_2$ 0.68mM and $MgCl_2$ 5mM).

3.7.4 Purification of Adenoviruses

Adenoviral particles are purified by Cesium Chloride (CsCl) gradient centrifugation.

Day 1. A gradient containing 1.5, 1.35, 1.25 g/mL of CsCl solutions was prepared (from bottom, to the top), and the viral homogenate was added on the top of the tube. A first ultracentrifugation was performed at 35000 rpm for 2 h in a swinging SW40Ti rotor.

After the centrifuge, two bands of adenoviral particles could be observed between 1.35 and 1.25 CsCl layers. The upper band corresponded to empty viral capsids and thus removed. The lower

band was collected and submitted to a second ultracentrifugation for 24 h at 35000 rpm in a continuous gradient of CsCl 1.35 g/mL.

Day2. Two bluish bands were observed in the continuous gradient, the upper band was discarded and the lower band, containing the full viral particles collected.

To eliminate CsCl, PD-10 desalting columns (GE Healthcare) were used. Viruses were eluted from columns with PBS++ (PBS containing $CaCl_2$ 0.68mM and $MgCl_2$ 5mM) and kept in PBS ++ with 10% glycerol for storage at -80ºC in 2, 50 and 100 µL aliquots.

3.7.5 Titration of adenovirus

In this thesis three different titration methodologies have been used. Adenoviruses introduced in the section 4.1 have been titrated by plaque forming units (pfu/mL), whereas in section 4.2 and 4.3 by infective forming units (IFU). When Adwt was used alone (section 4.2) it was administered as vp/mL.

3.7.5.1 Physical quantification of viral particle by spectrophotometry

Viral DNA was quantified by measuring its absorbance at 260nm wavelength.

Different adenoviral dilution (1/5, 1/10, 1/20) were prepared from viral stock in lysis buffer (Tris-HCl pH7.4 10mM, EDTA 1mM, SDS 0.1%) and incubated 10 min at 56ºC. DNA was quantified at Nanodrop 100 (ThermoScientific) and the viral titer was extrapolated from the following formula:

vp/mL = DO_{260} ·dilution factor · 1.1 ·10^{12}

3.7.5.2 Titration by plaque-forming unit (pfu/mL)

Viral titration by plaque forming units considers the functional ability of the virus to infect the cells. It determines the number of infective particles (plaque-forming units) by detecting the late adenoviral protein expressed inside the cells with an immunostaining for the viral hexon, 18-20 hours following infection.

HEK293 ICO cells were infected with a series of adenoviral dilutions in a final volume of 200µL and incubated for a period of 18-20 h. The day after, cells infected by the virus were stained with an anti-hexon antibody (coming from a cellular hybridoma). Visualization was realized by recognition with a fluorescently marked secondary anti-mouse antibody.
Positive cells were directly counted under a fluorescence microscope (IX51 – Olympus) or photographed for posterior manual counting (ImageJ). The viral titer was determined with the following formula:
Pfu/mL= # stained cells ·dilution factor ·0.1 mL

3.7.5.3 Titration by viral infectious units (IFU)

This titration quantifies the viral genomes inside the cells 4 hours after infection.

A549 cells were used for this titration: 50000 cells/well were plated in 24MW plates in a final volume of 500µL. Next day, 1/100 and

1/1000 of the viral dilutions were prepared and used to infect the cells with 10µL of the dilution, in triplicate. Four hours later, cells were washed three times with PBS and collected upon trypsinization. Viral and cellular DNAs were extracted with a commercial kit, and the number of viral genomes/cells determined via qPCR using specific primers for hexon and albumin (Adhexo, Albumin, see table 3.1). The number of viral genomes was obtained by interpolation with a standard curve.

3.8 Functional Assay

3.8.1 MTT assay

MTT (3-(4,5-dimethylthiazol-2-yl)-2,5-diphenyltetrazolium bromide) is a colorimetric assay based on the conversion of thiazolyl blue tetrazolium bromide into insoluble blue formazan by metabolic active cells. The formazan deposits can be dissolved in DMSO and quantified at 560nm with a spectrophotometer as an indirect measurement of cell viability.

Cells were incubated with a battery of adenoviral doses for 3, 5 or 7 days. At the end of the treatment, culture medium was replaced by MTT solution at a concentration of 7.5mg/mL, dissolved in DMEM 10% medium. Cells or organoids were incubated for 30 minutes or 2 h, respectively. Medium containing MTT was replaced with DMSO, to dissolve precipitated crystals. In the case of organoids, an intermediated step was performed between MTT and DMSO with 2% SDS (in ddH_2O). 30 µL of SDS were added to each well and incubated for 1 hour at moderate shaking. Then, 100 µL of

DMSO was added. Absorbance was measured at a wavelength of 560 nm in a spectrophotometer (Synergy HT – BioTek), as a direct indication for cell viability.

Results are expressed as percentage of cell viability compared to an uninfected or untreated control (MOCK -100% viability). Using GraphPad Prism software, the values were transformed to logarithmic and then fitted to a sigmoid curve via a nonlinear regression (% viability vs viral dose or drug concentration). The ID_{50} values, representing the amount of virus or drug required to inhibit 50% of cell growth, were extrapolated from dose-response curves and plotted independently.

3.8.2 Colony formation assay

Adenoviral infection was performed as explained in 6.4.3.1, at the indicated doses (ranging from 10^2 to 10^4 pfu/well). Five days later, the infected organoids were collected, mechanically disaggregated and seeded in a new 96MW plate split with a 1:2 ratio. Twenty-four hours later, only the organoids not infected with virus, or with a low viral progeny inside, were able to reassemble and form a new round shaped organoid. The number of organoids with a round shape and with a diameter larger than 20 µM were counted and plotted.

3.8.3 Methylene Blue staining

Cells were incubated with methylene Blue dye (Sigma Aldrich) for 1 min. Then, the excess of dye was removed by washes with H_2O and plates were dried at RT for 1 hour. Stained cells correspond to the number of cells alive previous to the treatment.

3.8.4 Viral Yield assay

50000 cells/well for PANC-1 and 100000 cells/well for MIAPaCa-2 and CP15-Luc were seeded in 24 MW plate. The day after, cells were infected with the different adenoviral doses in 500 µL of medium. Four hours later, wells were washed three times with sterile PBS to remove adenoviral particles that did not enter the cells. At this point some cells were collected to assess for viral entry. Seventy-two hours after infection, supernatant or total cell extracts were harvested, centrifuged at 400g 5 minutes to remove cell debris, and used for genomic DNA extraction with commercial kits. In the case of total cell extracts 3 freeze and thaw cycles were performed before centrifugation.

For organoids, two confluent wells of organoids were infected with 50.000 pfu/well. Five days later, organoids were harvested, centrifuged and cellular pellet suspended in 300 µL of Advanced DMEM F12 medium. The cell suspension was submitted to three freeze and thaw cycles to release viral particles contained inside the cells. Lysates were centrifuge at 600g for 5 minutes and medium containing viral particles was harvested. Two hundred µL of the lysate were used for genomic DNA extraction.

Viral DNA was quantified by specific primers recognizing adenoviral hexon (Adhexo) and cellular albumin. The amount of viral DNA/cell was extrapolated by interpolation in a standard curve of known concentrations.

3.8.5 eGFP detection

eGFP expression was determined via 3 alternative methods:

- mRNA quantification via qRT-PCR (specific primers detailed in table 3.1)
- Flow cytometry: eGFP intensity was detected in cells with the help of a flow cytometer, Attune ™ Acoustic Focusing Cytometer (Applied Bioscience). Cells were harvested by trypsinization and analyzed, using mean fluorescence intensity (MFI) as parameter.
- Microscope imaging: eGFP expression was visualized in a fluorescent microscope emitting at wavelength of 480nm. At the indicated times, cells or organoids were analyzed in Olympus IX51 for fluorescence emission.

3.9 Animal Manipulation

All the animal's procedure met European`s guidelines 86/609/EEC and were revised and approved by the ethical committee of the University of Barcelona.

Animals were housed in plastic cages in controlled environmental condition of temperature (22 ± 2º), humidity (60%) and light, with water and food ad libitum.

The animals used in the study were immunosuppressed Athymic Nude *Fox1 nu/nu* mice, purchased from ENVIGO at the age of 6 weeks (ranging from 20 to 30 gr).

3.9.1 Subcutaneous tumor model

Subcutaneous tumors were generated either from human cell lines or organoids in Athymic Nude *Fox1 nu/nu* immunosuppressed mice to escape rejection of the human inoculated cells.

For PANC-1, $2 \cdot 10^6$ cells/tumor were injected in each mouse flank with the help of a 29G needle. Before implantation, cells were washed twice with PBS to remove FBSi, and then the desired number of cells was re-suspended in an appropriate volume of DMEM (not supplemented), mixed 1:1 with Matrigel (Corning®). One hundred µL of this solution was injected into each flank.

For the generation of subcutaneous tumor from IDIT1 organoids, $5 \cdot 10^5$ cells/flank were inoculated.

Following injection, tumors were measured twice a week with a digital caliper. The volume was calculated by measuring the length (D) and width (d) of the tumor, and applying the following formula:

Tumor Volume = $(D \cdot d^2 \cdot \pi) / 6$

Once the tumor reached 100 mm^3, adenoviral treatment or saline solution as a control were administered to the assigned group of animals. Animals were euthanized at the end of the experiment and tumors were isolated and stored at -80º, for molecular analysis of DNA/RNA/protein, or transferred to a 4% PFA solution, for histological studies.

3.9.2 Orthotopic tumor model

An orthotopic tumor model consists in the implantation of cells in the tissue of tumor origin. This model takes advantage of the organ microenvironment, and more faithfully recapitulates tumor histology and architecture and at long-term generates metastases.

In this study we generated orthotopic tumor models by implanting $5 \cdot 10^5$ cells from disaggregated organoids, in a mixture 1:1 of PBS: Matrigel.

Briefly, 30 minutes before the operation animals received the analgesic meloxicam Metacam ® (Boheringer Ingheleim). Then, nude mice were anesthetized with a mixture of isofluorane and oxygen and placed on their right side. This was cleaned with ethanol and a laparotomy at the level of the spleen was performed. Spleen and pancreas were gently externalized, and 100µL of mixture containing organoids was slowly injected in the head of the pancreas. The formation of a small bubble within the pancreatic parenchyma assured the correct implantation of the cells. Organs were re-introduced inside the abdominal cavity two min later to allow for Matrigel solidification. Muscle layer was closed with interrupted 4-0 silk sutures and the overlying skin with Autoclips® (Stoelting Europe). Iodine solution was applied to the region of surgery, and animals were maintained under a heating source. Metacam was administered for the next 2 days and autoclips were removed 7 days after surgery.

Tumor volumes was followed by palpation and once reached values that limited ethical statements animals were euthanized (2-3 months after organoids implantation). Following sacrifice by cervical

dislocation, animals were inspected for the presence of metastasis. If present, they were collected together with the orthotopic tumor, and stored in advanced DMEM F12, for organoids generation, or transferred to a 4% PFA solution, for histological analysis.

3.9.3 Administration Route

- Intraperitoneal administration: this route was used for administration of the analgesic Metacam with a 29G needle. The drug was administered at a concentration of 1/2mg/kg, diluted in saline solution to reach final volume of 100µL.
- Intravenous administration: this route was used for systemic administration of adenoviruses via tail vein injection. To ease the process, animals were immobilized with the help of a restrainer and heat light was applied to the tail, to favor vasodilation. Adenoviruses were injected at a dose of $5 \cdot 10^{10}$ vp/animal using a 29G needle.

3.10 Histological Analysis

Tissues stored in 4% PFA (paraformaldehyde) were processed to paraffin block and further cut to 5 µM sections in the histology unit of IDIBAPS (Institut d'Investigacions Biomèdiques August Pi i Sunyer).

Hematoxylin/eosin (H&E) staining of paraffin-embedded sections was used to evaluate tissue structure and was performed by the Histology Unit of IDIBAPS.

3.10.1 Organoids inclusion

Organoids were dissociated from matrigel by incubation with 1mL dispase (1mg/mL). Organoids were collected with PBS and settled in an 8mL flat bottom tube. When sedimented, organoids were fixed with 4% PFA for 30 min at RT. PFA was removed via decantation and washed twice with PBS. Then, organoids were dehydrated applying EtOH diluted in ddH_2O (25-50-70%). In the last wash of 70% EtOH organoids were stored at 4 ºC and sent to the IDIBAPS histology unit or to Dr. Clevers' laboratory for inclusion and slides preparation.

3.10.2 Immunohistochemistry (IHC)

Paraffin-embedded section were deparaffinized and rehydrated with pure Xylen followed by solution with EtOh/H_2O with increased concentration of H_2O (4% - 30% - 50% - 100%). Then, samples were incubated in sodium citrate buffer (pH 6.0, 10mM) at 95ºC for 5 min under pressure. Sections were blocked with PBS-Triton 0.3% + 10% FBS + 1% BSA for 90 min to avoid unspecific bindings. Then, sections were washed 3 times with PBS, and incubated O/N with primary antibodies anti-Cytokeratin 19 or anti-E1A (AntiCK-19, Abcam 52625, dilution 1:500 in PBS-0.1% BSA; AntiE1A, Santacruz Biotechnology sc-25, dilution 1:200 in PBS-0.1% BSA). The day after, endogenous peroxidases were blocked with Dual Endogenous Enzyme Block (Dako) for 10 min. After 3 X PBS washes, the reaction was developed with Dako EnVision + Dual Link System-HRP (DAB+) (Dako). Sections were counterstained

with Harris hematoxylin (Panreac) and samples visualized at NIKON e600 inverted microscope.

3.11 Bioinformatics analysis

For the study of miRNA-related characteristics and target genes the following bioinformatical resources were used:

- **miRBase**: searchable database of miRNAs annotation and sequences (Release 22.1).
- **miRWalk**: bioinformatics program integrating data from different database predicting targets for miRNAs. Data matching at least 4 of the considered databases were included as targets (miRWalk, miRanda, miRDB, Pictar2, PITA, RNA22 and TargetScan).
- **PANTHER-GO**: bioinformatics tool clustering targets related to a miRNA of interested. It helped with the identification of the pathways having more miR-222 targeted-genes, performing a gene ontology (GO) analysis. The predicted pathways having the lowest p-value were considered for further analysis (p value from to 10^{-16} to 10^{-5}).

Other softwares applied for sgRNA design or miRNA sponge design have been listed in the appropriate sections (3.2.1.1 and 3.2.2.1).

Bioinformatics tools not related to miRNA analysis were:

- **Nucleotide BLAST**: tool for alignment of two or more sequences. It was used to analyze results from DNA sequencing.
- **Unipro uGENE**: program that permits visualization of FASTA sequences. Useful for plasmids and adenoviral genome design.

3.12 Data representation and Statistical Analysis

All data obtained in this study are represented as mean ± Standard Error of the Mean (SEM). A minimum of 3 replicates and a maximum of 6 for experiment were considered. Data are represented via GraphPad Prism v5.0.

Data obtained are treated as non-normal population and differences were analyzed with a Mann-Whitney non-parametric test or with a Kruskal-Wallis non-parametric test with the help of Graph Pad. Differences were considered significative when p-value < 0.05. P values were marked with the presence of *: *p<0.05, **p<0.01, ***p<0.005.

For in vivo analysis, tumor growth along days was evaluated with mixed linear model in R v2.14.1 using package Ime4 (performed by Estela Nuñez). Differences within mean were evaluated with Tukey's range Test.

DNA Primers	Forward (5'→ 3')	Reverse (5'→ 3')	Th	Application
Kras	GGTGGAGTATTTGATAGTGTA	GGTCCTGCACCAGTAATATGC	55	Sequencing
miR-21	CCACACTCTGTCGTATCTGTG	AAGTGCCACCAGACAGAAGG	58	Sequencing
miR-93	TGAGGGAGACCAGACCCTTT	TTCTGCTTCCCCATGAACCT	58	Sequencing
miR-221	GTCCCAGCATTTCTGACTGTTGG	GGCTTGTGGGTGCTATGCCTTC	58	Sequencing
miR-222	GCTGGATCTCCAGCACCTAAG	CCCAAGCCCCAGCTGATAATG	58	Sequencing
miR-761	GATATTTGGGTGGGCTGTCCAGTC	CATCTCCTGATCCGTTGGCC	57	Sequencing
miR-3714	CCTTTAAGGTTGATTCCAGCACCAC	CTGGGAAGGGAAACTGAGTGGG	58	Sequencing
miR-4713	GGCTTTAAGGGTGGAAGGGTGG	CCCTTCCACTCTGTGCTGTGC	58	Sequencing
LentiCrispr_Val	GAGGGCCTATTTCCCATGATT	GGAGTGGGAATTGGCTCCGGTGCCC	60	Sequencing
miRVec_Val	CATGGTCCTGCTGGAGTTCG	CTTGCCAAACCTACAGGTGG	57	Sequencing
Step3/4	CCAGAAACGAAAGCCAAAAA	TAATGAGGGGGTGGAGTTTG	50	Sequencing
E4 miRNA cua	gaaaactacaattcccaacacatacaagttactccgcccctaa CTTTTATTTTATCGAATCTGC	cgtggcgcggggcgtgggaacggggcgggtgacgtaggtt ACATTGATTATTGACTAG	50	Cloning

Hexo1/2	GCCGCAGTGGTCTTACATGCACATC	CAGCACGCCGCGGATGTCAAAG	58	qRT-PCR
Albumin	GCTGTCATCTCTTGTGGGCTGT	GGCTATCCAAACTCATGGGAG	58	qRT-PCR

Table 3.1. List of DNA primers for PCR or qRT-PCR used in the study.

ssDNA for sponges	Sponge sequence	Final Primer sequence
Primer Scramble Fw	GTTCTTGCTGCACACGTAGCTGTAAG GTGTAGAACGCCAGCTAACGTAGTG GATCTCATGTACACAACGACGTGAG TTCGATCGCTCCTCAA	**AATTC**TAATGAGTTCTTGCTGCACACGTAGC TGTAAGGTGTAGAACGCCAGCTAACGTAGTG GATCTCATGTACACAACGACGTGAGTTCGAT CGCTCCTCAA**G**
Primer Scramble Rv	TTGAGGAGCGATCGAACTCACGTCG TTGTGTACATGAGATCCACTACGTTA GCTGGCGTTCTACACCTTACAGCTAC GTGTGCAGCAAGAAC	**AATTC**TTGAGGAGCGATCGAACTCACGTCGT TGTGTACATGAGATCCACTACGTTAGCTGGC GTTCTACACCTTACAGCTACGTGTGCAGCAA GAACTCATTA**G**
Primer miR-222-S Fw	ACCCAGTAGGTCATGTAGCTGTACA CCCAGTAGGTCATGTAGCTGCATACC CAGTAGGTCATGTAGCTCGTAACCC AGTAGGTCATGTAGCT	**AATTC**TAATGAACCCAGTAGGTCATGTAGC TGTACACCCAGTAGGTCATGTAGCTGCATAC CCAGTAGGTCATGTAGCTCGTAACCCAGTAG GTCATGTAGCT**G**
Primer miR-222-S Rv	AGCTACATGACCTACTGGGTTACGA GCTACATGACCTACTGGGTATGCAG CTACATGACCTACTGGGTGTACAGCT ACATGACCTACTGGGT	**AATTC**AGCTACATGACCTACTGGGTTACGAG CTACATGACCTACTGGGTATGCAGCTACATG ACCTACTGGGTGTACAGCTACATGACCTACT GGGTTCATTA**G**

Table 3.2. List of primers used for the construction of miRNA sponges. Bold sequences represent EcoRI RS, red sequences represent extra stop codons inserted.

sgRNA Name	Forward (5'→ 3')	Reverse (5'→ 3')
sgmiR-21 #1	caccgTCATGGCAACACCAGTCGAT	aaacATCGACTGGTGTTGCCATGAc
sgmiR-93 # 1	caccgCTCCAAAGTGCTGTTCGTGC	aaacGCACGAACAGCACTTTGGAGc
sgmiR-221 # 3	caccGCAACAGCTACATTGTCTGC	aaacGCAGACAATGTAGCTGTTGC
sgmiR-222 # 1	caccgACGAAAGACAGGATCTACAC	aaacGTGTAGATCCTGTCTTTCGTc
sgmiR-761 # 3	caccgTGGCAAGCGGAGGAGCAGCA	aaacTGCTGCTCCTCCGCTTGCCAc
sgmiR-3714 # 2	caccgCGGTGATGGAGCACGTCACA	aaacTGTGACGTGCTCCATCACCGc
sgmiR-4713-5p # 5	caccgATTCGACCCTTATGGGAGCC	aaacGGCTCCCATAAGGGTCGAATc

Table 3.3 List of sgRNAs used for genome editing in this study.

Target gene	Forward (5'→ 3')	Reverse (5'→ 3')
BPTF	CGAAAAGGAGGAATCCGAGAGG	CGTAACATCAGGCTCACTCCAGC
DDX21	TCATCAAGGACGCACTATCATCT	CCTTTCAGGGTGATTTCCCTTT
eGFP	AAGATCCGCCACAACATCGA	AACTCCAGCAGGACCATGTG
c-MYC	AGTGCATTGACCCCTCAG	CCTGCCACTGTCCAACTTG
HES-1	TGGAAATGACAGTGAAGCAACT	GTTCATGCACTCGCTGAAGC
HPRT	GATATAAGCCAGACTTTGTTGGATTTG	CTTGAACTCTCATCTTAGGCTTTG
KPNA-2	CGTCTTCACAGATTCAAGAACAAGG	CCTCTTCAGCATCTGGTCATCC
KRT-19	CTACAGCCACTACTACACGAC	CAGAGCCTGTTCCGTCTCAAA
NOLC-1	TTCCTGCGCGATAACCAACTC	CCTGTAACTTTCGCTCTGGGA
NOTCH-1	ATCCAGAGGCAAACGGAG	CACATGGCAACATCTAACCC
SOX-9	GCCGAGCTCAGCAAGAC	TACTTGTAATCCGGGTGGTC
TCOF-1	CGATAACCAACTCTCAGAGGTGG	CTAAGAGGGAAGAGGCATTGG
uPAR	GCCTTAACCGAGGTTGTGTGT	CATCCAGGCACTGTTCTTCA

Table 3. 4. List of primers used for gene expression analysis via qRT-PCR.

miRNA	Recognizing sequence	Assay ID
miR-21	UAGCUUAUCAGACUGAUGUUGA	000397
miR-29c	UAGCACCAUUUGAAAUCGGUUA	000587
miR-93	CAAAGUGCUGUUCGUGCAGGUAG	001090
miR-99b	CACCCGUAGAACCGACCUUGCG	000436
miR-221	AGCUACAUCUGGCUACUGGGUCUC	000524
miR-222	AGCUACAUUGUCUGCUGGGUUUC	000525
miR-485	AGAGGCUGGCCGUGAUGAAUUC	001036
RNU6B	CGCAAGGAUGACACGCAAAUU CGUGAAGCGUUCCAUAUUUUU	001903

Table 3.5. TaqMan assays used in the study for miRNA expression analysis by qRT-PCR

Materials	Receipt / Provenience	Used for
Wash Media	DMEM Supplemented with 2% FBS, 1% P/S	Digestion media removal
Digestion Media	Wash media + Collagenase XI (0.125 mg/mL) + Dispase (0.125 mg/mL)	Tissue digestion and ducts liberation
Matrigel	Corning Matrigel - Phenol Red-free, LDEV-free, 10 mL	Organoids seeding Thaw on ice for 1 hours
Tryple Select	Thermofisher Scientific	Final tissue digestion
Growth media	Complete growth medium formulation at 2.3.2.1	Organoids feeding
75 cm^3 flask	Jet Biofill	Matrigel solidification

Table 3.6. Materials to prepare before starting organoids isolation.

Reagent	Concentration	Amount in 50mL	Healthy	Tumoral
Advanced DMEM F12	-	14 mL to reach 50 mL	+	+
L-Wnt3a	2 X	25 mL	+	+
Rspondin-1	10 X	5 mL	+	+
m-Nogging	10 X	5 mL	+	+
B-27	50 X	1 mL	+	+
Nicotinamide (NIC)	100 X	500 µL	+	+
N-acetyl-Cysteine (NAC)	400 X	125 µL	+	+
Primocin	500 X	100 µL	+	+
A-485	1000 X	50 µL	+	+
h-FGF-10	1000 X	50 µL	+	+
h-EGF	1000 X	50 µL	+	+

h-gastrin	1000 X	50 µL	+	+
Prostaglandin-E_2 (PGE_2)	1000 X	50 µL	+	-
Y-27632 - RhoK inhibitor	500 X	100 µL	1 week after isolation	

Table 3.7. Reagents required for preparation of 50mL of complete growth medium for organoids.

L-Wnt-3a testing	Media proportion	X 7 wells (500µL/well)
L-Wnt-3a control medium	100% DMEM 10%	3.5 mL DMEM 10%
L-Wnt-3a conditioned medium	50% L-Wnt-3a + 50% DMEM 10%	1.750 ml L-Wnt-3a + 1.750 ml DMEM 10%
Rspo-1 Testing	**Media proportion**	**X 7 wells (500µL/well)**
Rspo-1 control medium	10% Advanced DMEM F12 + 90% DMEM 10%	350□l Advanced DMEM F12 + 3.150ml DMEM 10%
Rspo-1 conditioned medium	10% DMEM 10% + 90% Rspo-1	350□l Rspo-1 + 3.150ml DMEM 10%
L-Wnt-3a/Rspo-1 conditioned medium	50% L-Wnt-3a + 10% Rspo-1 + 40% DMEM 10%	1.750ml L-Wnt-3a + 350□l Rspo-1 + 1.4ml DMEM 10%

Table 3.8. Preparation of media to be tested in TOP/FOP Assays.

4. Results

4.1 Organoids as a translational model to screen for therapies

PDAC is one of the major clinical problems in the field of oncology. Its survival has not increased in the last 30 years, and the only curative treatment remains surgical removal of the tumor [6,207]. Oncolytic virotherapy has been envisioned as an alternative promising approach for cancer treatment, with many viruses being tested in clinical trials, either alone or in combination with chemotherapies [186,208].

In vitro oncolytic virus screening is mostly performed in cell lines and eventually in mouse xenografts. However, *bidimensional* cultures poorly reproduce the heterogeneity of a tumor, whereas the use of patient-derived xenografts (PDX) is often too time-consuming for guiding in personalized therapies.

The 3D organoids model has recently shown its potential as a personalized medicine application in testing anti-cancer drugs and evaluating tumor diversity [116,209]. In the current project we have evaluated the potential of tumor organoids to help on virotherapy treatment decisions.

4.1.1 Generation of a patients-derived organoids from PDAC and healthy tissues

We obtained healthy and tumor pancreatic tissue, from patients diagnosed with PDAC undergoing surgery at the Hospital Clinic of Barcelona. Following established protocols [199,210], we obtained 5 lines of PDAC-derived organoids from 11 PDAC tumors and 8

from 16 healthy pancreas, when possible adjacent and matching the PDAC tumors.

Tissues were submitted to mechanical and chemical disruption. Following pancreatic ducts release, cells were seeded in matrigel, and supplemented with organoids complete medium. (Fig 4.1.1 A)

Organoids growth was evaluated by their morphologic appearance since day 1. We observed an epithelial cell layer with a round-shaped structure enlarging with days (Fig 4.1.1 B). Established tumor derived organoids could be passaged, maintained in culture and unlimited propagated. Normal pancreas derived organoids ceased to proliferate after a maximum of 10 passages.

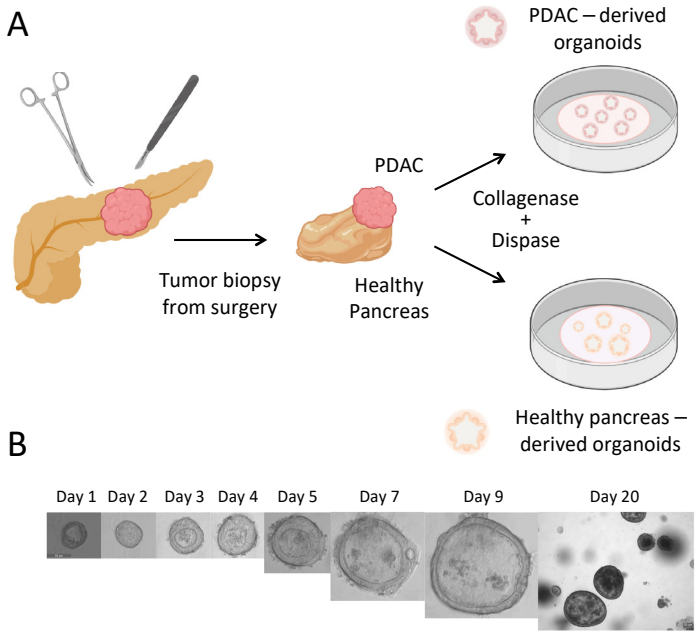

Figure 4.1.1. Schematic representation of organoids generation. ***A****. After surgery, a pathologist examined the tissue and PDAC region was separated from healthy pancreas. If available, both tissues were submitted to a preliminary mechanic disruption with the help of a surgical blade, followed by enzymatic digestion. When pancreatic ducts were observed, cells were seeded in matrigel, further supplemented by medium.* ***B****. IDIT4 organoids follow up from the first day of appearance until the first day of passaging (day 20).*

4.1.2 Characterization of PDAC-derived organoids confirms their malignant origins and ductal phenotype

Once organoids from PDAC tissues were established, the confirmation of their transformed pancreatic origin was assessed by molecular characterization of the mutational status of *KRAS*. This gene is mutated in 90% of PDAC tumors, and protein codon 12 is the hot-spot mutation. Sequence analysis of the region [196] revealed that the seven lines of organoids used in the study (5 lines generated by our group plus 2 kindly provided by Dr. Hans Clevers laboratory) presented a *KRAS* mutation (Table 4.1.1), confirming their tumor origin.

Organoids ID	*KRas* Status	Mutation	AA Change
IDIT1	Mutated	12:25398285(-): G/C	G12R
IDIT2	Mutated	12:25398285(-): G/C	G12R
IDIT3	Mutated	12:25398284(-): G/T	G12V
IDIT4	Mutated	12:25398284(-): G/A	G12D
IDIT5	Mutated	12:25398284(-): G/A	G12D
IDIT6	Mutated	12:25398284(-): G/A	G12D
IDIT7	Mutated	12:25398284(-): G/T	G12V

Table 4.1.1. KRAS Mutational status in PDAC derived organoids.

IDIT5, IDIT6 and IDIT7 were further characterized at histological and immunohistochemical (IHC) level. H&E staining of whole mount organoids were compared to the PDAC tissue of origin, showing strong morphologic similarities such as dysplastic cell organization and nuclear irregularities. CK19 IHC revealed strong immunoreaction of the ductal marker in patient tumors and established organoids (Fig 4.1.2 A, B).

To confirm the ductal origin of organoids, RNA from all PDOs was obtained and analyzed for ductal markers expression. Both normal and PDAC organoids showed enrichment in SOX9 and CK19 ductal markers compared to the tissue of origin (Fig 4.1.2C).

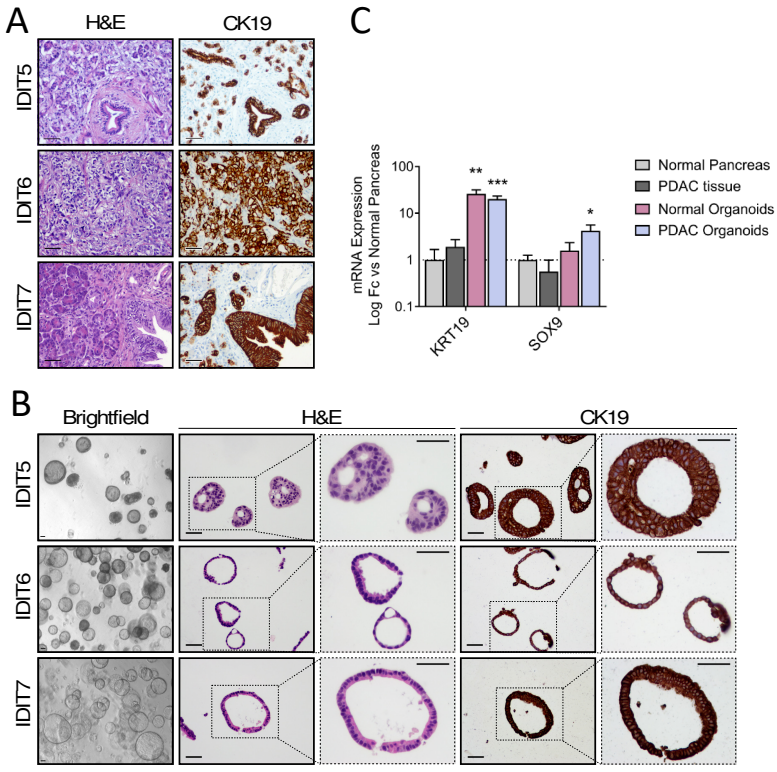

Figure 4.1.2. Human PDAC derived organoids maintain characteristics of tumors of origin and are enriched in ductal markers. ***A****. Representative histological sections of*

human pancreatic tumors. Left panels correspond to H&E staining. Right panels show CK19 immunoreactivity staining (scale bar 50 µm). ***B.*** *PDAC derived organoids from matching tumors: Bright field images (scale bar 50 µm). H&E staining of organoids and CK19 immunoreactivity (scale bar 50 µm).* ***C.*** *qRT-PCR analysis of ductal lineage markers (KRT19 and SOX9) from PDAC organoids (n=7), normal pancreas organoids(n=4) organoids, tumor tissue of origin (n=4) and adjacent normal pancreas (n=6). Data are represented as mean ± SEM; *p<0.5, **p<0.01, ***p<0.05 Mann- Whitney U Test.*

4.1.3 Adenoviruses efficiently infect and replicate in PDOs

We first evaluated whether adenoviruses were able to infect and replicate in organoids. To that end, reporter non-replicative adenovirus AdGFPLuc and replicative-competent Adwt-E expressing the eGFP protein were used (Fig 4.1.3).

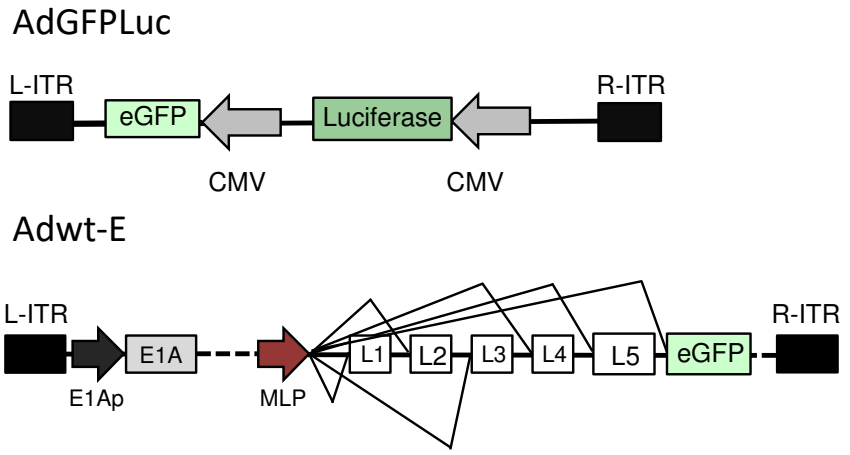

Figure 4.1.3. Schematic representation of reporter adenoviruses used in the following experiments. *AdGFPLuc is a replication-deficient reporter adenovirus. It contains a double reporter genes system composed by an eGFP and a Luciferase, each one encoded by its own CMV promoter. Adwt-E is a replication competent Ad5wt, in which an eGFP has been inserted after L5 with an extra splicing site acceptor for transcription from the MLP promoter.*

IDIT4 organoids were infected with high doses of both viruses and infection was followed up by eGFP detection under a fluorescent

microscope (Fig 4.1.4 A). Outer layers of organoid cultures showed susceptibility to adenoviral infection, as shown by eGFP expression, in line with what has been previously reported [211]. Interestingly, whereas eGFP signal was stable at all the time-points analyzed after AdGFPLuc infection, fluorescence signal observed by the Adwt-E infection dramatically increased after 96h (Fig 4.1.4 A). Presence of eGFP in the inner layers of organoids infected with Adwt-E suggested viral replication and spreading in PDOs. Positive E1A immunostaining confirmed viral replication within the organoid in Adwt-E, whereas no staining was detected in the AdGFPLuc-infected PDOs, in line with the lack of E1A (Fig 4.1.4 B).

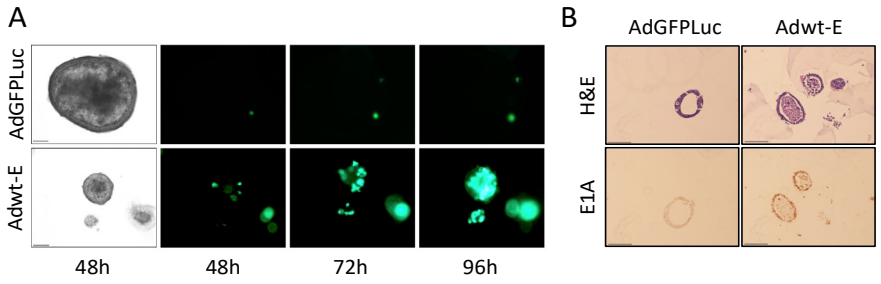

Figure 4.1.4. Adenoviruses are able to infect PDAC derived organoids. ***A****. Representative images of time-course eGFP expression in IDIT4 tumor organoids infected with 5·10^5 pfu/well of AdGFPLuc or Adwt-E (scale bar 100 µm). Images were taken with an inverted fluorescent microscope at the indicated time points. Representative images are shown, n=3.* ***B****. Histological sections of IDIT4 obtained 24 hours PI with AdGFPLuc and Adwt-E. Organoids were fixed in 4% PFA and further processed to obtain paraffin-embedded blocks. Tissue slides were stained with H&E to visualize morphology or were hybridized with anti-E1A antibody for adenoviral detection.*

To better characterize the dynamics of adenoviral replication in organoids, we set up an experiment in which naïve organoids were infected with viral extracts from sequential passages of infected organoids. For this, organoids were infected with AdGFPLuc or

Adwt-E and on day 5, harvested and submitted to freeze and thaw cycles, to release viral particles (Passage1 P1, Fig 4.1.5 A). The lysate was used to infect naïve IDIT4 organoids, generating P2, and 5 days later the same procedure was applied to generate P3. eGFP fluorescence was monitored through all the passages P1, P2 and P3. The cultures infected with the replication competent adenovirus displayed high fluorescence levels in all the passages, witnessing for strong adenoviral replication within the organoids. eGFP fluorescence from AdGFPLuc-infected cultures was only detected in P1, evidencing the lack of viral replication (Fig 4.1.5 B). We further measured the content of viral particles in P1, P2 and P3 lysates. Quantification of the adenoviral genomes revealed that Adwt-E viral DNA was abundant and at similar levels in all the passages, whereas AdGFPLuc genomes were only detected in P1, at values corresponding to the input dose (Fig 4.1.5 C).

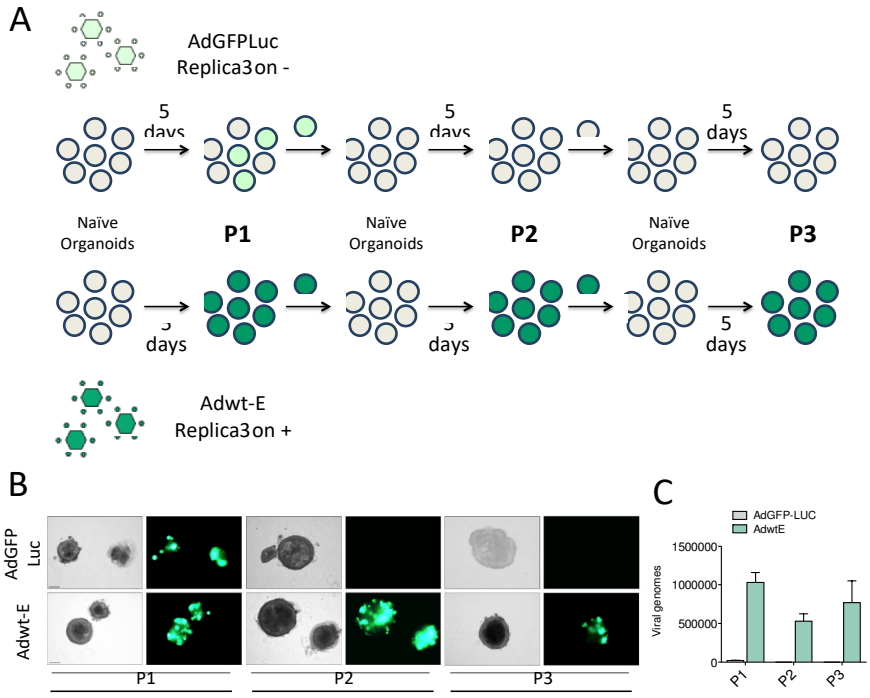

Figure 4.1.5. Adenoviruses are able to replicate in organoids and re-infect adjacent cells. ***A****. Schematic representation of the experiment.* ***B****. Rounds of adenoviral infection in IDIT4 organoids. Naïve organoids were infected with 5·10^5 pfu/well of AdGFPLuc or Adwt-E and 5 days later (P1) were harvested, followed by three cycles of freeze and thaw. Supernatants were used to infect fresh organoids and 5 days later (P2) the same procedure was repeated to generate P3. GFP expression was visualized at P1, P2 and P3 in organoids infected with Adwt-E, but only at P1 in AdGFP-Luc infected organoids (scale bar 100 µm). Representative images are shown, n=3.* ***C****. Quantification of viral genomes content in P1, P2 and P3 organoids passages infected with AdGFPLuc or Adwt-E (n=3). Supernatants obtained in each passage after freeze and thaw cycles (described in B) were quantified via qRT-PCR using specific primers for adenoviral hexon.*

4.1.4 Oncoselective adenoviruses display viral attenuation in organoids from healthy pancreas

To assess oncoselectivity and potency of adenoviral therapies, two different oncolytic viral backbones were used in the following

experiments: the AdNuPARmE1A and ICOVIR15 backbones. AdNuPARmE1A has been previously generated in our laboratory and incorporates SPS sequences responding to NOTCH activation and a uPAR promoter, highly upregulated in PDAC, controlling the E1A gene [172]. ICOVIR15, kindly provided by Dr. Ramon Alemany has an E1A modified promoter with 8 E2F binding sequences and a SP1 binding sequence plus a 24bp deletion in the E1A gene to redirect E1A transcription towards Rb/p16 altered pathway. Moreover, it bears an RGD motif inserted in the fiber gene (Fig 4.1.6) [168].

With the purpose of studying oncoselectivity, an eGFP was inserted in the adenoviral backbones to monitor adenoviral infections. AdNuPARmE1A-E and ICOVIR15-E were tested in PDAC (IDIT1) and healthy pancreas (IDIS0) derived organoids. Adwt-E was used as a non-selective control virus (Fig 4.1.6).

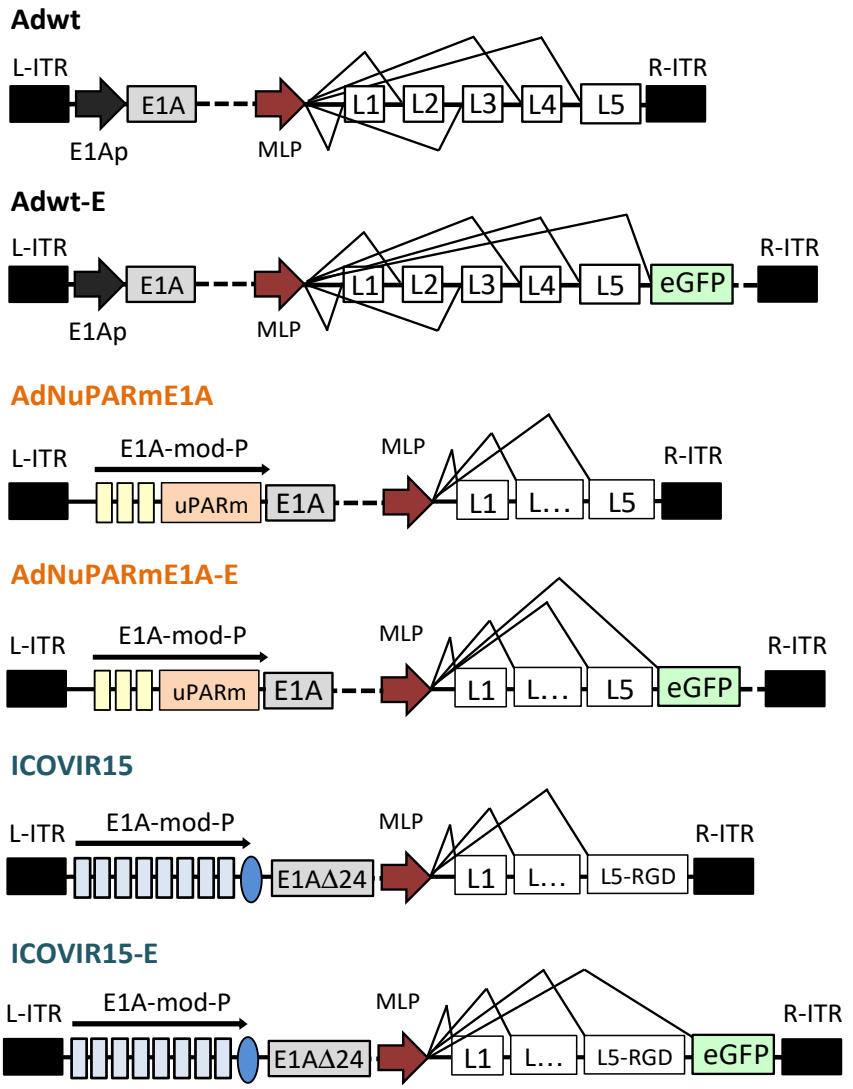

Figure 4.1.6. Backbones of the oncolytic adenoviruses used in the following experiments. *Adwt-E has already been introduced in 4.1.3; Adwt has the same backbone without eGFP. AdNuPARmE1A controls E1A replication by the uPAR gene promoter and 3 Notch responsive sequences, named SPS. ICOVIR15-E presents an E1A promoter with additional E2F binding sites plus an SP1 binding site, Δ24 deletion in the E1A gene and an RGD motif in the L5 gene. AdNuPARmE1A-E and ICOVIR15-E further encodes for an eGFP, inserted in both genomes after L5 with an extra splicing site acceptor for transcription from the MLP promoter.*

Organoids were infected with 5000 pfu/well and eGFP expression was monitored 24, 48, and 72 hours PI. Fluorescence in PDOs from PDAC tumors similarly increased with time, independently of the virus used, according to viral replication and spread within the organoid (Fig 4.1.7 A). Interestingly, whereas eGFP expression expanded in normal organoids exposed to Adwt-E, infection with oncolytic adenoviruses displayed similar eGFP expression at all time points assessed, indicating the difficulty of both AdNuPARmE1A-E and ICOVIR15-E to replicate in normal tissue (Fig 4.1.7 B).

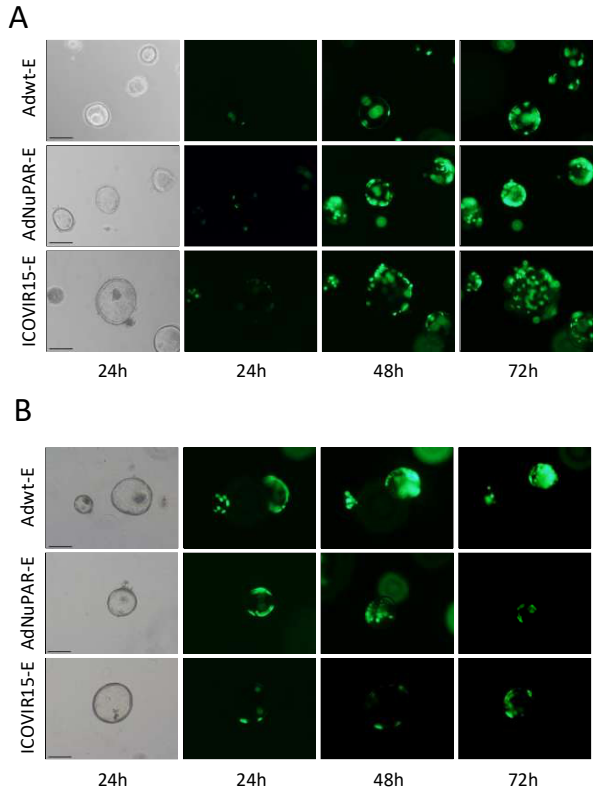

Figure 4.1.7. OVs selectively replicate in PDAC derived organoids. *Organoids were infected with 5000 pfu/well of Adwt-E and the oncolytic adenoviruses AdNuPARmE1A-E and ICOVIR15-E. Representative images of GFP expression at 24h, 48h and 72h after infection of PDAC IDIT1 organoids (**A**) or IDIS0 normal pancreas organoids (**B**).*

To validate healthy PDOs for testing adenoviral selectivity, we performed cytotoxicity studies by an adapted MTT assay on two healthy pancreas derived organoids. We infected the cultures with 3 different viral doses and 5 days later cytotoxic effects were evaluated. OVs displayed a diminished cytotoxic effect compared to Adwt (Fig 4.1.8). At all the analyzed doses, IDIS0 organoids maintained superior viability levels when infected with OVs than when infected with Adwt. IDIS6 organoids showed high sensitivity to viral lysis and differences in viral responses were observed upon infection at the low dose of 10^3pfu/well, where Adwt cultures showed significantly increased cytotoxicity.

Together these results support the oncoselective activity of AdNuPARmE1A-E and ICOVIR15-E and validate PDOs as a system to study this adenoviral property.

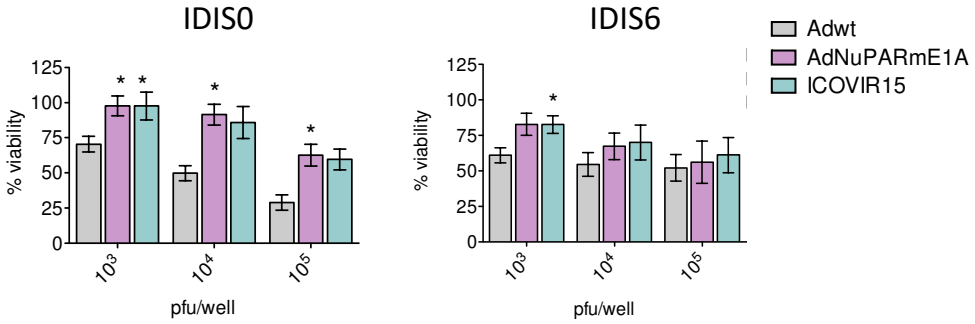

Figure 4.1.8. Oncolytic adenoviruses activity is hampered in healthy pancreas derived organoids. *Two different healthy pancreas PDOs were infected at the indicated doses with Adwt, AdNuPARmE1A and ICOVIR15. Five days later cytotoxicity effects were visualized by an adapted MTT assay. Data are represented as mean ± SEM, n≥4; *p<0.5, **p<0.01, ***p<0.05, Non parametric Mann- Whitney U Test.*

4.1.5 PDOs from PDAC exhibit different sensitivity to oncolytic adenoviruses

The idea of introducing organoids as a system for virotherapy screening was meant to evaluate potential inter-patient responses, what could help to identify patient-specific treatment. To that end, we tested the activity of oncolytic adenoviruses AdNuPARmE1A and ICOVIR15 (Fig 4.1.6) and compared their potency to that of the wild-type adenovirus Adwt in a panel of PDAC organoids.

As a proof of concept, AdNuPARmE1A and ICOVIR15 were screened for cytotoxicity in IDIT1 organoids. Organoids were seeded in 96MW plates and infected with 3 different adenoviral doses (10^3, 10^4, 10^5 pfu/well). Viability effects were evaluated on day 5, showing a dose dependent cytotoxicity for all the adenoviruses. Interestingly, IDIT1 organoids appeared more sensitive to AdNuPARmE1A. In fact, at the lowest dose, viability of the AdNuPARmE1A-infected IDIT1 organoids reached values lower than 50%, whereas at the same dose ICOVIR15-infected organoids still maintained viability higher than 75% (Fig 4.1.9 A). Analogous results were observed in organoid-formation assays. In these experiments, the viability of the organoids was indirectly measured as their ability to form new organoids once mechanically disaggregated, after 5 days of infection. AdNuPARmE1A-infected organoids formed significantly less organoids than ICOVIR15-infected ones at the two doses tested (Fig 4.1.9 B, upper and lower panel).

To investigate if the oncolytic efficacy in organoids could predict the *in vivo* response to the viruses, IDIT1 organoids were

subcutaneously injected into the flanks of nude mice. When tumors reached 100 mm^3, animals received a systemic dose of saline solution, ICOVIR15 or AdNuPARmE1A at $5 \cdot 10^{10}$ viral particles (vp)/animal. Treatment with both viruses strongly inhibited tumor growth, but the antitumor effect was significantly higher in animals receiving the AdNuPARmE1A virus, consistent with the *in vitro* data (Fig 4.1.9 C).

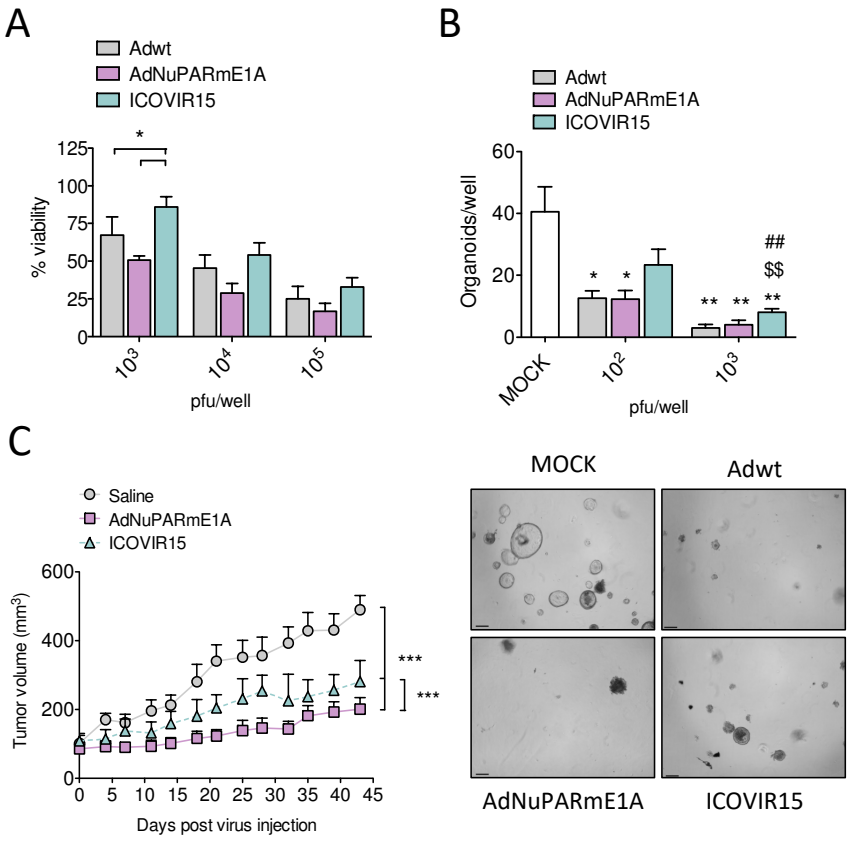

Figure 4.1.9. IDIT1 organoids show increased sensitivity to AdNuPARmE1A in vitro and in vivo. ***A.*** *In vitro cytotoxicity of Adwt, AdNuPARmE1A and ICOVIR15 in IDIT1 organoids. IDIT1 organoids were infected with the indicated doses and 5 days later, cell viability was assessed by MTT assay. Data are represented as mean ± SEM, n>3; *p<0.05, Non parametric Mann-Whitney U test.* ***B****. Organoids forming capacity of IDIT1 infected organoids. IDIT1 organoids were infected with the indicated viral doses and 5 days later, cells were harvested, softly disaggregated and re-seed in 96MW plate with a 1:2 dilution.*

*The day after, formed organoids were counted (discriminating for round-shaped structures with dimension > 20 µm). Upper panel represents the count for viable organoids 24 hour after re-seeding. Data are represented as mean ± SEM, n=6; *p<0.5; **, $$, ##p<0.01; * statistic significance compared to MOCK control, $$ compared to Adwt, ## compared to AdNuPARmE1A, Non parametric Mann Whitney U test. In lower panel, representative images of nascent organoids 24 hours after re-seeding are shown (scale bar 100 µm).* ***C****. In vivo antitumoral effects of oncolytic adenovirus in IDIT1 subcutaneous tumors. Tumor-bearing mice were intravenously injected with $5 \cdot 10^{10}$ vp/mice AdNuPARmE1A, ICOVIR15 or saline and tumor growth was monitored for 42 days (n=8, ***p<0.005, Differences within means were evaluated with Tukey's range Test).*

Next, we analyzed the cytotoxic activity of AdNuPARmE1A and ICOVIR15 in 4 additional PDOs (IDIT2, IDIT4, IDIT5, IDIT6). We observed dose-dependent effects, with patient-susceptibility differences to adenoviral infections. At the doses of 10^4 pfu/cell, IDIT2 and IDIT6 reached 50% of viability, whereas IDIT4 and IDIT5 maintained values higher than 75% (Fig 4.1.10). According to these data, two main degrees of viral sensitivity among patients could be identified. IDIT1, IDIT2 and IDIT6 patients showed good susceptibility to adenoviral infections, with high cytotoxicity at the lowest dose applied (Fig 4.1.9A and Fig 4.1.10). IDIT4 and IDIT5 required highest amount of OVs to reach remarkable cytotoxicity (Fig 4.1.10). The differences in adenoviral sensitivity could be potentially explained by differential Coxsackie and adenovirus receptor (CAR) expression on the surface of the organoids, in line with the variability observed in GI tumors and pancreatic cancer cell lines [165,212]. Comparative analysis of the OVs AdNuPARmE1A and ICOVIR15 activities in organoids revealed similar oncolytic response to both viruses in IDIT4 and IDIT5 patients. However, AdNuPARmE1A showed enhanced cytotoxicity in IDIT1 and

IDIT2 PDOs, (Fig 4.1.9 A, B and Fig 4.1.10) whereas ICOVIR15 was more potent in IDIT6 PDOs (Fig 4.1.10).

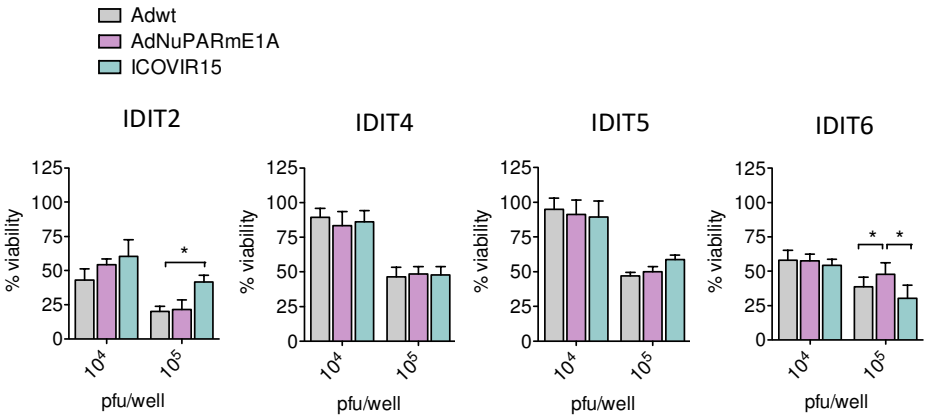

Figure 4.1.10. Oncolytic adenoviruses show patient-dependent sensitivity. *Four different PDOs cultures were infected with the indicated doses of Adwt, AdNuPARmE1A and ICOVIR15, and cytotoxic effects were visualized 5 days later by MTT assay. Data are represented as mean ± SEM, n>3; *p<0.05, Non parametric Mann-Whitney U test.*

To understand the increased response of AdNuPARmE1A in IDIT1 and IDIT2 organoids, we analyzed the expression of uPAR and HES1 genes, which share regulatory sequences with the virus, as well as that of NOTCH1, as a marker of the NOTCH pathway. We performed qRT-PCR analysis in the different organoids and observed increased upregulation of the 3 genes in IDIT1 and IDIT2 organoids (Fig 4.1.11). This result suggests that the higher potency of AdNuPARmE1A in these two organoids could be related to the control sequences inducing active transcription of E1A.

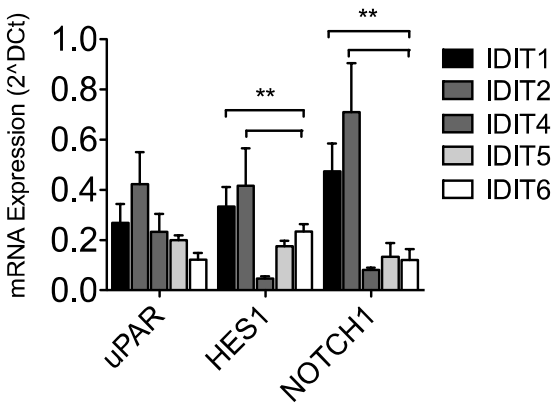

Figure 4.1.11. PDAC derived organoids show different level of activation of uPAR and NOTCH pathways. *mRNA expression of the indicated genes from 5 different PDOs was analyzed and results are expressed as 2^DCt. Data are represented as mean ± SEM, n≥4; **p<0.01, Non Parametric Mann- Whitney U Test.*

4.1.6 Combining viral oncolysis with chemotherapy or treatment with miR-99b-armed oncolytic virus increases the anti-cancer effects in PDOs

To further evaluate the benefit of PDOs for testing optimized based adenoviral treatments, we studied the effects of combining adenovirus with chemotherapy or the use of adenovirus armed with transgenes that could synergize with adenoviral activity.

To ascertain the potential benefit of combining the standard of care chemotherapy for PDAC, gemcitabine + nab-Paclitaxel, with the AdNuPARmE1A in PDOs, IDIT1 and IDIT2 organoids were treated with AdNuPARmE1A and the indicated drugs, alone or in combination. Cytotoxicity assays revealed small differences in sensitivity to chemotherapy between the two PDOs. The strongest cytotoxicity effects were observed in the combination treatments,

reaching similar response in both organoids with viability values of 25% at the conditions tested (Fig 4.1.12). These results highlight the feasibility of testing combination treatments in organoids for prospective therapies.

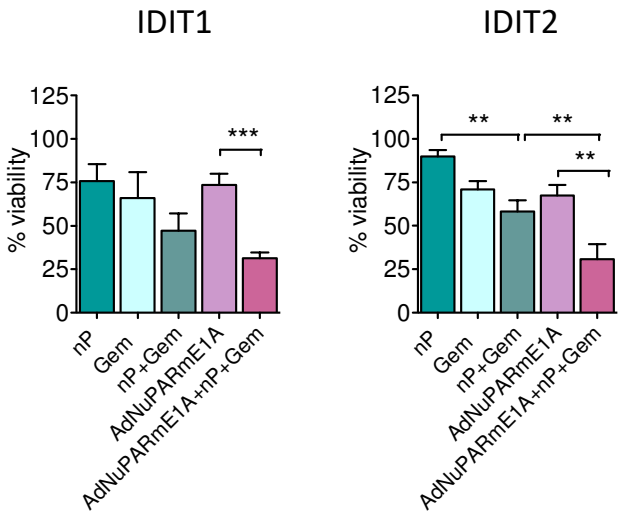

Figure 4.1.12. Combination of adenovirus with gold standard chemotherapy drastically decreases viability of PDAC organoids. *AdNuPARmE1A sensitive PDAC organoids were treated with 100nM nab-paclitaxel, 2.5 ng/ml of gemcitabine or 5000 pfu/well of AdNuPARmE1A, alone or in combination and 5 days later cell viability was assessed by MTT assay. Data are represented as mean ± SEM **p<0.01, ***p>0.005, n≥4, Non-parametric Mann-Whitney U test.*

Previous results from our laboratory showed that the reintroduction of certain miRNAs, whose expression is suppressed in PDAC, could help adenovirus during infections. ICOVIR15-miR99b and ICOVIR15miR-485 armed OVs displayed enhanced antitumor response in cell lines and xenografts, due to their role in regulating viral transcriptional repressors[190]. In this project we tested the activity of these armed oncolytic viruses (Fig 4.1.13 A) in the ICOVIR15-sensitive IDIT6 organoids. ICOVIR15-miR99b but not ICOVIR15-miR485 showed significantly higher activity than the

parental ICOVIR15 (Fig 4.1.13 B), confirming the role of this miRNA as an adenoviral sensitizer in PDAC.

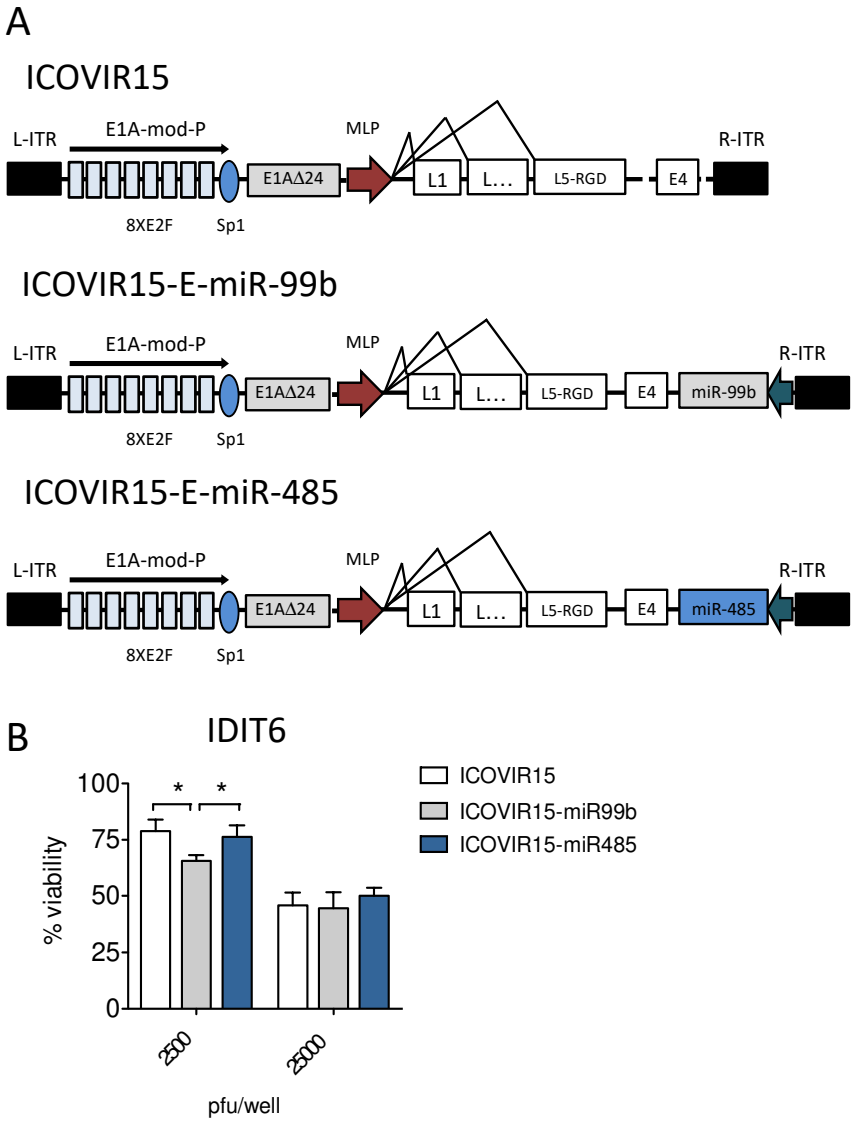

Figure 4.1.13. miR-99b rescue improves adenoviral oncolysis in IDIT6 organoids. ***A.*** *Schematic representation of the viruses used in the experiment. ICOVIR15 was already detailed in figure 4.7. ICOVIR15-miR-99b/miR-485 have an ICOVIR15 backbone endowed with sequences expressing indicated miRNAs under CMV promoter in a region between E4 and R-ITR.* ***B.*** *IDIT6 organoids were seeded and infected with the indicated doses of*

*adenoviruses. Five days post infection cytotoxicity was visualized by MTT assay. N>4 *p<0.05, Non parametric Mann-Whitney U test.*

These results further highlight the patient-dependent sensitivity to oncolytic adenovirus and provide increased value to the viral screening in PDOs.

4.1.8 Organoids derived from orthotopic tumors and metastatic foci in mice mirror responses of patient-PDO to oncolytic viruses

At the time of PDAC diagnosis, very often, distant metastases are already present. Thus, it is fundamental that the developed therapies could act both in the primary tumors and in the metastatic foci. We took advantage of PDOs to generate a personalized model of metastases and characterize their response to OVs.

We implanted a suspension of $5 \bullet 10^5$ cells obtained from disaggregation of IDIT6 organoids in the pancreas of athymic nude mice. Tumor growth was followed up by palpation and 2-3 months later, animals were euthanized and inspected for the appearance of primary tumor and metastases (Fig 4.1.14 A). Of 7 animals implanted, 6 developed tumors in the pancreas, with metastatic foci either in liver or diaphragm.

Analysis of tumor tissues revealed the presence of glandular structures resembling human PDAC lesions, with positive immunostaining for the ductal marker CK19 (Fig 4.1.14 B).

We established organoids from individual tumors and metastases. First, we perform a karyotype of the different organoid lines, and

compared with IDIT6 before implantation and with healthy pancreas derived organoids.

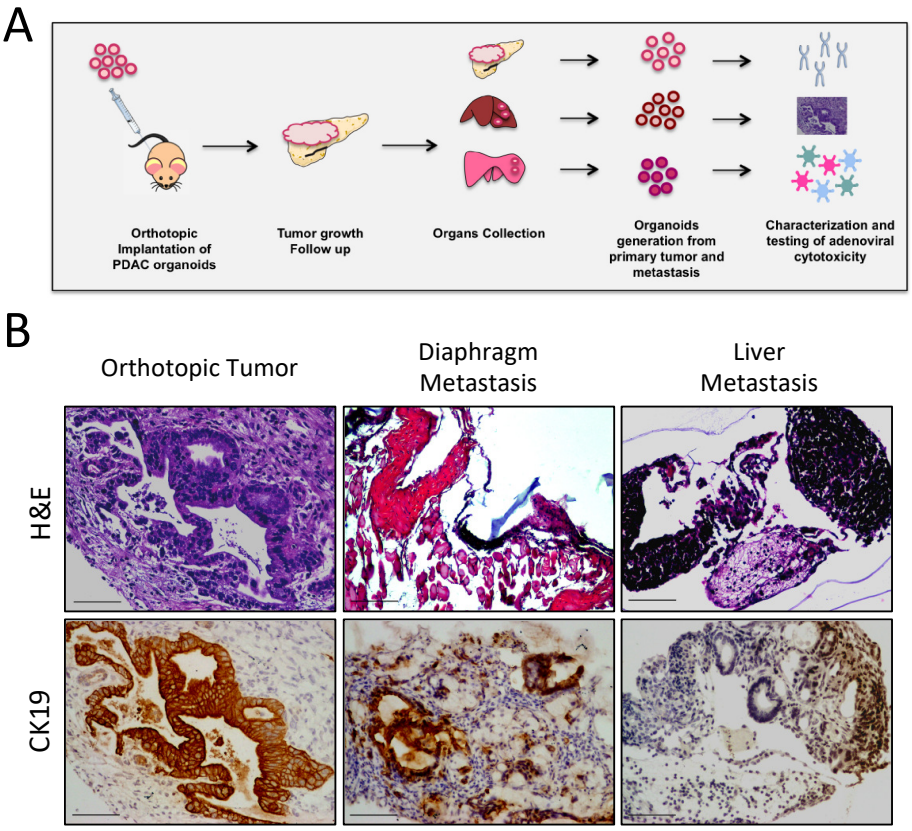

Figure 4.1.14. Schematic representation of the in vivo metastasis model experiment and histological characterization of tumors and metastasis. ***A****. Athymic nude mice were orthotopically implanted with 5•10^5 IDIT1 or IDIT6 organoids (n=3 for IDIT1, n=7 for IDIT6). Tumors in the pancreas and derived metastases were histologically characterized and collected for organoids generation. Karyotyping analysis and sensitivity to OA was evaluated in organoids.* ***B****. H&E and CK-19 staining orthotopic tumor and its derived metastasis.*

Healthy organoids showed a diploid chromosome number, whereas aneuploidy was evident in all the tumor-derived organoids and was superior in the metastatic organoids. These showed the highest

percentage of nuclei with more than 69 chromosomes, in line with the genetic drift likely taking act during the development of metastasis. Original IDIT6 PDOs presented an aneuploidy similar to the orthotopic tumors derived organoids (Fig 4.1.15 A, B).

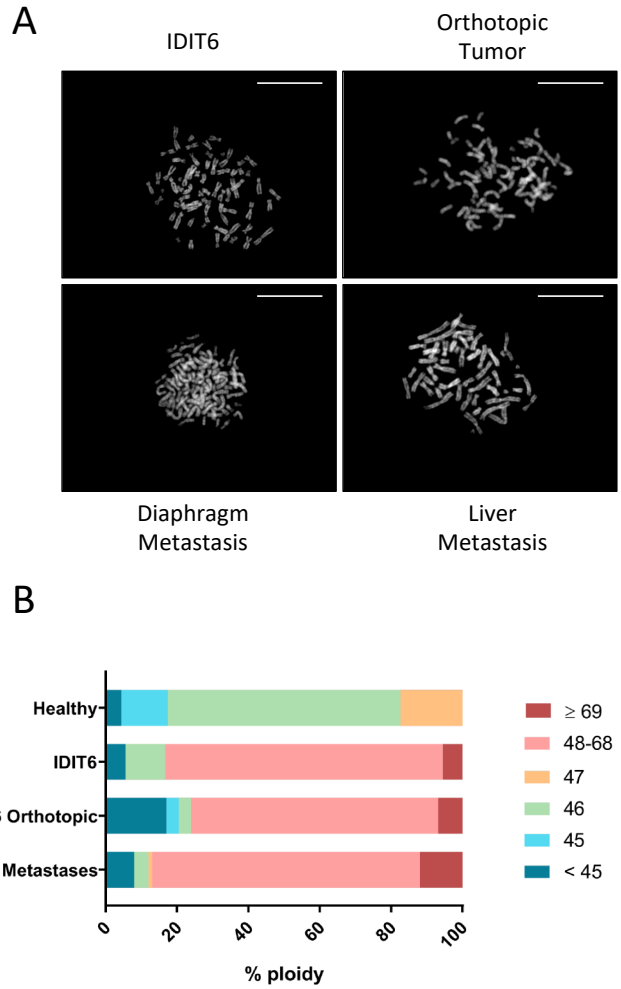

Figure 4.1.15. Chromosomal instability analysis in orthotopic tumors and metastases derived from IDIT6 implanted organoids. *Metaphases were induced in the different lines via COLCEMID treatment (0.1 µg/mL) for 24 h. A minimum of 15 metaphases for sample was counted.* ***A****. Panel shows representative images of the different samples' karyotypes.* ***B****. Percentage of ploidy in each group of samples is represented. A karyotype of healthy pancreas derived organoids is taken as reference.*

Next, we evaluated the OVs activity on primary tumor derived organoids and their corresponding metastasis. Interestingly, we observed that ICOVIR15 displayed enhanced cytotoxicity compared to AdNuPARmE1A in organoids from all primary IDIT6 tumors and their metastatic foci, mirroring what already observed in IDIT6 original organoids (Fig 4.1.16 A, B).
A similar experiment was performed on a reduced number of animals, orthotopically implanted with IDIT1 organoids. In this experiment 2/3 operated animals developed pancreatic tumors 3 months later, and one of them presented diaphragm metastasis. Again, we observed that tumor and metastasis derived organoids reproduced IDIT1 PDO behavior, being AdNuPARmE1A the most potent of the two adenoviruses (Fig 4.1.16 C).

These results show that oncolytic virotherapy acts similarly in primary tumors and metastases, despite the latter having increased genomic instability. Interestingly, tumor evolution seems not to interfere with viral activity, at least in the tested conditions. These findings suggest the predictive ability of PDOs to identify highly active oncolytic adenoviruses and in the future could facilitate the selection of successful treatments to eradicate both primary tumors and metastases.

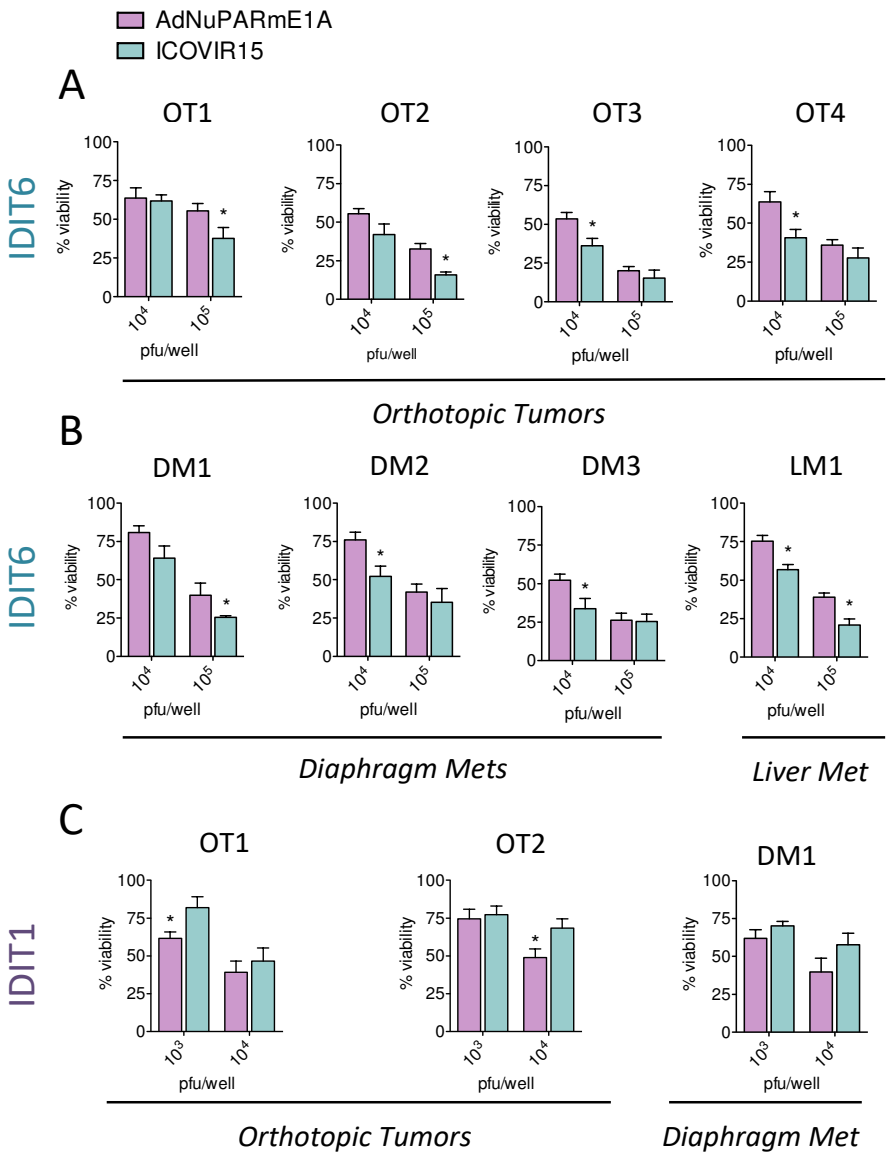

Figure 4.1.16. Primary tumor and metastases derived organoids from PDOs implanted in nude mice mirror PDOs sensitivity to adenoviruses. ***A, B, C****. Orthotopic tumors and metastases derived IDIT6/IDIT1 organoids from 4 or 2 different animals, respectively, were infected at the indicated doses with AdNuPARmE1A and ICOVIR15. Five days later cytotoxicity was analyzed via MTT assay. n=5, *p<0.05, Non Parametric Mann Whitney U test.*

4.2 Influence of miRNA deregulation in PDAC on adenoviral oncolysis

Altered miRNAs expression in malignancies has been widely demonstrated [213,214]. These small post-transcriptional regulators are involved in all the processes of cancer biology. Their alteration has proven fundamental for tumor cells to acquire resistance to apoptosis, to induce high cellular proliferation, migration and chemoresistance [81,215–218].

MiRNAs also play important roles in host-virus interactions. Recently our group showed that the reintroduction in an adenoviral backbone of miR-99b and miR-485, poorly expressed in PDAC, facilitated adenoviral oncolysis and improved the antitumor activity in mouse models [190]. These results suggest that exploiting miRNA modulation can be a good strategy to ameliorate the therapeutic activity of oncolytic adenoviruses. However, very often in tumors miRNAs are highly upregulated. We hypothesized that the cellular deregulation triggered by excessive abundance of miRNAs might generate a context that would limit adenoviral replication in PDAC.

In this thesis we have screened for potential miRNA candidates upregulated in PDAC and studied whether their normalization by miRNA sponges engineered in adenovirus could improve the oncolytic activity.

4.2.1. Impact of miR-93 and miR-21 removal on adenoviral fitness

In a recent miRNome study of PDAC samples, authors identified 31 miRNAs significantly upregulated [219]. Among those, miR-93 and miR-21 were within the group of the most upregulated miRNAs (table 4.2.1). We decided to evaluate the impact of miR-93 and miR-21 KO on adenoviral infections.

	Discovery phase (NGS)	Cohort 1 (q-PCR)	Cohort 2 (q-PCR)
microRNA	FC vs Healhty	FC vs Heahty	FC vs Healthy
miR-21-5p	11.18	7.84	10.20
miR-93-5p	2.75	6.59	77.77

Table 4.2.1. Expression levels of miR-21 and miR-93 in PDAC (data from [219]).

For this, we generated by lentiviral transduction PANC-1 knockout cells for miR-93 (PANC-1-miR93 KO) and the corresponding control cells modified with a lentivirus containing no sgRNA (PANC-1-Ctrl). For the experiments, the pool of PANC-1-miR93 KO cells and two individual clones were used (PANC-1-miR93 KO/1, PANC-1-miR93 KO/2). To confirm the genetic knockout, we sequenced the miR-93 region and analyzed the expression of the miRNA (Appendix 8.1). As shown in fig 4.2.1 A, miR-93 was completely abolished both in the cellular pool (left graph) and

individual clones (right graph). Next, we tested the cytotoxic response of the generated cells to adenoviral infection. For this, cells were incubated with serial dilutions of Adwt adenovirus and 7 days later viability was evaluated. The pool (Fig 4.2.1 left panel) and the different clones (Fig 4.2.1 right panel) of PANC-1-miR93 KO cells showed a shift to the right in the dose-response curves, indicating that knockout cells were less sensitive to adenoviral oncolysis. Moreover, the ID50 values of miR93 KO cells were clearly superior to that of control cells, confirming its reduced sensitivity to viral killing (Fig 4.2.1 C). We assessed viral production 48h after adenoviral infection in PANC-1-miR93 KO and PANC-1-Ctrl cells and observed that viral progeny was diminished in all the PANC-1-miR93 KOs (Fig 4.2.1 D). Similar results were observed in MIA PaCa-2-miR93 KO cells, although the loss of sensitivity was less evident (Fig 4.2.2 B, C), in line with the observation that some residual miR-93 expression was present in the cells (Fig 4.2.2 A).

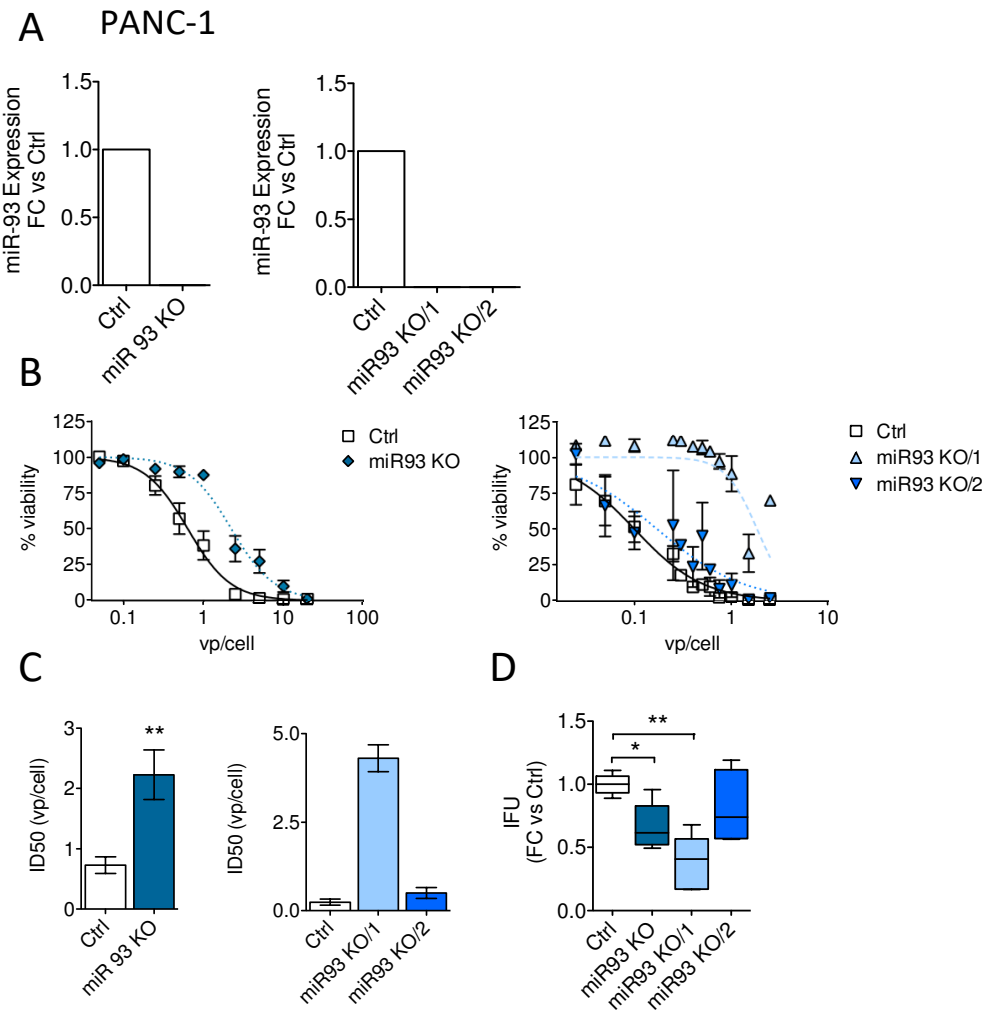

Figure 4.2.1 Effects of miR-93 KO in PANC-1 cells. ***A****. Evaluation of miR-93 expression. Both pool KO (left) and clones KO/1-2 (right) were analyzed via qRT-PCR using TaqMan specific probes. Results are represented as FC with PANC-1-Ctrl, n=1.* ***B****. Viability Curves in miR93 KO (left) and miR93 KO/1-2 (right) after 7 days of treatment with Adwt. 5000 cells were seeded and the day after infected with serial dilutions of Ad5wt. Results were visualized 7 days later by MTT assay.* ***C****. ID50 values for PANC-1 Ctrl, miR93 KO (left) and miR93 KO/1-2. Data were extrapolated from viability curves by non-linear regression with the help of GraphPad Prism v5.0.* ***D****. Viral yield assay evaluating viral particles contained in total cell extracts 48 hours after infection. 50000 cells/well were seeded and the day after infected with 1 IFU/cell. 48 hours later cells were scraped and both cellular and supernatant were collected and analyzed for viral particles in the lysate. N>3, data are represented as mean ± SEM. p*<0.05, **p<0.01 Non parametric Mann-Whitney U test.*

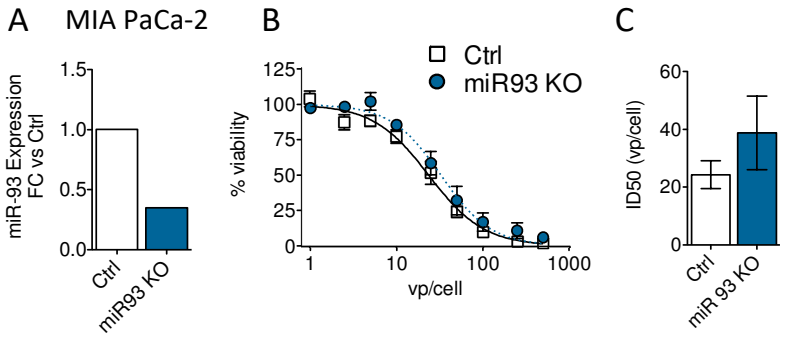

Figure 4.2.2 Effects of miR-93 KO in MIA PaCa-2 cells. ***A****. Evaluation of miR-93 expression. MIA PaCa-2 miR93 KO were analyzed via qRT-PCR using TaqMan specific probes. Results are represented as FC with Mia PaCa-2-Ctrl, n=1.* ***B****. Viability Curves in MIA PaCa-2-miR93 KO and MIA PaCa-2-Ctrl after 7 days of treatment with Adwt. 5000 cells were seeded and the day after infected with serial dilutions of Ad5wt. Results were visualized 7 days later by MTT assay.* ***C****. ID50 values for MIA PaCa-2-Ctrl and miR93 KO. Data were extrapolated from viability curves by non-linear regression with the help of GraphPad prism v5.0. N=3, data are represented as mean ± SEM.*

Altogether these results indicate that the cellular reshaping of miR-93 create conditions that influence adenoviral activity. However, miR-93 downregulation seems to hinder viral replication.

Next, we evaluated the effects of miR-21 modulation in adenoviral oncolysis. PANC-1-miR21 KO and PANC-1-Ctrl cells were generated as already described. Sequencing of the genomic region containing the miRNA and further qRT-PCR quantification in KO and control cells showed reduced or null miR-21 expression in the pull of KO cells and in the individual clones KO/1, KO/2, respectively (Fig 4.2.3 A, Pool: left panel, clones: right panel). The effects of Adwt cytotoxic activity on miR-21 KO PANC-1 cells were evaluated after 7 days of infection. MiR-21 removal negatively impacted adenoviral activity in PANC-1 KO/1 and 2,

displaying ID50 values 10 and 5-fold higher than control cells, respectively (Fig 4.2.3 B, C right panels). No differences in adenoviral ID50 were observed between PANC-1-Ctrl and PANC-1-miR-21 KO pool, in line with the residual miRNA expression observed in this line (Fig 4.2.3 A, B, C left panels). Again, we did not observe any differences in adenoviral activity in MIA PaCa-2-miR-21 KO (Fig 4.2.4 B, C), in line with the presence of some residual miR-21 levels (Fig 4.2.4 A).

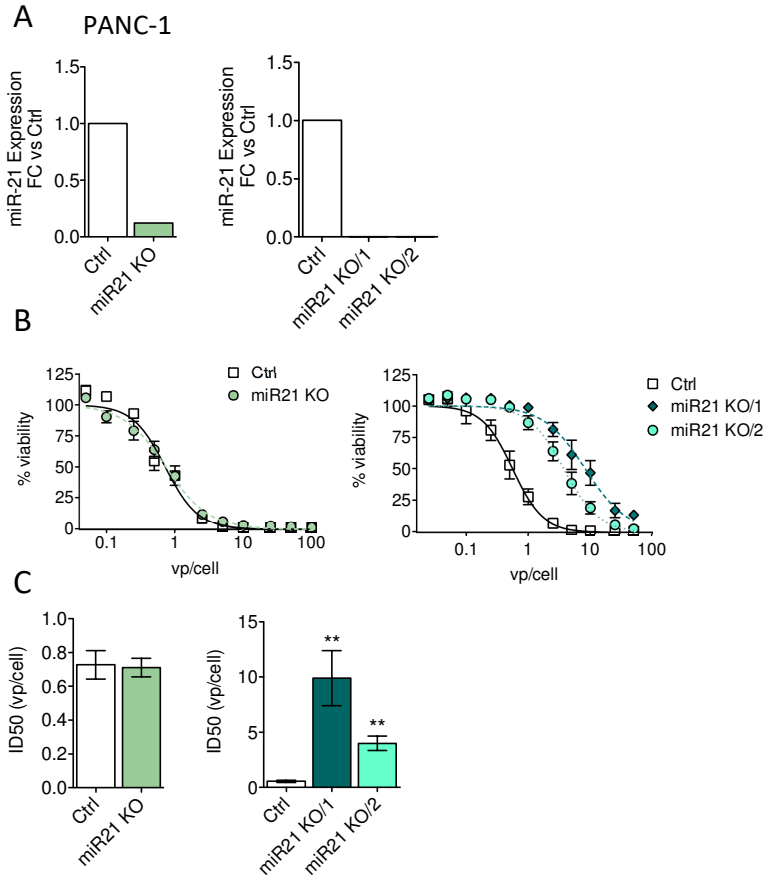

Figure 4.2.3 Effects of miR-21 KO in PANC-1 cells. ***A****. Evaluation of miR-21 expression. Both pool (left) and clones (right) were analyzed via qRT-PCR using TaqMan specific probes. Results are represented as FC with PANC-1-Ctrl, n=1.* ***B****. Viability Curves in miR21KO pool (left) and miR21 KO/1-2 clones (right) after 7 days of treatment with Adwt.*

5000 cells were seeded and the day after infected with serial dilutions of Ad5wt. Results were visualized 7 days later by MTT assay. ***C****. ID50 values for PANC-1 Ctrl, miR21 KO (left) and miR1 KO/1-2 (right). Data were extrapolated from viability curves by non-linear regression with the help of GraphPad prism v5.0. N>3, data are represented as mean ± SEM.p*<0.05, **p<0.01, non parametric Mann-Whitney U test.*

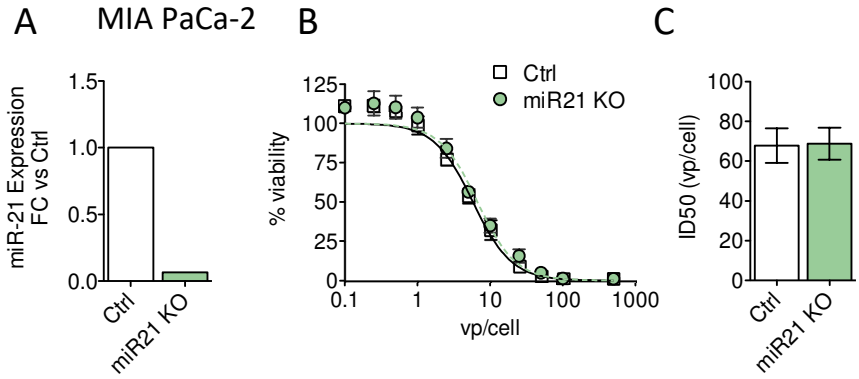

Figure 4.2.4 Effects of miR-21 KO in MIA PaCa-2 cells. ***A.*** *Evaluation of miR-21 expression. MIA PaCa-2-miR21 KO cells were analyzed via qRT-PCR using TaqMan specific probes. Results are represented as FC with Mia PaCa-2-Ctrl, n=1.* ***B****. Viability Curves in MIA PaCa-2-miR21 KO and MIA PaCa-2-Ctrl after 7 days of treatment with Adwt. 5000 cells were seeded and the day after infected with serial dilutions of Ad5wt. Results were visualized 7 days later by by MTT assay.* ***C****. ID50 values for MIA PaCa-2-Ctrl and miR21 KO. Data were extrapolated from viability curves by non-linear regression with the help of GraphPad prism v5.0. N=3, data are represented as mean ± SEM.*

4.2.2 Identification of new miRNA candidates

Previous results evidenced that removal or downregulation of specific miRNAs was modulating adenoviral activity. To identify whether any of the most upregulated miRNAs in PDAC could interfere with adenoviral oncolysis we moved to a hypothesis-driven strategy.

We selected miRNAs upregulated in PDAC (a shortlist from the top 30 from [219]) that could regulate genes participating in two significant aspects of the virus-host interactions. From both aspects,

we selected relevant molecules and, by bioinformatics prediction, we identified the presence of candidate PDAC upregulated miRNAs target sites in their 3' UTR. The two virus-host interactions considered are listed below:

1) Upon adenoviral infection, cells undergo an immunogenic cell death (ICD), characterized by the emission of immunostimulatory damage-associated molecular patterns (DAMPs). DAMPs generation is mediated by the c-GAS/STING pathway, the main sensor of dsDNA inside the cytosol, critical for activating interferon responses (reviewed in [220,221]). Recent reports showed that miR-93 contributes to the establishment of an immunosuppressor tumor microenvironment by downregulating the expression of c-GAS [222]. We observed impaired adenoviral cytotoxicity in cells KO for miR-93, which could be linked to augmented c-GAS in the cell, easing adenoviral recognition. In this scenario, we hypothesized that miRNAs controlling inhibitors of the c-GAS/STING pathway could influence adenoviral infections, and that the inhibition of these miRNAs could improve oncolysis. Thus, we elaborated a shortlist of upregulated miRNAs in PDAC acting on target genes that are inhibitors of the c-GAS/STING pathway. However, miRNAs not having targets in this pathway were also considered for further analysis, with the condition that targets were encountered in the second virus-host interaction aspect considered.

2) Adenoviral infections induce massive changes in host cells, some of whom consist in the enrichment of proteins aiding adenovirus during its replication process [223]. Reyes and collaborators published a list of molecules whose amounts are strongly enriched along the course of an adenoviral infection, co-localizing with adenovirus during its replication inside the cells. We hypothesized that those proteins could be necessary for the adenoviral replication cycle and that upregulated miRNAs targeting these genes could interfere with viral activity. In consequence, we elaborated a shortlist of upregulated miRNAs in PDAC that target the expression of such genes.

Considering common miRNAs fulfilling both criteria, or at least the second criteria targeting a minimum of 3 genes, we end up with a final list identifying 4 miRNA candidates: miR-222, miR-761, miR-3714, miR-4713 (Fig 4.2.5, table 4.2.2, Appendix 7.2).

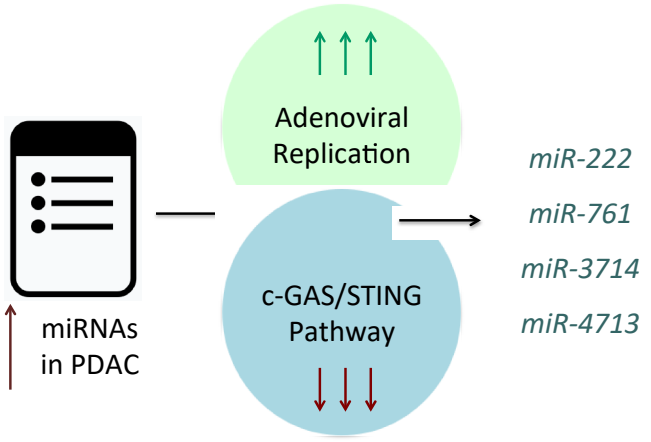

Figure 4.2.5 Schematic representation of the hypothesis-driven strategy for the identification of new miRNA candidates interfering with adenoviral oncolysis in PDAC.

	Discovery phase (NGS)	Cohort 1 (q-PCR)	Cohort 2 (q-PCR)
microRNA	FC vs Healhty	FC vs Heahty	FC vs Healthy
miR-761	2.00	2.19	3.13
miR-3714	2.49	1.76	3.58
miR-4713-5p	3.84	2.19	26.29
miR-222-3p	FC =2.70 [224]; FC = 32 [225]		

Table 4.2. 1. Expression levels of new candidate miRNAs (data from [219])

4.2.3 Impact of miR-222, miR-761, miR-3714 and miR-4713 on adenoviral activity

We generated PANC-1 KO cell lines for all the identified miRNAs by CRISPR/Cas9, as previously described. Genomic alterations were validated by DNA sequencing and miRNA expression analysis (Fig 4.2.6, Appendix 7.1). Infection of the 4 PANC-1 KO cell lines with serial dilutions of Adwt demonstrated variability in the cytotoxic response. PANC-1-miR-761 KO and PANC-1-miR-4713 KO showed right-shifted dose-response curves, resulting in Adwt increased ID50 (Fig 4.2.7 A upper panel, B), suggesting that downregulation of these miRNAs was interfering with viral activity.

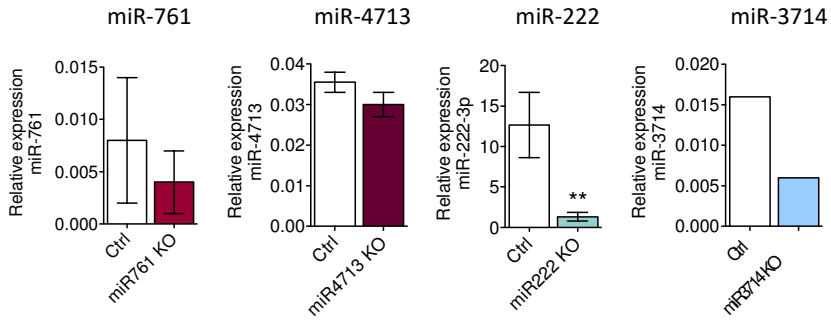

Figure 4.2.6 miRNA expression in miRNA PANC-1 KO cells engineered by CRISPR/Cas9 editing. *miRNA expression was detected via qRT-PCR using specific TaqMan probes. Values are represented as 2^-ΔCt. N≥1, Data are represented as mean ± SEM.**p<0.001, Non Paramentric Mann Whitney U test.*

Interestingly, Adwt ID50 values were significantly reduced in PANC-1-miR-222 KO and PANC-1-miR-3714 KO cells compared to PANC-1-Ctrl, suggesting that downregulation of these miRNAs in PDAC tumors could facilitate viral activity (Fig 4.2.7 A lower panel, B). However, despite being highly abundant in PDAC tissues[80], miR-3714 expression in PANC-1 cells was barely detectable. Thus, we discarded this miRNA and considered only miR-222 for further characterization.

We generated MIA PaCa-2-miR222 KO cells (Fig 4.2.8 A), and similarly to PANC-1-miR-222 KO, we observed increased sensitivity to adenoviral infection in the miR222 KO cells, when compared to MIA PaCa-2-Ctrl cells. We detected a shift to the left in the Adwt dose-response curve (Fig 4.2.8 B) that resulted in decreased ID50 values (Fig 4.2.8 C). Next, we assessed viral particles production in PANC-1 and MIA PaCa-2-miR222 KO cells by infecting with Adwt or with the tumor-selective virus AdNuPARmE1A (introduced in section 4.1). Quantification of viral

particles released 72 hours PI evidenced increased viral yield in the KOs cells, with the highest number of particles produced with Adwt infections (Fig 4.2.9). This result endorsed what was observed in the cytotoxic assay, and supported the idea of inhibiting miR-222 to facilitate adenoviral oncolysis.

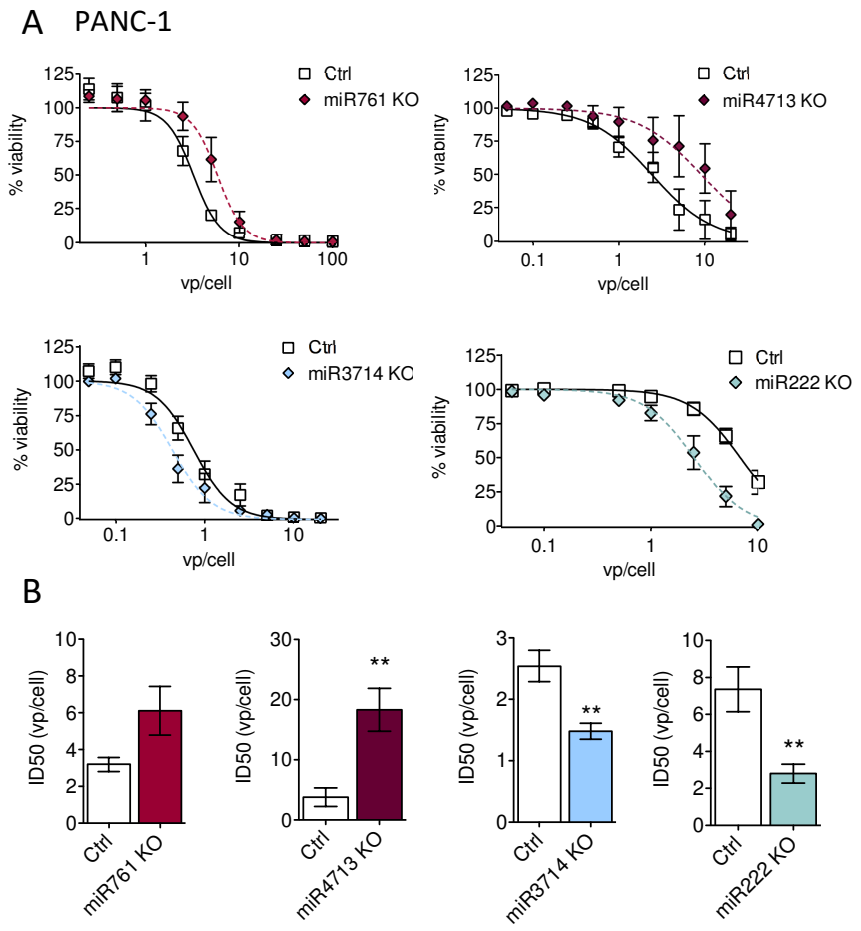

Figure 4.2.7 Cytotoxic effects of Adwt in miRNA PANC-1 KO cells. ***A****. Viability Curves in PANC-1 miR761 KO, PANC-1 miR4713 KO, PANC-1 miR222 KO, and PANC-1 miR3714 KO after 7 days of treatment with Adwt. 5000 cells were seeded and the day after infected with serial dilutions of Ad5wt. Results were visualized 7 days later by MTT assay.* ***B****. ID50 values for KO cell lines. Data were extrapolated from viability curves by non-linear regression with the help of GraphPad Prism v5.0. N>3, Data are represented as mean ± SEM. . **p<0.01, Non parametric Mann-Whitney U test.*

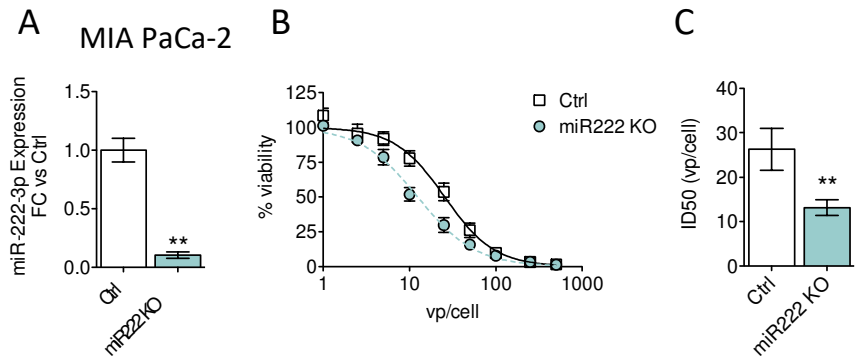

Figure 4.2.8 Cytotoxic effects of Adwt in miR-222 KO in MIA PaCa-2 cells. ***A.*** *miR-222 expression in MIA PaCa-2-miR222 KO cells analyzed via qRT-PCR using specific TaqMan probes. Results are represented as FC with Mia PaCa-2-Ctrl, n>3.* ***B****. Viability Curves in MIA PaCa-2-miR222 KO and MIA PaCa-2-Ctrl after 7 days treatment of with Adwt. 5000 cells were seeded and the day after infected with serial doses of Ad5wt. Results were visualized 7 days later by MTT assay.* ***C****. ID50 values for MIA PaCa-2-Ctrl and miR222 KO. Data were extrapolated from viability curves by non-linear regression with the help of GraphPad prism v5.0. N>3, Data are represented as mean ± SEM. **p<0.01 Non parametric Mann-Whitney U test.*

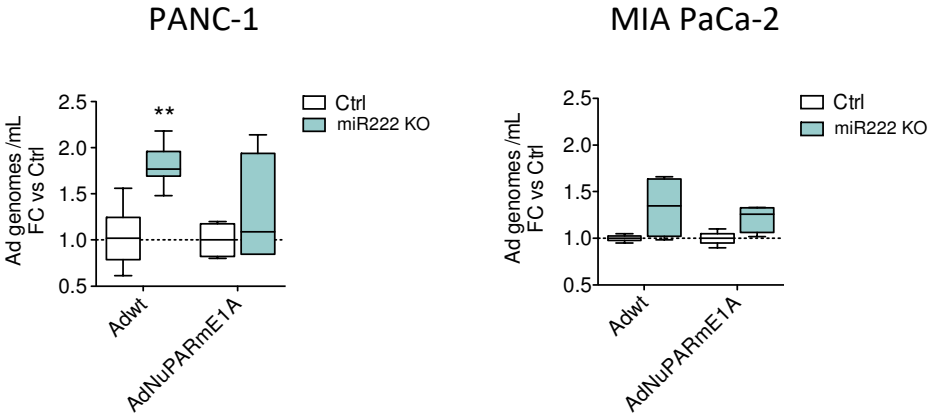

Figure 4.2.9 Viral release in PANC-1 and MIA PaCa-2 miR222 KOs. *50000 PANC-1 and 150000 MIA PaCa-2 cells were seeded and the day after infected with 1 (PANC-1) or 2 (MIAPaCA-2) IFU of either Ad5wt or AdNuPARmE1A. Four hours later, cells were washed three times with PBS and 500 µL of fresh medium were added to each well. Seventy-two hours after infection supernatants were collected and the amount of viral particles present were detected by qRT-PCR with adenoviral hexon specific primers. **p<0.01, Non parametric Mann-Whitney U test. N>4, data are represented as mean ± SEM.*

MiR-222 is located in the short arm of the X chromosome, as part of a cluster region in tandem with miR-221. Both miRNAs share the seed sequences, are separated only by 727 bp (Fig 4.2.10) and have common transcriptional regulators, leading to similar alteration profiles [90]. In fact miR-221 is also highly upregulated in PDAC [80].

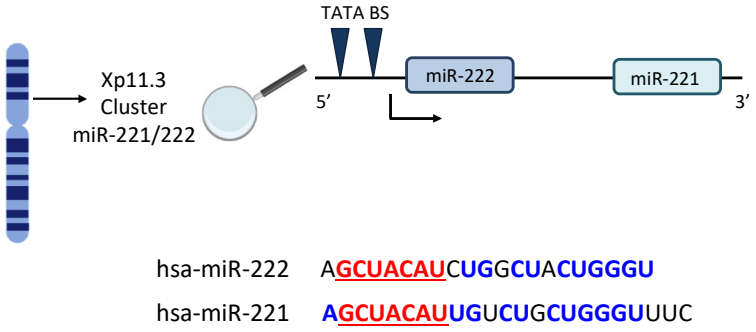

Figure 4.2.10 Schematic representation of miR-222 location in the human genome. *Both sequences of miRNAs in the cluster are represented. Seed sequence is highlighted in red and sequence identity in blue. TATA BS meaning TATA box binding site.*

Considering these features, we checked if the increased sensitivity to Adwt in PANC-1-miR222 KO was specific of miR-222 and independent of miR-221. Expression analysis of miR-221 content in PANC-1-miR222 KO showed similar miRNA levels in KO and PANC-1-Ctrl cells (Fig 4.2.11 A), witnessing miR-222 KO specificity.

Since miR-221 and miR-222 shared the seed sequence, very likely the inhibition of miR-222 through a sponge construct would also downregulate miR-221 content. With this in mind, we explored the effects of inhibiting miR-221 in adenoviral activity. PANC-1-miR221 KO cells were generated and confirmed by DNA

sequencing (Fig 4.2.11 B, Appendix 7.1). When cells were challenged with a battery of Adwt dilutions, the cytotoxic response was similar in miR221 KO and Ctrl cells (Fig 4.2.11 C), indicating that miR-221 depletion was not altering adenoviral activity.

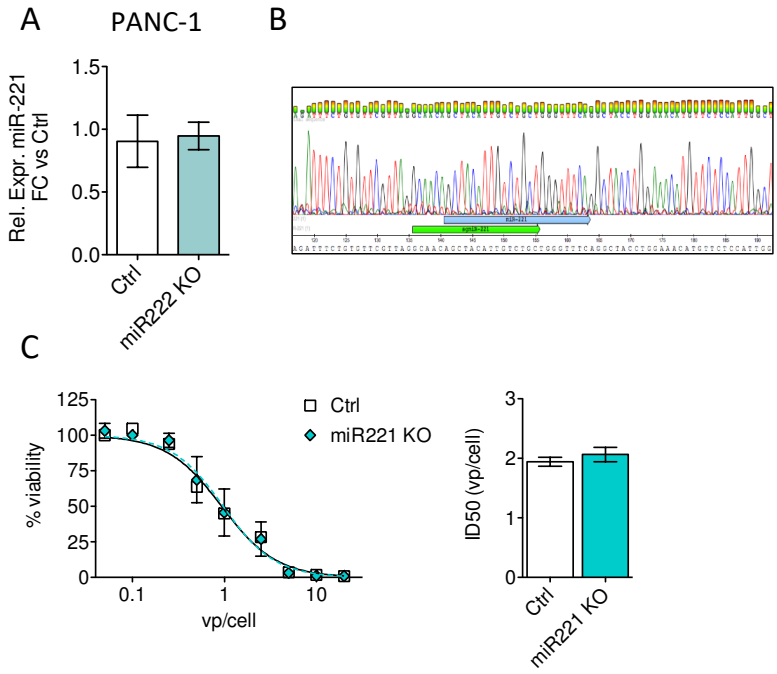

Figure 4.2.11 Influence of miR221 KO on adenoviral oncolysis. ***A.*** *Evaluation of miR-221 expression in PANC-1 cells KO for miR-222.* ***B****. Validation of miR-221 KO in PANC-1 cells. After sgRNA insertion, double or triple peaks can be observed, meaning that genetic editing led to a mixture of rearrangement.* ***C****. Cytotoxicity assay in PANC-1-Ctrl and PANC-1-miR221 KO. 5000 c/w were seeded and the day after infected with serial dilution of Adwt, ranging from 0 to 50 vp/cell. Results were visualized 7 days later by MTT assay. Left panel represents viability curves, right panel represents ID50 values. ID50 values were extrapolated from viability curves by non-linear regression with the help of GraphPad Prism v5.0. N=3, data are represented as mean ± SEM.*

4.2.4 Generation of miR-222 sponges

Previous results supported the idea that miR-222 inhibition could facilitate adenoviral activity. One of the strategies developed to

inhibit miRNAs, are the so-called miRNA sponges. These are artificial constructs containing miRNAs binding sites, mimicking the target sequences on mRNAs and acting as miRNA decoy. Optimal miRNA sponges are generally constituted by 4-8 repeated tandem sequences with complementarity to the miRNA of interest, and separated by 4 nt. Introduction of a buldge in the nucleotides between the position 9-12 of the sponges demonstrated to increase the sequestration activity of the constructs[226,227].

We designed miRNA sponges as 4 tandem repeats of the sponge sequences separated by 4 random nucleotides spacers [175,194,227]. The sponge sequence consisted of a 21 nucleotide sequence with a bulged region in nucleotides 9 to 12 flanked by 9 and 8 nucleotides of perfect complementarity to miR-222 [226]. Scramble control sequence and miR-222 sponge sequences were generated with the miRNA song software [228](Fig 4.2.12 A).

Among the sequences predicted by the software to work as miR-222 sponge sequence, we selected the one characterized by the lowest energy score, meaning high affinity, and the highest number of target sites, selecting 4 target sites/sponge sequence. The affinity prediction of this sequence was equivalent for both miR-221 and miR-222. Some miRNA off-targets with very low affinity were identified for miR-222 sponge (miR-370-3p, miR-3692-5p, miR-4731-5p, miR-6861-5p, miR-147b, miR-1301-3p), however their expression is poor in PDAC, reducing their potential interference. For the selection of the Scramble sponge we used the same software and picked up a sequence that recognized individual target sites having high-energy score and that were not expressed in PDAC.

To evaluate the sponge's activity, we cloned both constructs in the 3'UTR of the eGFP gene controlled by a CMV promoter in the miRVec vector, generating miRVec-eGFP-miR222-S and miRVec-eGFP-Scramble (Fig 4.2.12 B). HEK-239T cells were transfected and eGFP expression was analyzed as a surrogate of sponge functionality. Visualization of eGFP 48h later under a fluorescence microscope revealed very low eGFP expression in miRVec-eGFP-miR-222-S transfected cells, compared to cells receiving miRVec-eGFP-Scramble (Fig 4.2.12 C). The result was confirmed in quantification analysis by flow cytometry (Fig 4.2.12 D). Low eGFP expression in miRVec-eGFP-miR-222-S transfected cells was also detected by eGFP mRNA quantification (Fig 4.2.12 E). The sponge effect resulted in a reduced expression of miR221 and miR222 levels, ranging from 30 to 50% (Fig 4.2.12 F).

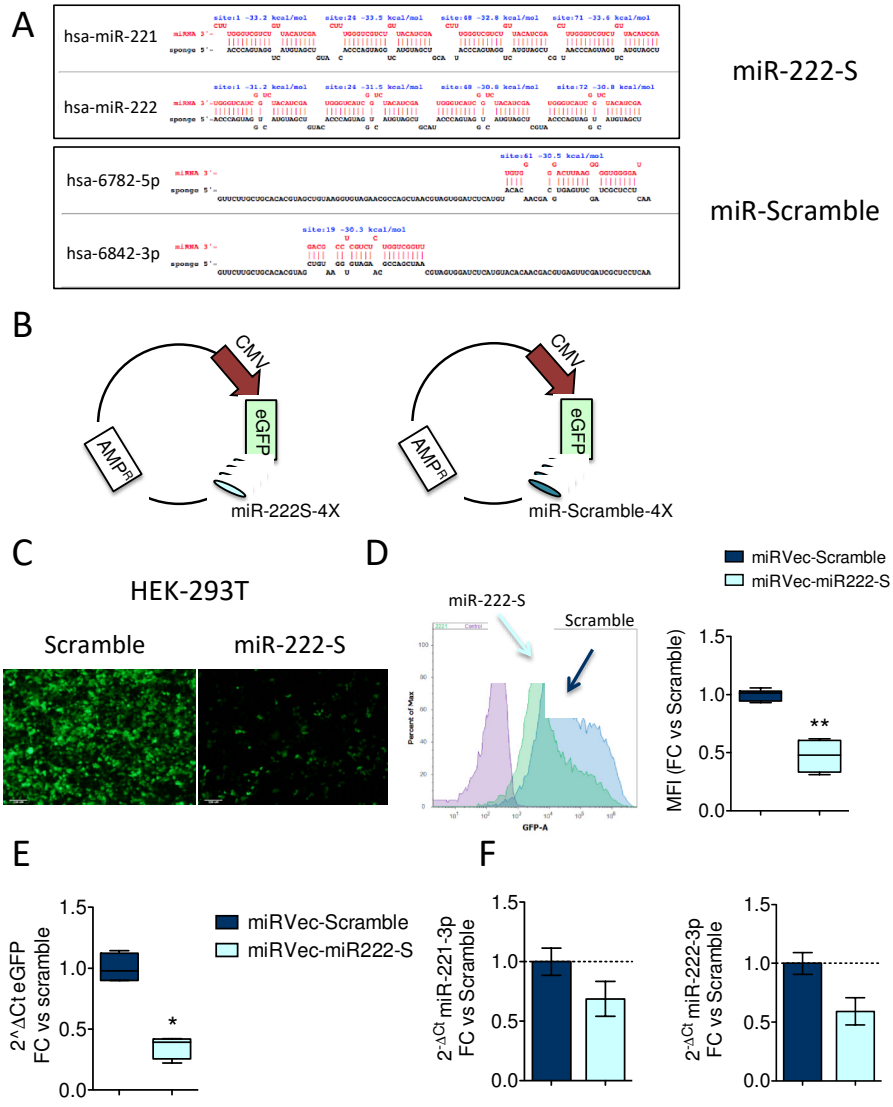

Figure 4.2.12 Generation of miRVec plasmids containing Scramble sequence or sponges for miR-222 and their validation in HEK-293T cells. ***A****. miRNAsong output for sponge sequence of Scramble and miR-222. Most scored on-targets are showed for both sequences.* ***B.*** *Schematic representation of miRVec vectors: miRVec-eGFP-miR-222-S (left) and miRvec-eGFP-Scramble (right).* ***C****. Visualization of eGFP expression by fluorescence microscope 48 hours after transfection of miRVec-eGFP-Scramble or miRVec-eGFP-miR-222-S in HEK-293T cells. Scalebar 100µM.* ***D****. Quantification of eGFP intensity by flow cytometry 48h after plasmids transfections in HEK-293T cells. Left panel shows curves of fluorescence intensity, quantified in right panel (MFI).* ***E****. Quantification of eGFP expression*

by qRT-PCR. Values are represented as fold change compared to miRVec-eGFP-Scramble. ***F****. Quantification of miR-221 and miR-222 after miRNA sponges transfection. Values are represented as fold change compared to miRVec-eGFP-Scramble. N>4, data are represented as mean ± SEM. *p<0.05, **p<0.01, Non parametric Mann-Whitney U test.*

4.2.5 Generation of AdNuPAR-E-miR-222-S and evaluation of its potency *in vitro* and *in vivo* in PDAC models

To evaluate the potential translational application of miR-222-Sponges in adenoviral activity, we inserted miR-222 sponges in the oncolytic viral backbone AdNuPARmE1A. The whole fragment of CMV-eGFP-miR-222-S or the scramble counterparts were cloned in the region between E4 and R-ITR and viruses were generated [190,205] (Fig 4.2.13).

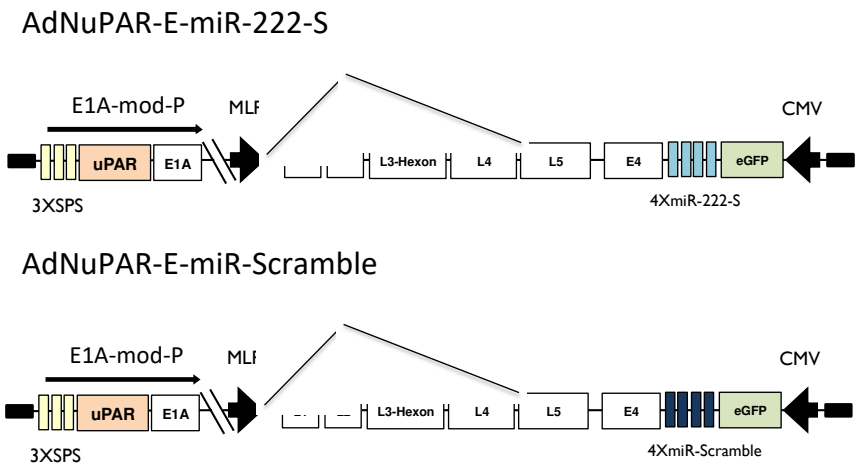

Figure 4.2.13 Schematic representation of AdNuPAR-E-miR-222-S and AdNuPAR-E-miR-Scramble backbones*. AdNuPARmE1A backbone was modified by the insertion of a construct comprising the CMV promoter with the eGFP and the sponge sequences, between the E4 and the right ITR.*

PANC-1 cells were infected with 10 IFU of both AdNuPAR-E-miR-Scramble and AdNuPAR-E-miR-222-S and mRNA eGFP expression was quantified. AdNuPAR-E-miR-222-S infected cells displayed reduced eGFP expression in line with miR-222 sponge control (Fig 4.2.14 A). Moreover, confirming the sponge activity, we observed a reduction of 25% and 30% for miR-221 and miR-222 expression, respectively, quantified at 24h, when compared to AdNuPAR-E-miR-Scramble infected cells (Fig 4.2.14 B).

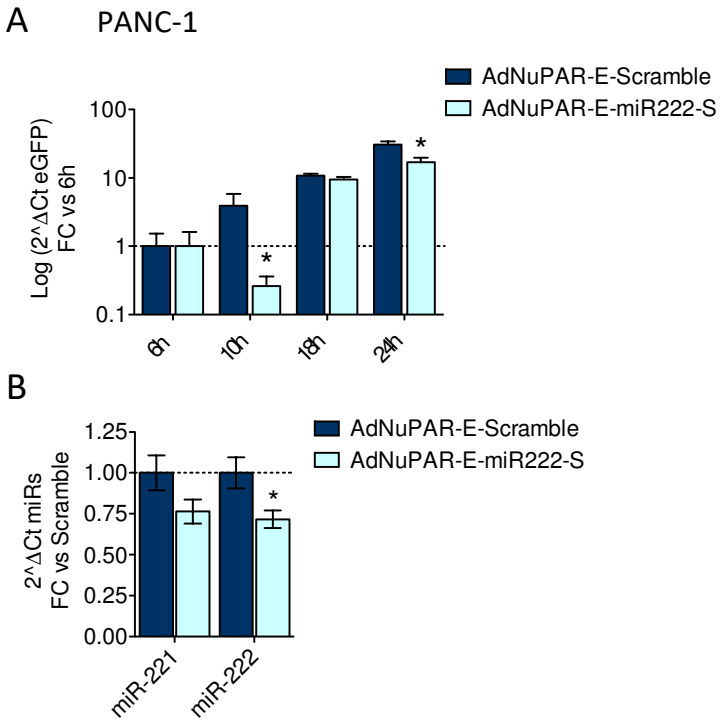

***Figure 4.2.14 Functional validation of sponges in AdNuPAR-E-miR-222-S infected PANC-1 cells. A**. 150000 c/w were seeded in 12 MW plate, and the day after infected with 10 IFU. Cells were collected at the indicated time points and eGFP expression was analyzed by qRT-PCR. Values are represented as fold change from the value at 6h for each virus. **B**. miRNAs quantification at 24 hours PI. MiR-221 and miR-222 were analyzed by qRT-PCR using TaqMan specific probes. Results are represented as FC with AdNuPAR-E-Scramble-infected cells. N>3, data are represented as mean ± SEM. *p<0.05, Non parametric Mann-Whitney U test.*

Then, we challenged adenoviral potency of AdNuPAR-E-miR-222-S and AdNuPAR-E-miR-Scramble in the PDAC cell lines PANC-1, MIA PaCa-2 and CP-15 Luc. Cells were treated with different viral dilutions and 7 days later viability was assessed by MTT assay. In all the cell lines, the viability curves for AdNuPAR-E-miR-222-S showed a shift to left, indicating increased sensitivity resulting in significantly lower ID50 with respect to Scramble-infected cells (Fig 4.2.15 A, B, C). Enhanced potency of AdNuPAR-E-miR-222-S was corroborated in a viral yield assay. We infected PANC-1, MIA PaCa-2 and CP-15 Luc with 1, 5 or 10 IFU respectively, and 72 h PI we collected cell supernatant containing viral particles.

Quantification of AdNuPAR-E-miR-222-S virions released from PANC-1 and MIA PaCa-2 cells showed a 1.5-fold increase in viral production of AdNuPAR-E-miR-222-S compared to AdNuPAR-E-Scramble. No significative differences were observed in CP15-Luc cells (Fig 4.2.16).

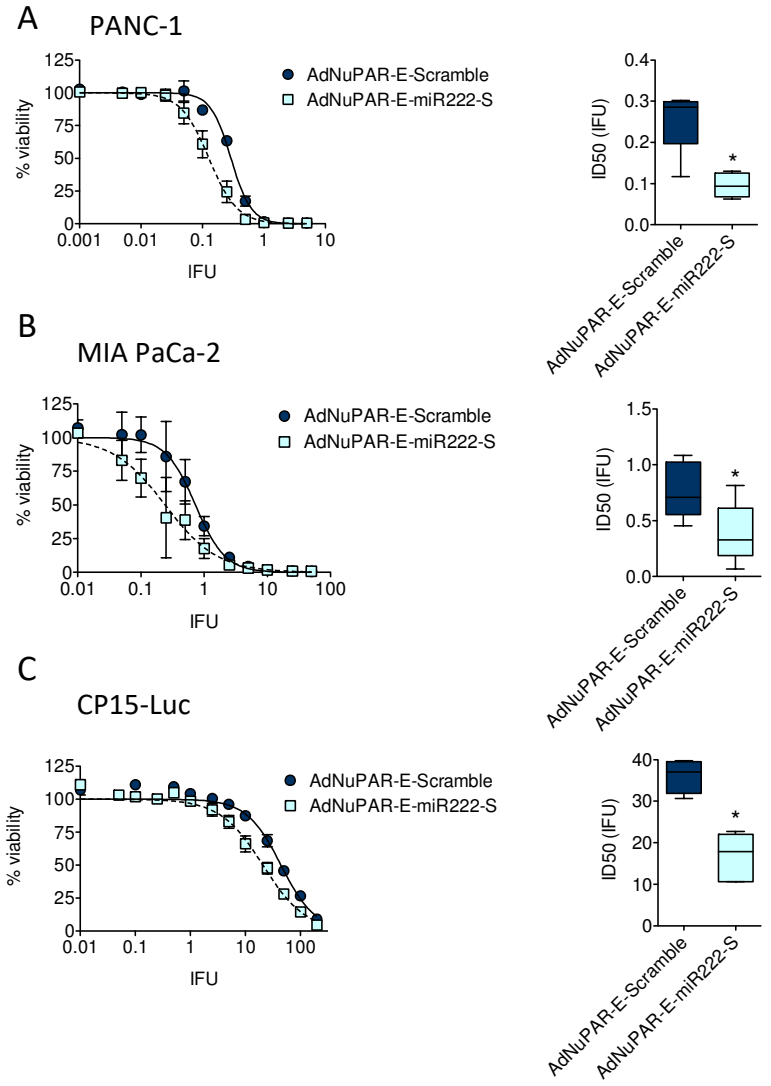

Figure 4.2.15 Cytotoxicity effects of AdNuPAR-E-miR-222-S in PDAC cell lines. A, B, C. *5000 cells of PANC-1, MIA PaCa-2 or CP15-Luc were seeded and the day after infected with serial doses of Ad5wt. Results were visualized 7 days later by MTT assay. Viability curves are represented by the panels on the left, ID50 values on the right. ID50 values were extrapolated from viability curves by non-linear regression with the help of GraphPad prism v5. N>4, data are represented as mean ± SEM. *p<0.05, Non parametric Mann-Whitney U test.*

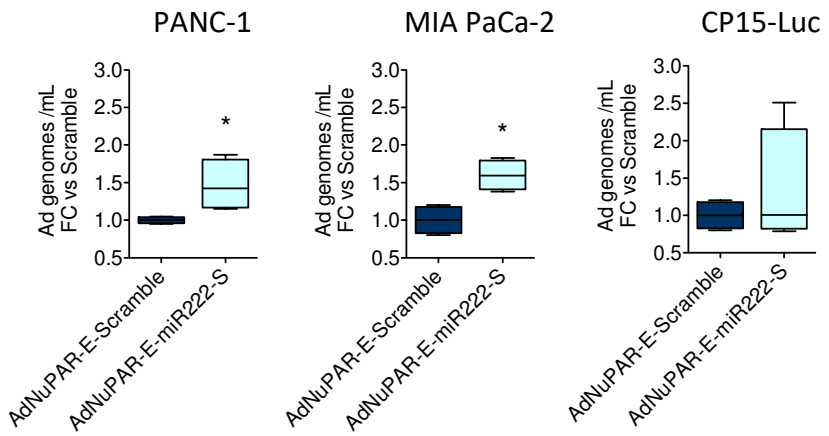

Figure 4.2.16 Viral release from AdNuPAR-E-Scramble and AdNuPAR-E-miR-222-S-infected PDAC cells. *50000 (PANC-1) or 100000 (MIA PaCa-2 and CP15-Luc) c/w were seeded and the day after infected with 1 (PANC-1), 5 (MIAPaCa-2) or 10 (CP15-Luc) IFU of both viruses. Four hours later, cells were washed three times with PBS and 500 µL of fresh medium were added to each well. Seventy-two hours after infection supernatants were collected and the amount of viral particles present were detected by qRT-PCR with adenoviral hexon specific primers. N =4, data are represented as mean ± SEM. *p<0.05, Non parametric Mann-Whitney U test.*

We also explored AdNuPAR-E-miR-222-S activity in PDAC derived organoids. We selected three different patients and first we analyzed miR-222 expression, confirming high miR-222 levels in all of them ($2^{\wedge-\Delta Ct}$ mean values: 35, 64 and 19 for IDIT4, IDIT5 and IDIT6, respectively). IDIT4, IDIT5 and IDIT6 PDOs were infected with 3 different doses of both OVs. Fluorescence intensity monitored during infections revealed no differences between viruses in terms of eGFP expression (Fig 4.2.17 A, B, C left panels). However, AdNuPAR-E-miR-222-S triggered highest cytotoxic effects than the Scramble OV, which was statistically significant at the 10^5 IFU/well doses in IDIT5 and IDT6 organoids (Fig 4.2.17 A, B, C right graphs).

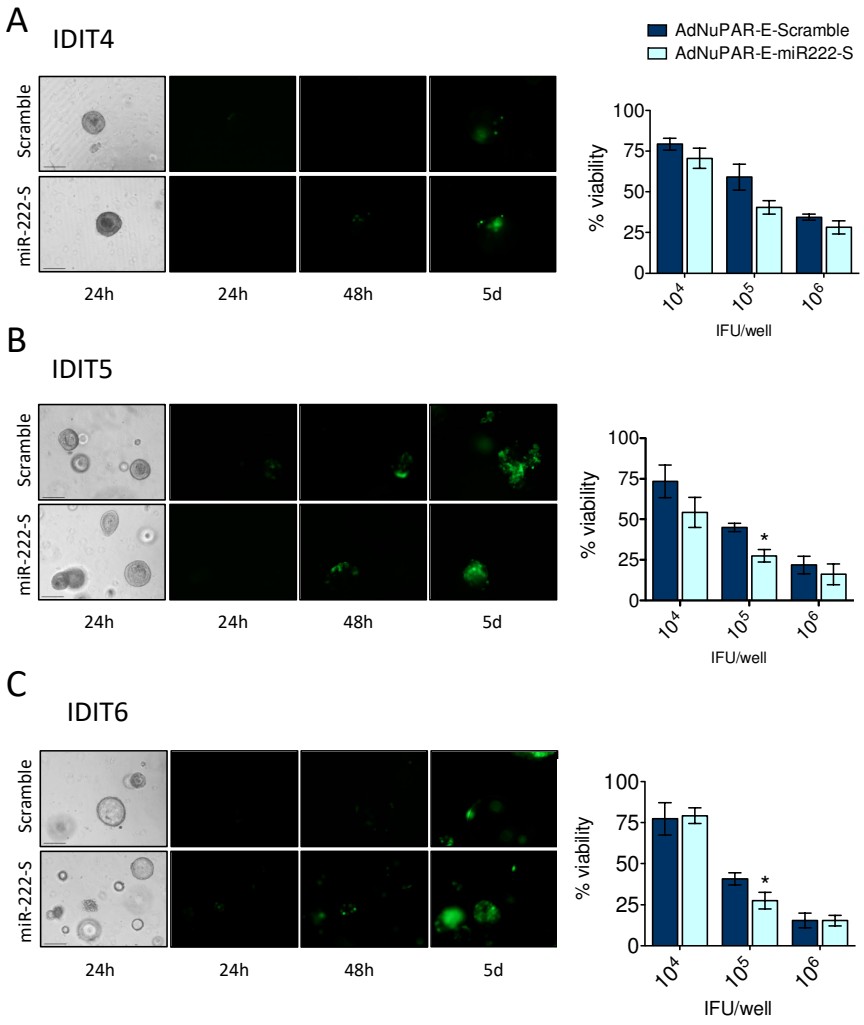

Figure 4.2.17 AdNuPAR-E-miR-222-S cytotoxicity in PDOs. A, B, C. *IDIT4, 5 and 6 organoids were infected with the indicated doses of viruses. Infection was monitored via eGFP detection in a fluorescence-inverted microscope 24, 48h and 5 days after infection. Cytotoxicity of the two viruses was measured on day 5 via an MTT assay. *p<0.05 Non parametric Mann-Whitney U test. N=5, data are represented as mean ± SEM.*

Altogether these results highlight that miR-222 sequestration by a sponge approach facilitates oncolytic adenoviral activity.

To evaluate the therapeutic effects of the AdNuPAR-E-miR-222-S *in vivo*, athymic nude mice bearing PANC-1 tumors received intravenously administrations of either saline solution or AdNuPAR-E-Scramble or AdNuPAR-E-miR-222-S ($5 \bullet 10^{10}$ vp/animal) and tumor growth was monitored twice a week. Both oncolytic viruses controlled tumor progression. Interestingly, AdNuPAR-E-miR-222-S displayed increased potency and the inhibition of tumor growth was consistently higher than that exerted with the Scramble virus (Fig 4.18 A, B).

These results highlight the therapeutic potential of arming adenoviruses with miR-222 sponges as a strategy to enhance viral oncolysis in PDAC tumors.

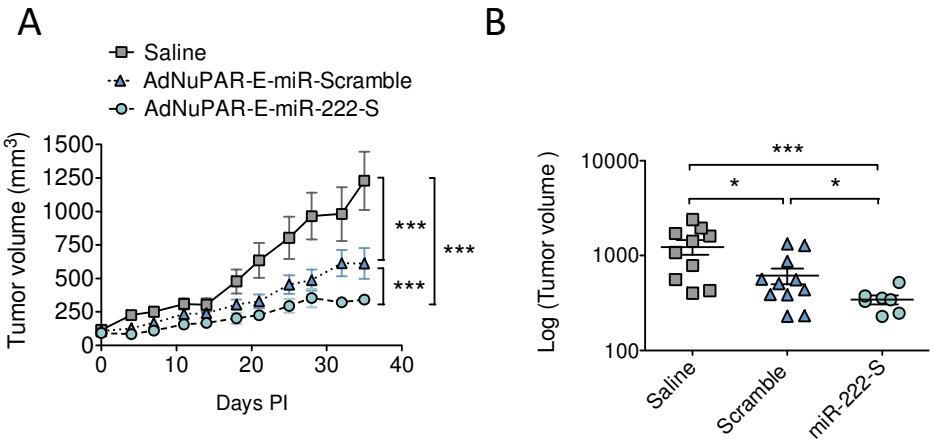

Figure 4.2.18 In vivo antitumor effects of AdNuPAR-E-miR-222-S. *Athymic nude mice were subcutaneously injected in both flanks with $2 \cdot 10^6$ c/flank of PANC-1 cells. When tumors reached 100mm³ animals were assigned to a group and treated either with Saline, AdNuPAR-E-Scramble or AdNuPAR-e-miR-222-S.* ***A.*** *Tumor growth follow-up. ***p<0.001 Tukey's Multiple comparison test.* ***B.*** *Tumor volumes at end point. The panel shows tumors mean volumes at the moment of sacrifice Number of tumors ≥8, data are represented as mean ± SEM. *p<0.01, ***p<0.001, Non parametric Mann-Whitney U test.*

4.2.6 Mechanistic insights of miR-222 on adenoviral activity

To elucidate the molecular mechanisms related to miR-222 modulation and adenoviral boosting, we analyzed miR-222 target genes by the PANTHER-GO software, based on gene ontology principles. We considered processes with p-values lower than 10^{-5}, and with potential impact in the adenoviral life cycle (table 4.2.3).

Gene ontology	Pathway	Hits	Expected hits	P value
Molecular Function	Nucleic Acid Binding	161	84.05	1.66E-16
Molecular Function	RNA binding	94	36.95	1.30E-15
Cellular Component	Nucleus	237	153.9	2.59E-15
Molecular Function	Organic cyclic compound binding	203	124.9	1.40E-14
Cellular Component	Cytosol	180	116.6	1.37E-11
Biological Process	Intracellular membrane-bounded organelle	289	228.3	5.29E-9
Biological Process	Cell cycle	75	39.39	1.69E-5

Biological Process	Gene expression	162	114.9	5.55E-5

Table 4.2.2. Pathways of hsa-miR-222 targets with potential effects on adenoviral infection

Using data extracted from Reyes and collaborators we selected 5 genes with miR-222 target sites whose expression was 2-fold higher during an adenoviral infection (data available from [223]):

- BPTF (Bromodomain PHD Finger Transcription Factor)
- DDX21 (Nucleolar RNA Helicase 2)
- KPNA2 (Karyopherin Subunit Alpha 2)
- NOLC1 (Nucleolar and coiled-body phosphoprotein 1)
- TCOF1 (Tetracle Ribosome biogenesis factor 1).

The interactions between miR-222 and the targets were bioinformatically predicted, but no experimental validation was performed, and no data were available from the literature. Nevertheless, we evaluated whether the depletion of miR-222 was associated with changes in any of the candidate target genes. For this, we analyzed the expression of each gene in PANC-1 and MIA PaCa-2 miR-222 KO cells. Interestingly, we observed that all the targets genes displayed higher expression in miR-222 KO than in the Ctrl cells reaching values up to 2/3-fold higher, suggesting miR-222 regulation (Fig 4.2.19 A). Next, we analyzed their expression in AdNuPAR-E-miR-222-infected PANC-1 cells and observed increased levels of the target genes in AdNuPAR-E-miR-222-

infected cells when compared to Scramble infected cultures, suggesting that miR-222 sponge rescued the expression of the target genes. (Fig 4.2.19 B left graph). Similar studies in MIA PaCa-2 cells showed a tendency to rescue the expression of the target genes, although no statistical significance was achieved (Fig 4.2.19 B right panel).

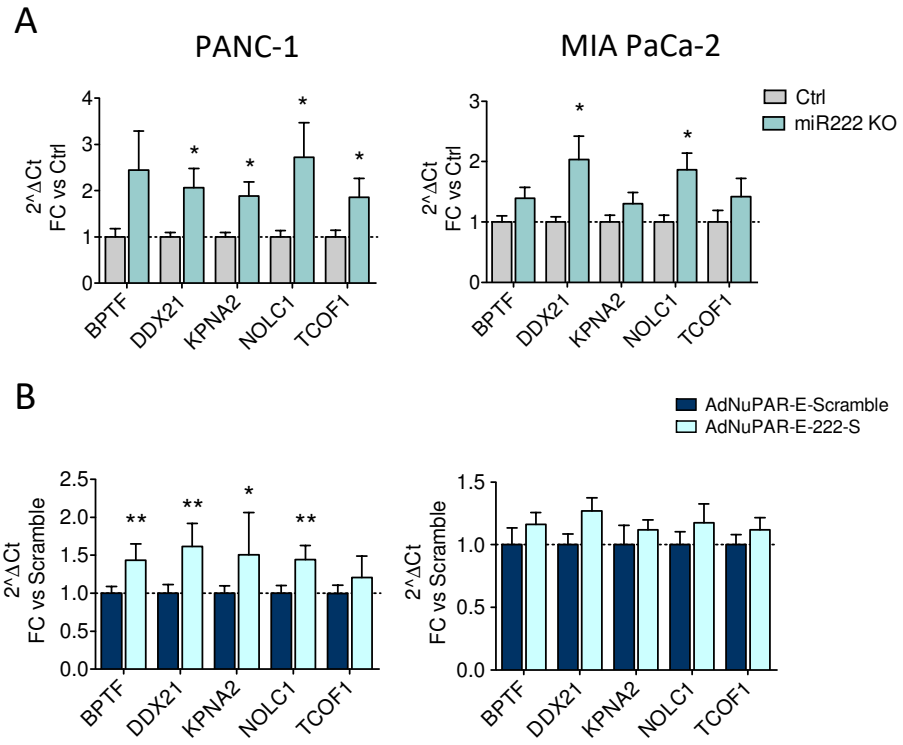

Figure 4.2.19 Identification of miR-222 molecular targets suspected to be implicated in oncolysis. ***A.*** *RNA from PANC-1 and MIA PaCa-2 cells KO for hsa-miR-222 was analyzed via qRT-PCR to evaluate expression of indicated targets. Values are represented as FC compared to level of expression in Ctrl cells.* ***B.*** *Expression of identified targets in PANC-1 cells infected with AdNuPAR-E-miR-222-S. Values are represented as FC comparing expression levels when infecting with AdNuPAR-E-Scramble. N>4, data are represented as mean ± SEM. *p<0.05, **p<0.01, Non parametric Mann-Whitney U test.*

NOLC1 and TCOF1 are proteins related to ribosomal biogenesis with a role on protein production [229]. BPTF is a chromatin remodeler, modulating gene transcriptional activity, and DDX21 helps RNA loops resolution during transcription acting as a transcriptional co-activator [230,231]. KPNA2 is a nuclear importin, favoring translocation of molecules to the nucleus [232].

Considering the molecular functions of the described targets, we hypothesized that changes in their expression could impact the virus, probably at several levels. We speculated that the protein VII of the adenovirus, strongly associated with the viral DNA, could bind KPN2A through any of the three NLS motifs and, as a consequence, facilitate the nuclear import of viral DNA [233]. KPN2A could also facilitate the nuclear translocation of other viral proteins needed for viral replication and or viral assembly. Thus, we decided to analyze the intracellular viral DNA content at different times PI in PANC-1 cells infected either with AdNuPAR-E-Scramble or AdNuPAR-E-miR-222 (2.5 IFU). Cells were harvested at 4, 8, 16, 20, 24 and 30h PI, and the intracellular viral DNA quantified. We observed a tendency to increased viral DNA content in AdNuPAR-E-miR-222-S infected cultures at 24h and 30h PI (fig 4.2.20).

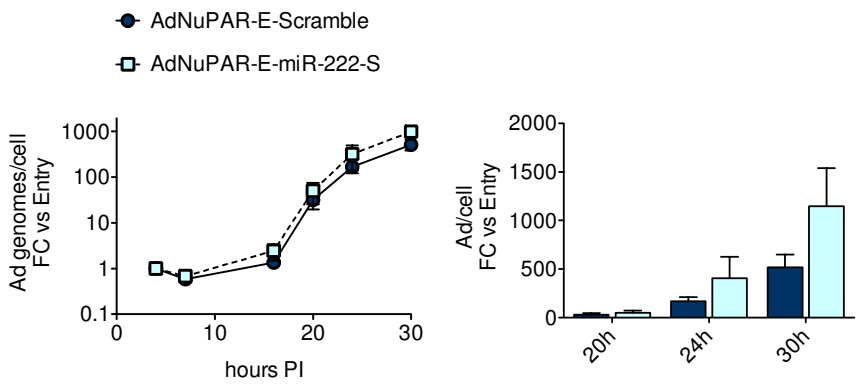

Figure 4.2.20 Intracellular viral DNA content of cells infected with AdNuPAR-E-miR-222-S and AdNuPAR-E-Scramble. *Monitoring of intracellular viral particles production during an infection with AdNuPAR-E-Scramble and AdNuPAR-E-miR-222-S. 50000 PANC-1 cells were seeded in 24MW plate. The day after, cells were infected with 2.5 IFU of both viruses and samples collected at the indicated time points. Cells were harvested and lysed to quantify viral genome by qRT-PCR using specific primers for adenoviral hexon. Results are represented as amount of viral genomes/cell, relativized to 4h values. Left panel represents the time course-follow up of the experiment, in right panel the last 3 time points are represented. *p<0.05, Non parametric Mann-Whitney U test. N=4, data are represented as mean ± SEM.*

Further studies are definitively needed to fully elucidate the miR-222 molecular mechanisms impacting adenoviral fitness, and it is likely that several of the identified targets could mediate in different processes of the adenoviral cycle.

4.3 Effects of miRNA reactivation on oncolytic adenovirus activity.

Modulation of miRNAs in malignancies demonstrated a critical role in the management of adenoviral potency ([94,190]; section 4.2). We wondered whether broadening the restoration of miRNA activity in cancer cells with the use of specific drugs could generate benefits on adenoviral oncolysis. THZ1, is a recently discovered drug with inhibitory effects on cyclin dependent kinase 7 (CDK7) and super enhancer driven genes, such as the MYC oncogene [234]. Particularly, THZ1 has been described to markedly downregulate MYC expression, leading to massive reprogramming of MYC-transcriptional regulation [234,235]. Since MYC-activation has been related to the repression of miRNAs as a consequence of MYC-binding to miRNA promoters, treatment with THZ1 could restore miRNAs expression.

We decided to investigate whether miRNA-modulation by THZ1 treatment could impact on adenoviral oncolysis and evaluate whether this strategy could have any advantage over miRNA-arming oncolytic viruses.

4.3.1 THZ1 cytotoxicity in PDAC cells and its effects in modulating miRNA expression

Treatment of PDAC in *in vitro* models with THZ1 has been poorly described [236]. To evaluate its effects, we screened its cytotoxicity in a battery of PDAC cell lines: ASPC-1, CAPAN-1, MIA PaCa-2 and PANC-1. Cells were treated with serial dilutions of the drug, and the effects were visualized 3 days later by MTT assay. Apart from ASPC-1, all the remaining cell lines showed relevant sensitivity to the drug, with ID50 at the micro (CaPan-1) and nanomolar (MIA PaCa-2 and PANC-1) order (Fig 4.3.1 A, B).

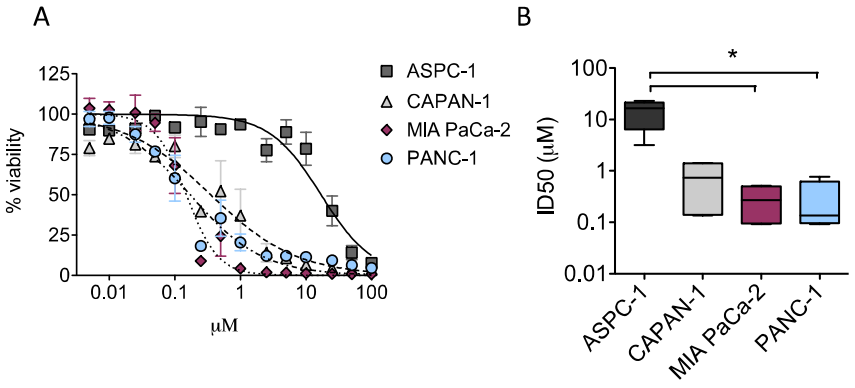

Figure 4.3.1 Cytotoxic effects of THZ1 in PDAC cell lines. ***A****. Viability Curves summarizing THZ1 effects at escalating doses 3 days after treatment. 5000 cells/well were seeded and the day after administered with serial dilution of THZ1. Results were visualized 72 hours later by MTT assay.* ***B****. ID50 values of the 4 different PDAC lines relative to THZ1 administration. Data were extrapolated from viability curves by non-linear regression with the help of GraphPad prism v5.0. N=4, data are represented as mean ± SEM. *P<0.05 Kruskal-Wallis test, with individual differences calculated via Dunn's Multiple Comparison Test.*

Next we analyzed the effects of THZ1 on MYC expression and consistent with previous data [235,237], we confirmed that THZ1 was

inhibiting MYC expression both in MIA PaCa-2 and PANC-1 cells (Fig 4.3.2 A).

MYC binding sites have been identified in the promoter regions of at least 10 pri-miRNAs, correlating their widespread repression to MYC-promoted tumorigenesis [75]. MiR-29c/b cluster's promoter was one of the genomic regions to which MYC directly associated [75]. We performed a bioinformatic study to reveal other miRNAs potentially repressed by MYC. Analyzing miRNA promoters in Genecard, we identified binding sites for MYC in the regulatory region of miR-99b and miR-485, two miRNAs previously reported to sensitize cells to adenovirus oncolysis [190].

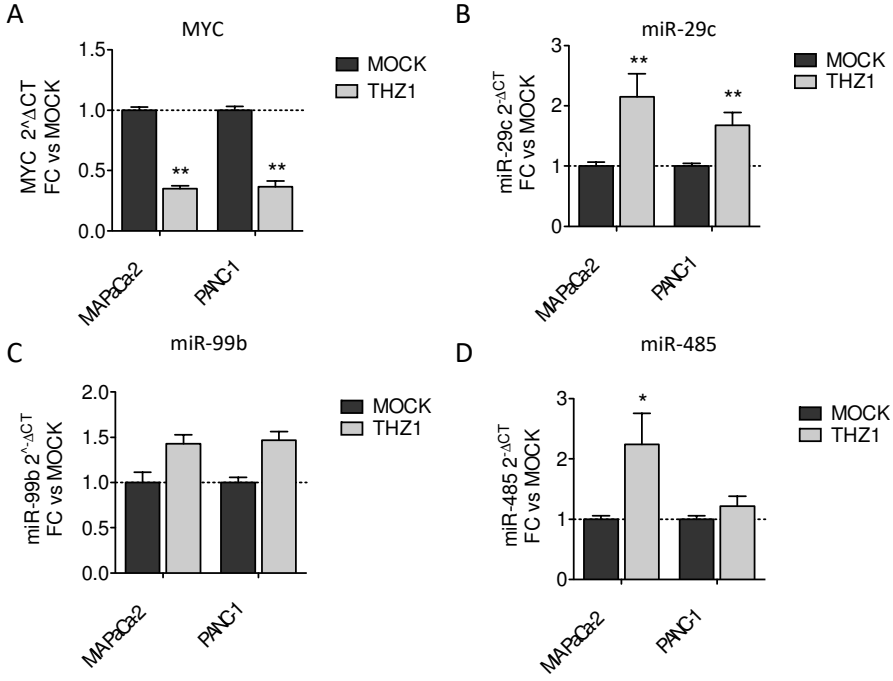

Figure 4.3.2 THZ1 effects over MYC and MYC-regulated miRNAs expression. ***A****. MYC Expression after 6 hours of treatment with THZ1. 150000 cells/well were seeded in a 12MW plate. The day after, medium was replaced with DMEM 10% containing 500nM*

THZ1 or DMEM 10% alone (500µL/well). 6 hours later cells were harvested by trypsinization and cellular pellet used for RNA extraction. MYC expression was quantified in MOCK and THZ1 treated cells via qRT-PCR. ***B,C,D****. miR-29c (****B****), miR-99b (****C****), miR-485 (****D****) expression after 6 hours of treatment with THZ1. Experiment was performed as in A. miRNAs quantification was performed by qRT-PCR using specific TaqMan probe assays. N≥4, data are represented as mean ± SEM. *p<0.05, **p<0.01, non-parametric Mann-Whitney U test.*

Considering these findings, we studied whether THZ1 treatment had any impact on the expression of MYC-repressed miRNAs. We analyzed the cellular content of miR-29c, and the potential MYC targets miR-99b and miR-485 in THZ1-treated cells. Interestingly, we observed that miR-29c expression was restored both in MIA PaCa-2 and PANC-1 cells, whereas miR-485 was only rescued in MIA PaCa-2 cells. Increased expression of miR-99b upon treatment was also observed in both cell lines although it did not reach statistically significance (Fig 4.3.2 B, C, D).

4.3.2 Cytotoxic effects of THZ1 and virotherapy combined treatment in PDAC cells

Considering the rescue observed in oncolytic sensitizer miRNAs after THZ1 treatment (Fig 4.3.2 B, C, D), we hypothesized that the drug could have positive effects on adenoviral oncolysis. Thus, we explored the impact of a combination treatment of THZ1 and Adwt adenovirus. MIA PaCa-2 and PANC-1 cells were treated with a battery of THZ1 and Adwt doses, alone or in combination. Cytotoxic effects were visualized 3 days later, revealing the presence of a moderate synergism in MIA PaCa-2 cells (Table 4.3.1). In these cells the combination treatment benefits Adwt and

THZ1 effects, resulting in ID50s significantly decreased when compared to unimodal treatment (Fig 4.3.3 A, B, C upper panel). A synergistic analysis by analyzing the combination index (CI) revealed that the combined treatment was synergistic. In contrast, PANC-1 cells did not benefit from the combination, showing individual or combined treatment with THZ1 analogous cytotoxicity effects (Fig 4.3.3 A, B, C lower panel).

These results suggested that the synergistic effects of Adwt and THZ1 treatment observed in MIA PaCa-2 cells could be at least partially explained by the restoration of the MYC-repressed miR-29c and miR-485.

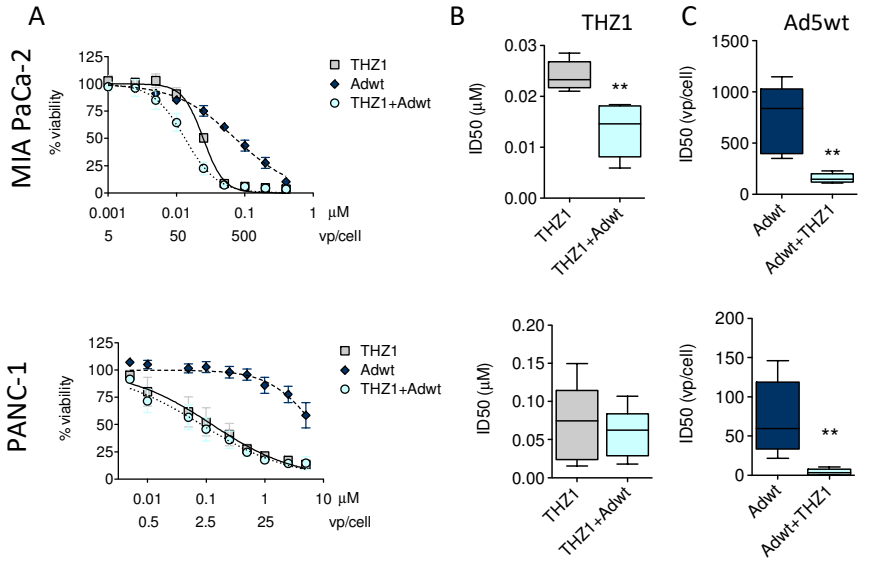

Figure 4.3.3 Cytotoxic effects of combination treatment of THZ1 and Adwt in PDAC cell lines. ***A****. Viability Curves for two different PDAC cell lines. Upper panel represents MIA PaCa-2 cells, lower panel represents PANC-1.* ***B****. ID50 relative to THZ1, calculated for both cell lines when the drug is used alone or in combination with Ad5wt. Upper panel represents MIA PaCa-2, lower panel PANC-1* ***C****. ID50 relative to Ad5wt, alone and in combination with THZ1. Upper panel represents MIA PaCa-2, lower panel PANC-1. N=4, data are represented as mean ± SEM. ** p<0.01, non parametric Mann-Whitney U test.*

Cell line	CI1 THZ1	CI2 Ad5wt	CI+C2	Synergy CI<0.8
MIAPaCa-2	0,56	0,21	0,77	YES
PANC-1	0,79	0,058	0,85	NO

Table 4.3.1. Evaluation of synergism between THZ1 and Ad5wt.

4.3.3 Comparative efficacy study of ICOVIR15-miR-29c with the combination regimen THZ1 and ICOVIR-15 in PDAC *in vitro* models

Interestingly, in our group Maria Rovira performed an *in vitro* library screening of miRNA-engineered adenoviruses, challenged in PDAC cells. This study identified an adenovirus expressing miR-29c being strongly enriched at the end of the bioselection strategy (data not published).

This observation, together with the results showing restored expression of miR-29c after THZ1 treatment associated to improved adenoviral oncolysis, prompted us to investigate whether miR-29c could be a sensitizer of adenoviral oncolysis. To that end, we introduced the ICOVIR15-E-miR29c previously generated in the laboratory and ICOVIR15-E (same of section 4.1) was used a control (Fig 4.3.4 A).

To test the OV functionality, we assessed miR-29c levels induced after ICOVIR15-E-miR-29c infection. Detection of miR-29c 24h PI

in PANC-1 cells revealed increased expression in a dose dependent manner (Fig 4.3.4 B).

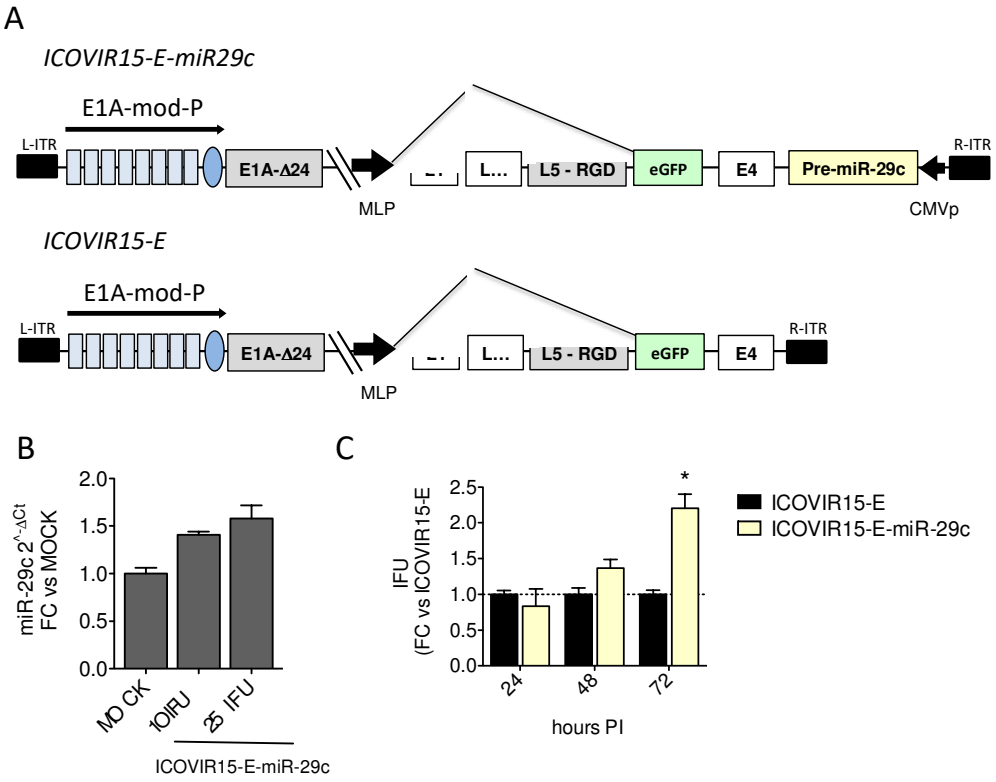

Figure 4.3.4 Evaluation of effects induced after miR-29c introduction in an oncolytic viral backbone. ***A****. Schematic representation of ICOVIR15-E-miR29c and its parental backbone ICOVIR15-E. Upper backbone represents ICOVIR15-E-miR29c, in which the genetic sequence of pre-miR-29c under a CMV promoter was inserted in the region between E4 and R-ITR. Lower backbone represents ICOVIR15-E, introduced in section 4.1.* ***B****. Quantification of miR-29c expression in PANC-1 cell line after infection with ICOVIR15-E-miR29c. 150.000 c/w were seeded in 12MW plate and the day after infected with the indicated doses of virus. Twenty-four hours later cells were harvested and miR-29c quantified by qRT-PCR using specific TaqMan probe assays. Values are represented as fold change values compared to MOCK condition.* ***C.*** *Infective Units in A549 cells coming from previously infected PANC-1 cell extract. 80.000 cells/well of PANC-1 were seeded in a 24MW plate and infected with 25 IFU. 24, 48, 72 hours post-infection cells and supernatant were harvested and submitted to freeze and thaw cycles. Lysates were centrifuged and supernatant used to infect A549 cells, previously seeded at 200.000 cells/well. 4 hours PI, A549 cells were washed three times with PBS and collected. Cellular*

*pellets were collected to quantify viral particles inside the cells by qRT-PCR using adenoviral hexon specific primers. N≥3, data are represented as mean ± SEM. *p<0.05, non parametric Mann-Whitney U test.*

Next, we studied whether miR-29c expression was triggering any effects on viral production. For this, PANC-1 cells were infected with 25 IFU of ICOVIR15-E or ICOVIR-15-E-miR29c and total cell extracts were collected 24, 48 and 72h PI. To estimate the number of infective virions produced, all the extracts were used to re-infect naïve A549 cells. After 4 hours of incubation, A549 cells were harvested and the content of viral genomes was measured. Interestingly, ICOVIR15-E-miR29c adenovirus produced the double amount of viral particles when compared to the parental virus ICOVIR15-E at 72 hours PI (Fig 4.3.4 C).

To further estimate the potency of ICOVIR15-E-miR29c, we designed an experiment that could illustrate the effects of consecutive infections, simulating what occurs during *in vivo* treatment. For this, PANC-1 cells were infected with a dose of either ICOVIR15-E or ICOVIR15-E-miR29c for 72 hours. Then, the supernatant was collected (I1) and used to re-infect naïve PANC-1 cells in 4 consecutive steps (I2, I3, I4) (represented in fig 4.3.5 A). The staining of viable cells with a dye revealed accumulating cytotoxic effects of ICOVIR15-E-miR29c at every round of infection (Fig 4.3.5 B). For every step, we collected the cell supernatant and quantified the virions released from cells. After 4 round of infections ICOVIR15-E-miR29c produced 30-fold more viral particles than ICOVIR15-E, calculated with respect of the viral particles released at I1 (Figure 4.3.5 C).

These preliminary results confirm the role of miR-29c in boosting adenoviral oncolysis, although the mechanism supporting miR-29c adenoviral sensitization remains to be elucidated.

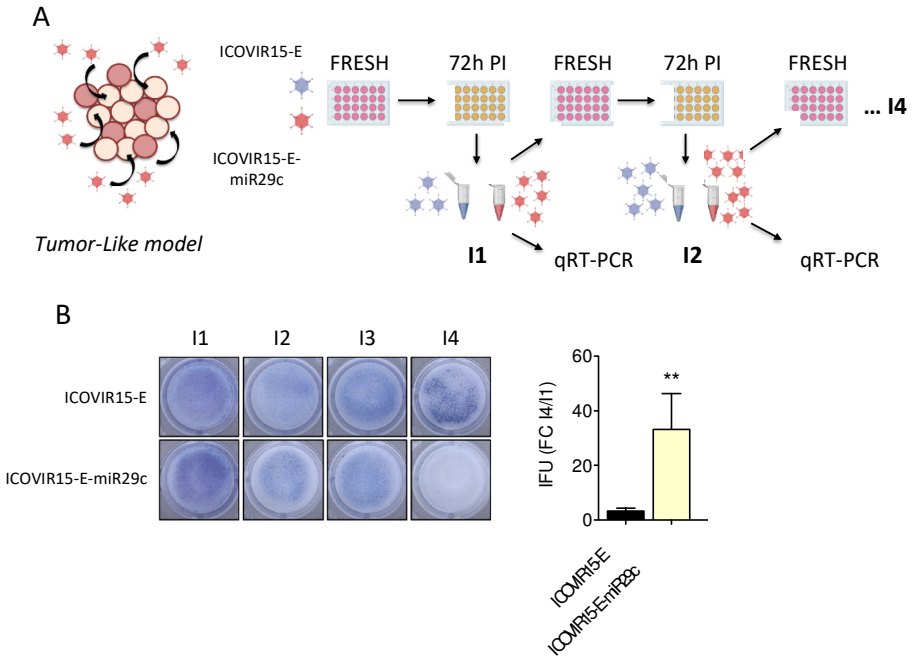

Figure 4.3.5. In vitro tumor-like model to further evaluate improved cytotoxicity of ICOVIR15-E-miR29c in comparison to the parental backbone. ***A****. Schematic representation of the experiment. Fresh PANC-1 cells were infected with 1 IFU of both ICOVIR15-E and ICOVIR15-E-miR29c. 72 hours later supernatant was collected (I1). Part of I1 was used to further infect naïve PANC-1 cells and 200µL went for viral particle quantification. The same procedure was repeated up to I4.* ***B****. Results obtained from the experiment. Left panel show methylene blue staining performed at the end of every round of infection. Bars graph on the right shows quantification of viral particles in I4 compared to the ones in I1 for each of the two viruses. **p<0.01, Non parametric Mann Whitney U test. N≥3, data are represented as mean ± SEM.*

To evaluate whether the combined THZ1 and ICOVIR15-E treatment had any advantage with respect to the restoration of miR-29c through ICOVIR15-E-miR-29c, we designed an experiment to compare the treatments. MIA PaCa-2 cells were exposed for 72 hours to serial doses of THZ1, THZ1 + ICOVIR15-E, ICOVIR15-E

alone and ICOVIR15-E-miR-29c. Results were visualized 3 days later by MTT colorimetric assay.

Both ICOVIR15-E-miR-29c and the THZ1 + ICOVIR15-E treatments improved the cytotoxicity of the parental ICOVIR15-E virus, although the combination of THZ1 plus ICOVIR15-E showed a tendency to higher cytotoxicity. This is not surprising since THZ1 cytotoxicity may also respond to mechanisms independent of miR-29c (Fig 4.3.6 A, B, C).

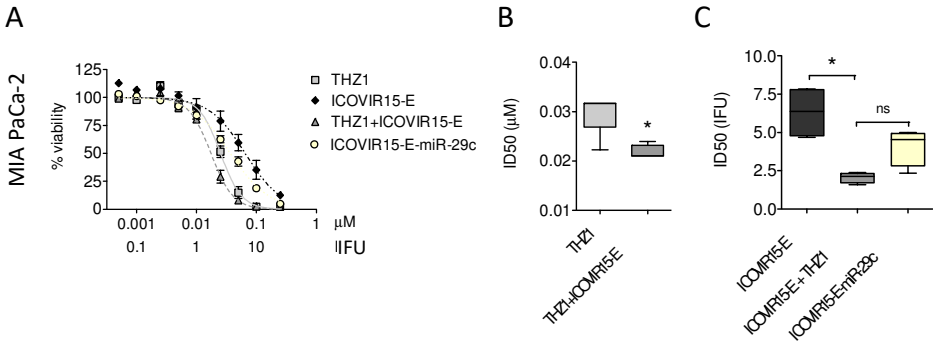

Figure 4.3.6. Evaluation of the cytotoxic effects exerted by ICOVIR15-E in combination with THZ1 compared to ICOVIR15-E-miR29c. ***A****. Viability curves at increasing doses of drug and/or adenoviruses, showing cytotoxicity 72 hours after treatment. 5000 cells/well were seeded and the day after administered with serial dilution of THZ1 and/or indicated adenoviruses. Results were visualized 72 hours later by MTT assay.* ***B, C****. ID50 values relative to THZ1 administration (B) and adenovirus treatment (C). Data were extrapolated from viability curves by non-linear regression with the help of GraphPad prism v5.0. N =4, *p<0.05, Two tailed non parametric Mann Whitney U test.*

Current studies are insufficient to identify the optimal treatment and further evaluations are required, in particular in *in vivo* studies. However, the presence of a sensitizing miRNA in an oncolytic virus backbone has the advantage to self-boost its own expression and propagate the infection. In contrast, the combination treatment will

probably require continuous administration of the drug what could trigger some undesired side effects.

5. Discussion

PDAC is a neoplastic malignancy with a very dismal prognosis. The majority of patients already presents with unresectable carcinomas at the time of diagnosis. Available therapies contribute very little to increase patients' survival, and surgical removal of the tumor remains the only available cure [7].

Predictivity of 2D cell lines for the screening of therapies in PDAC is extremely poor. PDXs, in which freshly resected human tumors are implanted into immunosuppressed mice, recapitulate various elements of tumor biology and can be more predictive of tumor-response to different treatments. The use of humanized PDX models in the presence of an intact human immune system is a very attractive strategy. However, all these models are complex and very time consuming for a broad preclinical testing of personalized treatments [95,105,238]. The advent of organoids introduced a revolution in the study of cancers, permitting the analysis of patients-derived tissues and their response to treatments in a simpler model within a short time frame. Organoids maintain genomic and histopathologic similarities with their tumor of origin and several studies have shown its predictive value in terms of response to therapies. These characteristics are converting the organoids system in a valuable tool for the study of PDAC *in vitro*.

Genetic heterogeneity of PDAC tumors makes this malignancy less suitable for treatment with conventional chemotherapies. Oncolytic virotherapy is showing promising results in clinical trials for the treatment of solid tumor. However, oncolytic adenoviruses as

monotherapy are not strong enough to completely ablate tumor mass, and they are often co-administered with chemotherapy or immune modulators [132,139].

Improvement of oncolytic adenoviral potency is investigated by arming adenoviruses with transgenes to provide additional antitumor functions. More recently, our group showed that the introduction of miRNAs sensitizers of adenoviral oncolysis can also improve adenoviral antitumor efficacy *in vivo* in PDAC xenografts [190].

Considering the state of art, this thesis focused on the development of organoids technology to evaluate its utility for predicting patient-specific responses to oncolytic adenoviruses in PDAC. Moreover, we explored different strategies to modulate the deregulated miRNome in PDAC to boost adenoviral oncolysis.

5.1 Organoids as a predictive translational model to screen for personalized oncolytic adenoviral therapies

In the current work, for the first time, we demonstrate the feasibility of PDAC organoids as a valuable tool to study oncolytic virotherapy.

The capacity of adenoviruses to transduce organoids was already described in intestinal organoids, and in this study the authors showed with a replication-deficient adenovirus the expression of a transferred transgene up to 7 days [211]. Our data supports the infectivity of organoids cultures in a different model, the PDAC organoids. With the use of a replication-competent adenovirus armed with eGFP, we were able to show that adenoviruses not only infect organoids, but also replicate and spread to adjacent cells, as we demonstrated by monitoring eGFP and viral production after several organoid passages. These results suggested the potential of PDAC organoids to study oncolytic virotherapy.

One of the concerns of oncolytic adenoviral treatments is safety, mostly associated to limiting viral lysis to cancer cells, leaving healthy cells unharmed [240]. The availability of non-transformed pancreatic tissues allowed us to demonstrate the utility of organoids in the study of adenoviral oncoselectivity. Low eGFP spread in the infected IDIS0 and IDIS6 over time suggested impaired viral replication of AdNuPARmE1A and ICOVIR15. In the cytotoxicity studies some mortality was observed in healthy organoids when infected at at 10^5 pfu/well, likely due to the high presence of viral DNA and proteins inside the cells, generating cytotoxicity. In AdNuPARmE1A-infected normal organoids, some of the residual activity, observed with eGFP monitoring or with the cytoxicity effects, could also be linked to the expression of stemness and embrionary genes in the pancreatic progenitors giving rise to healthy organoids [210]. Notch activation levels regulate pancreatic

development and the fate of pancreatic progenitors [241,242]. It is highly probable that the active Notch signaling in these cells could stimulate AdNuPARmE1A, resulting in viral production. The fact that AdNuPARmE1A and ICOVIR15 activity in IDIS0 and IDIS6 was diminished with respect to that of Adwt, was in line with the good safety profile of both viruses in immunocompetent mice [172,173]. Of course, organoids screening will not substitute the toxicity studies in animals, but they might offer a first analysis to select for optimal candidates.

One of the attractive interests of organoids is their potential predictivity in terms of therapeutic-response to treatments. Besides general sensitivity of the five studied PDAC organoids to adenoviral infections, we identified inter-patient diversity in the response to adenoviruses. The dissimilarity was aligned with the variable expression of genes encoding cellular factors that regulate viral activity. For instance, the Notch-sensitive uPAR-regulated oncolytic adenovirus AdNuPARmE1A was more effective in PDOs with upregulated Notch signaling pathway and uPAR transcriptional activity. Although we did not investigate further mechanisms behind ICOVIR15 activity, it is likely that the study of *RB* mutational status and its pathway could help in this direction. Moreover, ICOVIR15 has a fiber characterized by the insertion of an RGD motif, lacking in AdNuPARmE1A, permitting adenovirus entry both via integrin and CAR recognition. Considering the gradual loss of CAR observed in gastro-intestinal tumors[165],

expression profiles of integrins and CAR in PDOs could help to explain the different grades of cytotoxicity observed.

Our study also showed the utility of the well-defined model of PDOs to screen for armed oncolytic viruses that bear inserted transgenes that provide enhanced viral fitness. The increased viral cytotoxicity of ICOVIR15-miR-99b and AdNuPAR-E-miR-222-S, with respect to their corresponding parental virus in different PDOs, supports this notion.

However, the lack of stromal elements from the tumor microenvironment in the current organoids system limits the evaluation of novel oncolytic adenoviruses engineered with transgenes modulating TME to facilitate viral oncolysis. The generation of more complex patient-derived models including CAFs, immune cells and organoids would expand the number of oncolytic adenoviruses to test, and thus enlarge the merits of this approach.

Studies in a higher number of PDAC organoids and with an extended battery of viruses will increase the robustness of validating the organoids model for virotyping. In this study all the organoids were originated from patients undergoing surgical operation. In the future we aim to incorporate organoids from PDAC biopsies obtained by EUS-guide fine needle aspiration, as has been lately demonstrated to successfully generate organoids with high efficiency [115,243]. This new paradigm would allow the therapeutic testing at the time of initial tumor diagnosis.

The possibility to establish a correlation between organoids-sensitivity to oncolytic viruses with patient-responses to the treatment would be a step forward to position organoids as a clinical meaningful platform to predict patient-oncolytic response. Unfortunately, we could not perform this correlation since the studied viruses were not in clinical trials. The concordance between PDOs and patient-response to treatment has been nicely studied in a pharmacotyping study in PDOs, in which chemorefractory PDOs showed sensitivity to alternative therapeutic agents [115].

The heterogeneous nature of cancer highlights the need of joining forces to develop combination therapies. Oncolytic viruses undergoing clinical trials showed better response rate when administered in combination regimens. The oncolytic adenoviruses LOAd703 [244] and VCN-01 [185] are currently administered with the combination of gemcitabine and nab-paclitaxel for the treatment of local and advanced PDAC [126,132]. Our results validated the benefit of combining the standard chemotherapeutic regimen of gemcitabine + nab-Paclitaxel with oncolytic adenoviruses using the preclinical models of PDOs, recapitulating the synergism already observed in pancreatic cancer cell lines, 3D spheroids and PDXs [172,245].

The high metastatic ability of PDAC makes this malignancy to be already a systemic disease at the moment of diagnosis [246]. Systemic administration of oncolytic adenoviruses can be a valuable strategy to reach both primary tumors and metastatic foci. However,

availability of metastases from PDAC patients is very limited, and generally obtained post mortem, restricting organoids generation to a very small number of patients [115]. In this study, we addressed the study of oncolytic adenoviruses in metastasis-derived organoids with the generation of a model of metastasis induced by the orthotopic implantation of PDOs in mice. The formation of metastatic foci in diaphragm and liver, recapitulating common features of PDAC metastatic evolution, supported the model [247]. Interestingly, the small metastases showed extreme propensity to form organoids, probably due to a strong amount of CSC in the invasive front of pancreatic tumors, populating metastasis in a high number and thus facilitating organoids generation [248].

Our metastatic model evidenced a significant degree of aneuploidy in line with the genomic complexity and instability of PDAC tumors. Higher chromosomal alterations were present in the metastatic foci confirming a parallel evolution of chromosomal instability with the invasive phenotype [249,250]. Interestingly, AdNuPARmE1A and ICOVIR15 tested in organoids derived from primary tumors and metastases showed similar responses and matched PDO sensitivity. However, this might not be the case for any oncolytic adenovirus, since preferential killing of high-metastatic versus low metastatic cells have been reported for the replication-selective adenovirus vector OBP-401 [251]. Ideally, to elucidate the optimal adenoviral activity in metastatic nodules, OA screening should be performed in PDOs derived from patient metastases. However, in the absence of metastatic biopsies, our

results provide an indication that OA screening in PDOs derived from primary tumors still reflects their activity in metastatic foci.

All together, these results show that virotyping in organoids is feasible and inter-patient sensitivities can be identified, suggesting that PDOs may represent in the future an easy-to-handle platform to help on virotherapy-based, personalized treatment decisions.

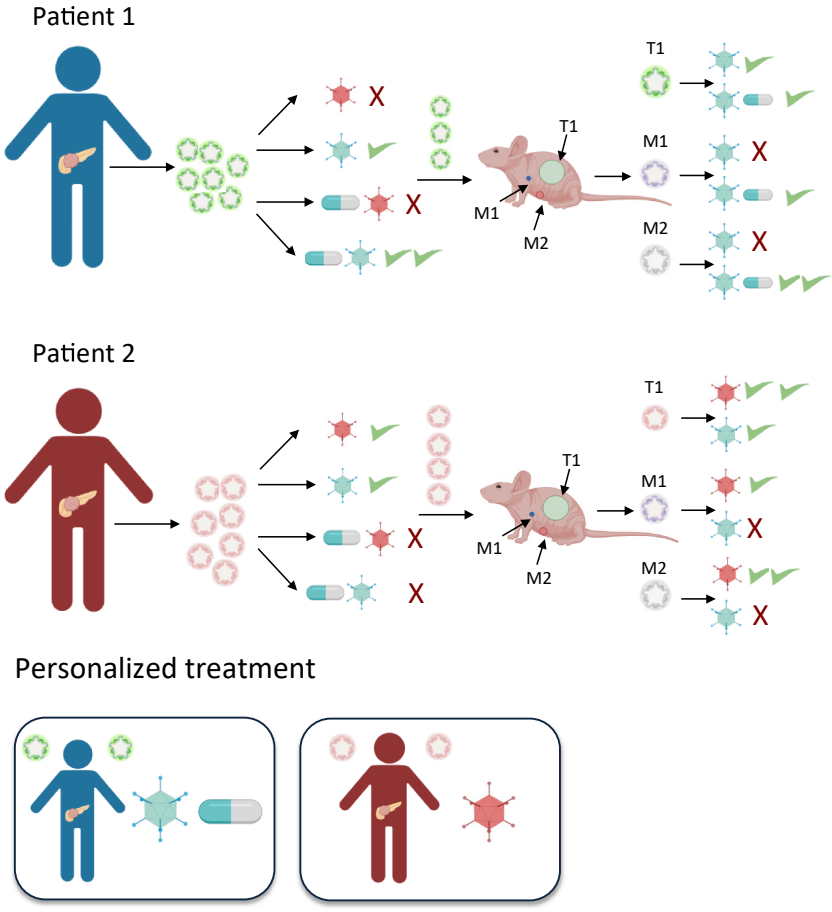

Figure 5.1 PDOs can help on virotherapy-based, personalized treatment decisions. T stays for tumor (orthotopic) and M stays for metastasis.

5.2 miRNAs impact adenoviral infection. Enhanced adenoviral oncolysis in PDAC can be achieved by inhibition of miR-222 content or reestablishment of miR-29c activity.

MiRNAs were shown to play a role in the replication and propagation of viruses, including the activation of cellular antiviral responses or the promotion of viral infections. In fact, normal miRNA profiles are profoundly altered during an adenoviral infection in the context of normal cells. The adenovirus manipulates miRNAs to propagate, whereas the cells reshape miRNAs to counteract the viral infection, generating a complex crosstalk between miRNA pathways and viral infections [93,252]. In PDAC cells there is an important deregulation of miRNA levels [253,254]. This perturbed miRNome might either favor adenovirus infection or, on the contrary, interfere with viral propagation. Deciphering the role of miRNAs in adenovirus infection can contribute to the development of more efficacious oncolytic viral therapies.

In this work, we broadened the concept of miRNAs in oncolysis, showing that miRNAs expression impacts adenoviral fitness in different directions. We explored the consequences provoked by the removal of upregulated miRNAs in PDAC or by the restoration of miRNAs whose expression is gradually lost in PDAC and observed

that their modulation could impact positively or negatively the adenoviral life cycle.

With the generation of miRNA KOs, we evaluated the role of upregulated miRNAs in PDAC during adenoviral infections. In contrast, by the treatment with the transcriptional regulator THZ1, we rescued miRNAs poorly expressed in PDAC, what helped us to study their effects on oncolysis.
We showed how miR-21 and miR-93 might have a key role for adenoviral propagation, since KOs of either miRNAs strongly interfered with adenoviral activity. Opposite effects were observed with miR-222 since its removal facilitated oncolysis. On the other hand, THZ1 treatment mediated the rescue of miR-99b and miR-485 and confirmed their role as adenoviral sensitizers [190]. Furthermore, this treatment facilitated the discovery of miR-29c as a novel miRNA that promotes adenoviral infection.

The impaired adenoviral activity observed in miR-21 and miR-93 KO cells could be, at least partially, related to the role of this miRNAs in repressing cells' innate immune response. Both miRNAs act by repressing the interferon response. In the case of miR-93 it regulates the c-GAS/STING pathway, inhibiting the production of type I interferon, thus creating the conditions to facilitate viral propagation (Wu et al., 2017). MiR-21 targets MyD88 and IRAK1, two components of the Toll-like receptor signaling pathway that leads to type I interferon production. The downregulation of these two molecules by miR-21 has been shown

to repress type-I interferon and promote Hepatitis C viral infections [255,256].

Moreover, miR-21 exerts anti-apoptotic effects, inhibiting tumor-suppressor molecules, and induce proliferation, actions probably required by the virus to complete its lytic cycle [257].

Among the intricate networks of interactions that occur between the virus and the host cell upon an infection there are important changes in the miRNAs profile. Studies monitoring miRNA levels during an adenoviral infection evidenced miR-93 as s stable miRNA at early time points and upregulated at later phases of infections. This suggests that miR-93 would be important to complete viral infection, in line with our observation that its KO hampered adenoviral fitness [93]. In the same study, the authors observed that miR-21 was highly downregulated only at 12h PI but no changes were observed at later time-points 24h and 36h PI, suggesting the need of fluctuating levels of this miRNA during the course of an infection, and that the presence of miR-21 particularly at late phases should be important to complete the adenoviral cycle. Thus, a scenario of steady-state KO of miR-21 will hamper viral fitness, whereas a minimal expression would be sufficient to maintain good viral activity This support the results obtained with miR-21 KO, in which residual levels of miR-21 in pools of PANC-1 and MIA PaCa-2 were sufficient to maintain normal adenoviral activity. On the contrary, adenoviral activity was strongly impaired in PANC-1 KO1/2, in which miR-21 levels were completely abolished.

Our data supports miR-222 as a miRNA that, at least in excess, can interfere with adenoviral replication. In fact, miR-222, KO both in PANC-1 and MIA PaCa-2 cells boosted adenoviral activity. Interestingly, the modulation of miR-222 content in the cells, by miR-222 sponges, after infection with AdNuPAR-E-miR222-S resulted in enhanced sensitization of adenoviral oncolysis.

The finding that miR-222 inhibition can favor viral fitness is not new. Screening in prostate cancer cells showed that miR-222 downregulation by miR-inhibitors favored adenoviral propagation [94]. Reduced levels of miR-222 were also observed upon Epstein Bar Virus (EBV) and Herpes Simplex Virus (HSV) infections, favoring their viral activity [258,259]. Both EBV and HSV are also dsDNA viruses and it could be speculated that miR-222 acts over mechanisms commonly exploited by the three viruses. In fact, a recent work comparing proteomes associated with replicated DNA of three DNA viruses Ad5, HSV1 and Vaccinia Virus (VACV) provides information about host factors and cellular pathways potentially exploited by the viruses during infections (Reyes 2017).

The same study identified enriched host factors that aid adenoviral replication during an adenoviral infection. Interestingly, through a bioinformatic analysis we identified that five of these genes: BPTF, DDX21, KPNA2, NOLC1 and TCOF1 contain in their 3'UTR miR-222 target sites, indicating their susceptibility to be regulated by miR-222. If so, it can be speculated that in PDAC cells some of those genes would be maintained at low levels limiting viral infection, as a consequence of the high upregulation of miR-222. These would be in line with the increased oncolysis triggered by

AdNuPAR-E-miR222-S, and with the rescued expression of these genes when miR-222 was inhibited, either by KO or by miR-222 sponges.

The infection of AdNuPAR-E-miR222-S cultures resulted in higher amounts of mature virions released when compared to the Scramble virus, accompanied by increased viral DNA inside the infected cells. Since viral DNA replication does not seem to be a limiting factor during an infection, it is likely that the potential role of the 5 identified molecules would facilitate AdNuPAR-E-miR222-S through the whole course of infection: by favoring both DNA synthesis, viral genes expression and viral protein translation.

By analyzing the function of these proteins, we can speculate some comprehensive mechanisms to explain the improved AdNuPAR-E-miR-222-S activity. After virion disassembly, the naked viral DNA enters to the nucleus by the nuclear pore complex. Viral DNA arrives at the pore complex associated to protein VII. Through its three potent nuclear localization signals (NLS) protein VII binds multiple import proteins and translocate into the nucleus together with the viral DNA[233]. KPNA2 recognizes NLS on proteins, mediating their translocation to the nucleus [232]. Then, protein VII could bind KPNA2 and promote the efficient nuclear entry of the viral genome [233]. Inside the nucleus, the expression of adenoviral genes happens gradually, starting with the early genes codifying for viral polymerase [260]. However, viral gene transcription is still dependent on the host cell machinery to transcribe viral mRNAs and translate them to proteins [261]. The cellular factors BPTF and DDX21 can help the adenovirus in the processes involving gene

expression. BPTF has chromatin remodeler activity and might re-direct cell chromatin conformation in favor of a permissive adenoviral lytic cycle [260,262]. DDX21 has a RNA/DNA helicase activity that might be helping in the transcription of the viral genes, resolving eventual conformational problems [263]. Interestingly, DDX21 activity is necessary for expression of CMV genes, resolving R-loop formation during viral genes transcription [264], exerting a similar role in HIV gene expression [265]. Finally, changes in the expression of TCOF1 and NOLC1 might also contribute to adenoviral infection. TCOF1 regulates ribosomal DNA transcription and processing, forming with NOLC1 a scaffold that recruits the ribosomal polymerase RNA POL I. Adenoviral infection of TCOF1 KO cells, impacted the localization of NOLC1 away from sites of Ad replication, reduced viral genome accumulation and diminished viral yield, suggesting a relevant role for TCOF1 in viral infections [223]. To sum up, the re-expression of these factors, by miR-222 downregulation, either individually or in combination, can facilitate adenoviral replication. However, to fully understand the position of these proteins as mediators of adenoviral lytic cycle, further investigations are required.

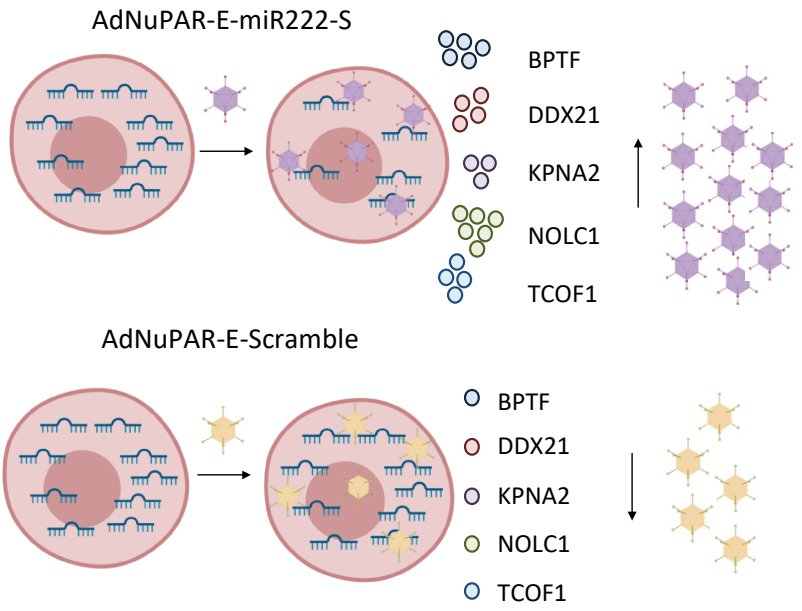

Figure 5.2. Molecular mechanism proposed for the improved adenoviral activity observed in AdNuPAR-E-miR222-S infected PDAC cells.

Apart from the cellular effects of AdNuPAR-E-miR222-S infection leading to superior viral yield and enhanced oncolysis, our data also showed a remarkable control of tumor progression when AdNuPAR-E-miR-222-S was administered *in vivo* in mice bearing tumors. Contributing to this antitumor effect there are probably the tumor suppressor effects of reducing miR-222 in the cells. The cluster miR-221/222 inhibits Cip/Kip family of cyclin dependent kinases (CDK) p27 and p57, resulting in uncontrolled proliferation [193,225]. Indeed, the good antitumoral activity observed with AdNuPAR-E-miR-222-S *in vivo* is probably the combination of enhanced oncolysis and the sequestration of the pro-tumorigenic miR-222, both contributing to hamper tumor growth.

Treatment with THZ1 suppressed MYC expression, in line with previous results [235]. Interestingly, we could demonstrate that this treatment rescued the expression of miRNAs with binding sites in their promoter region for MYC transcription factor, the miR-99b, miR-485 and miR-29c. Moreover, our data showed that THZ1 treatment was synergistic with adenoviral lysis, suggesting cooperating mechanisms. Although there might be several possibilities, we considered that the re-expression of miRNAs facilitating oncolysis, such as miR-99b and miR-485 could contribute to these effects. Interestingly, we could also demonstrate that miR-29c, when expressed from the virus, strongly boosted its fitness, achieving ICOVIR15-E-miR29c a viral yield 30 times higher than the parental ICOVIR15-E virus.

The mechanisms behind miR-29c sensitization have not been explored yet. However, data from the literature helped to formulate some hypothesis. Several studies demonstrated that miR-29c protected the expression of the deubiquitination enzyme A20, essential for the homeostasis of the immune system and inhibiting NFKβ activity, mechanism observed to reduce the antiviral response in cells infected by influenza virus [87].Other studies have shown that miR-29c indirectly inactivates STAT1 signaling, required by the cells to react against the virus [266–268].

Thus, similarly to what we observed with miR-93 and miR-21, miR-29c could act to counteract cell immune response to the virus,

emphasizing the idea that deregulation of miRNAs impacting on the host antiviral response can influence adenoviral oncolysis.

The ICOVIR15-E- miR29c could be a very good candidate for *in vivo* administration, since, in addition to the effects favoring adenoviral oncolysis, many tumor suppressor activities have been associated to this miRNA, with emphasis on its anti-proliferative role. Moreover, miR-29c tightly regulates ECM remodeling factors, such as MMP2 and SPARC, impairing tumor progression and formation of metastasis [84,86,269]. Considering the desmoplatic reaction taking place in PDAC tumors, the re-introduction of miR-29c could help to reduce ECM production, thus facilitating viral spread in the tumor.

Altogether, these results highlight the strong impact exerted by miRNAs on adenoviral infections. Different outcomes were observed depending on the miRNAs and on its targets, although in all the cases miRNA modulation impacted adenoviral fitness. Interestingly, we managed to boost adenoviral activity in PDAC cells with an altered miRNome by either inhibiting miR-222 or re-expressing miR-29c. We propose two novel oncolytic adenoviruses with increased potency, the AdNuPAR-E-miR-222-S and ICOVIR15-E- miR29c as good candidates for further development.

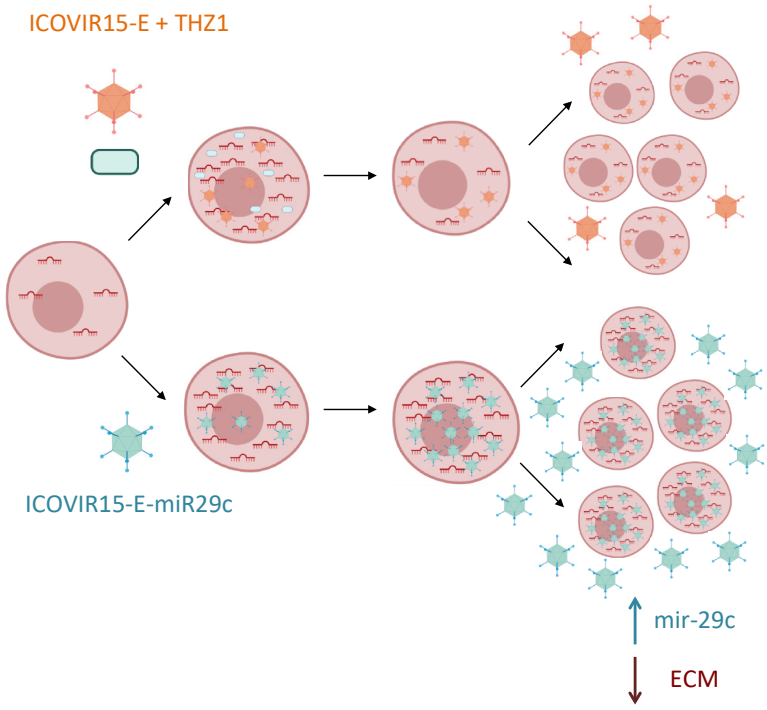

Figure 5.3 Re-expression of miR-29c favor adenoviral oncolysis, and its introduction in an oncolytic adenoviral backbone is envisioned to generate good antitumor effect in vivo.

6. Conclusions

1) Organoids can be successfully generated from patients' healthy pancreas and PDAC, and from primary tumors and metastases established in nude mice.

2) Adenoviruses infect and propagate in patient-derived organoids (PDOs).

3) PDOs can be used as a platform to identify patients' sensitivity to OVs and evaluate their effects in combination with chemotherapy.

4) Metastatic response to OV in mouse models, mirrored patients' response in PDOs primary tumors, suggesting that sensitivity to OV in primary tumors can predict metastases response to OV treatment.

5) Deregulation of miRNAs in PDAC has a strong impact on adenoviral oncolysis.

6) miRNA-222 sponges engineered in the AdNuPAR-E-miR-222-S downregulate miR-222 and improve adenoviral fitness, probably facilitating adenoviral DNA replication and viral particles production.

7) AdNuPAR-E-miR-222-S triggers high cytotoxic effects *in vitro* and a strong antitumoral activity *in vivo*.

8) THZ1 treatment restores the expression of MYC-regulated miRNAs and synergizes with adenovirus activity to enhance cytotoxicity of PDAC cells.

9) ICOVIR15-E-miR29c, by restoring miR-29c in PDAC cells, displays improved adenoviral oncolysis.

7. Bibliography

1. Dongmei, C. *et al. Atlas of Histology with Functional and Clinical Correlations*. *Assiut Journal of Environmental Studies* (2011).

2. Molnar, C. & Gair, J. Concepts of Biology-1st Canadian Edition. *Concepts Biol. Can. Ed.* (2015).

3. Logsdon, C. D. & Ji, B. The role of protein synthesis and digestive enzymes in acinar cell injury. *Nature Reviews Gastroenterology and Hepatology* (2013). doi:10.1038/nrgastro.2013.36

4. Collisson, E. A., Bailey, P., Chang, D. K. & Biankin, A. V. Molecular subtypes of pancreatic cancer. *Nature Reviews Gastroenterology and Hepatology* (2019). doi:10.1038/s41575-019-0109-y

5. Mcguigan A *et al.* REVIEW 4846 Pancreatic cancer: A review of clinical diagnosis, epidemiology, treatment and outcomes MINIREVIEWS 4862 Cryotherapy in the management of premalignant and malignant conditions of the esophagus 4870 Acute acalculous cholecystitis in children Ba. **24**, 43 (2018).

6. Siegel, R. L., Miller, K. D. & Jemal, A. Cancer statistics, 2019. *CA. Cancer J. Clin.* (2019). doi:10.3322/caac.21551

7. Pourshams, A. *et al.* The global, regional, and national burden of pancreatic cancer and its attributable risk factors in 195 countries and territories, 1990–2017: a systematic analysis for the Global Burden of Disease Study 2017. *Lancet Gastroenterol. Hepatol.* **4**, 934–947 (2019).

8. Saiki, Y. & Horii, A. Molecular pathology of pancreatic cancer. *Pathol. Int.* **64**, 10–19 (2014).

9. Distler, M., Aust, D., Weitz, J., Pilarsky, C. & Grützmann, R. Precursor lesions for sporadic pancreatic cancer: PanIN, IPMN, and MCN. *Biomed Res. Int.* **2014**, (2014).

10. Hruban, R. H., Maitra, A., Kern, S. E. & Goggins, M. Precursors to Pancreatic Cancer. *Gastroenterol. Clin. North Am.* **36**, 831–849 (2007).

11. Koorstra, J. B. M., Feldmann, G., Habbe, N. & Maitra, A. Morphogenesis of pancreatic cancer: Role of pancreatic intraepithelial neoplasia (PanINs). *Langenbeck's Arch. Surg.* **393**, 561–570 (2008).

12. Basturk, O. *et al.* A revised classification system and recommendations from the Baltimore consensus meeting for neoplastic precursor lesions in the pancreas. in *American Journal of Surgical Pathology* (2015). doi:10.1097/PAS.0000000000000533

13. Grant, T. J., Hua, K. & Singh, A. *Molecular Pathogenesis of Pancreatic Cancer. Progress in Molecular Biology and Translational Science* **144**, (Elsevier Inc., 2016).

14. Kleeff, J. *et al.* Pancreatic cancer. *Nat. Rev. Dis. Prim.* **2**, 1–23 (2016).

15. Makohon-Moore, A. & Iacobuzio-Donahue, C. A. Pancreatic cancer biology and genetics from an evolutionary perspective. *Nat. Rev. Cancer* **16**, 553–565 (2016).

16. Bailey, P. *et al.* Genomic analyses identify molecular subtypes of pancreatic cancer. *Nature* **531**, 47–52 (2016).

17. Waddell, N. *et al.* Whole genomes redefine the mutational landscape of pancreatic cancer. *Nature* **518**, 495–501 (2015).

18. Jones, S. *et al.* Core signaling pathways in human pancreatic cancers revealed by global genomic analyses. *Science* **321**, 1801–6 (2008).

19. Avila, J. L. & Kissil, J. L. Notch signaling in pancreatic cancer: Oncogene or tumor suppressor? *Trends Mol. Med.* **19**, 320–327 (2013).

20. Brzozowa-Zasada, M. *et al.* Notch signalling pathway as an oncogenic factor involved in cancer development.

Wspolczesna Onkol. **20**, 267–272 (2016).

21. Gao, J., Long, B. & Wang, Z. Role of Notch signaling pathway in pancreatic cancer. *Am. J. Cancer Res.* **7**, 173–186 (2017).

22. Harbuzariu, A., Oprea-Ilies, G. & Gonzalez-Perez, R. The Role of Notch Signaling and Leptin-Notch Crosstalk in Pancreatic Cancer. *Medicines* **5**, 68 (2018).

23. Anastas, J. N. & Moon, R. T. WNT signalling pathways as therapeutic targets in cancer. *Nat. Rev. Cancer* **13**, 11–26 (2013).

24. Stamos, J. L. & Weis, W. I. The β-catenin destruction complex. *Cold Spring Harbor Perspectives in Biology* (2013). doi:10.1101/cshperspect.a007898

25. Morris, J. P., Wang, S. C. & Hebrok, M. KRAS, Hedgehog, Wnt and the twisted developmental biology of pancreatic ductal adenocarcinoma. *Nat. Rev. Cancer* **10**, 683–695 (2010).

26. Perugorria, M. J. *et al.* Wnt–β-catenin signalling in liver development, health and disease. *Nat. Rev. Gastroenterol. Hepatol.* **16**, 121–136 (2019).

27. Makena, M. R. *et al.* Wnt/β-catenin signaling: The culprit in pancreatic carcinogenesis and therapeutic resistance. *Int. J. Mol. Sci.* **20**, (2019).

28. Madunić, J. The Urokinase Plasminogen Activator System in Human Cancers: An Overview of Its Prognostic and Predictive Role. *Thromb. Haemost.* **118**, 2020–2036 (2018).

29. Büchler, P. *et al.* Transcriptional regulation of urokinase-type plasminogen activator receptor by hypoxia-inducible factor 1 is crucial for invasion of pancreatic and liver cancer. *Neoplasia* **11**, 196–206 (2009).

30. Noh, H., Hong, S. & Huang, S. Role of urokinase receptor in tumor progression and development. *Theranostics* **3**, 487–495 (2013).

31. Smith, H. W. & Marshall, C. J. Regulation of cell signalling by uPAR. *Nat. Rev. Mol. Cell Biol.* **11**, 23–36 (2010).

32. Sorio, C. *et al.* Elevated urinary levels of urokinase-type plasminogen activator receptor (uPAR) in pancreatic ductal adenocarcinoma identify a clinically high-risk group. *BMC Cancer* **11**, (2011).

33. Hildenbrand, R. *et al.* Amplification of the urokinase-type plasminogen activator receptor (uPAR) gene in ductal pancreatic carcinomas identifies a clinically high-risk group.

Am. J. Pathol. **174**, 2246–2253 (2009).

34. Feig, C. *et al.* The pancreas cancer microenvironment. *Clin. Cancer Res.* **18**, 4266–4276 (2012).

35. Kalluri, R. The biology and function of fibroblasts in cancer. *Nat. Rev. Cancer* **16**, 582–598 (2016).

36. Karamitopoulou, E. Tumour microenvironment of pancreatic cancer: immune landscape is dictated by molecular and histopathological features. *Br. J. Cancer* **121**, 5–14 (2019).

37. Pereira, B. A. *et al.* CAF Subpopulations: A New Reservoir of Stromal Targets in Pancreatic Cancer. *Trends in Cancer* **5**, 724–741 (2019).

38. Moffitt, R. A. *et al.* Virtual microdissection identifies distinct tumor- and stroma-specific subtypes of pancreatic ductal adenocarcinoma. *Nat. Genet.* **47**, 1168–1178 (2015).

39. Öhlund, D. *et al.* Distinct populations of inflammatory fibroblasts and myofibroblasts in pancreatic cancer. *J. Exp. Med.* **214**, 579–596 (2017).

40. Neesse, A. *et al.* Stromal biology and therapy in pancreatic cancer: Ready for clinical translation? *Gut* **68**, 159–171 (2019).

41. Hermann, P. C. & Sainz, B. Pancreatic cancer stem cells: A state or an entity? *Seminars in Cancer Biology* (2018). doi:10.1016/j.semcancer.2018.08.007

42. Ercan, G., Karlitepe, A. & Ozpolat, B. Pancreatic cancer stem cells and therapeutic approaches. *Anticancer Res.* **37**, 2761–2775 (2017).

43. Penchev, V. R., Rasheed, Z. A., Maitra, A. & Matsui, W. Heterogeneity and targeting of pancreatic cancer stem cells. *Clin. Cancer Res.* **18**, 4277–4284 (2012).

44. Gzil, A. *et al.* Markers of pancreatic cancer stem cells and their clinical and therapeutic implications. *Mol. Biol. Rep.* **46**, 6629–6645 (2019).

45. Vaz, A. P., Ponnusamy, M. P., Seshacharyulu, P., Batra, S. K. & Diseases, A. HHS Public Access. (2015).

46. Chan, T. S., Shaked, Y. & Tsai, K. K. Targeting the Interplay Between Cancer Fibroblasts, Mesenchymal Stem Cells, and Cancer Stem Cells in Desmoplastic Cancers. *Front. Oncol.* **9**, 1–15 (2019).

47. Vincent, A., Herman, J., Schulick, R., Hruban, R. H. & Goggins, M. Pancreatic cancer. *Lancet* **378**, 607–620 (2011).

48. Neoptolemos, J. P. *et al.* Comparison of adjuvant gemcitabine and capecitabine with gemcitabine monotherapy in patients with resected pancreatic cancer (ESPAC-4): a multicentre, open-label, randomised, phase 3 trial. *Lancet* **389**, 1011–1024 (2017).

49. Neoptolemos, J. P. *et al.* Therapeutic developments in pancreatic cancer: Current and future perspectives. *Nat. Rev. Gastroenterol. Hepatol.* **15**, 333–348 (2018).

50. Conroy, T. *et al.* FOLFIRINOX or Gemcitabine as Adjuvant Therapy for Pancreatic Cancer. *N. Engl. J. Med.* **379**, 2395–2406 (2018).

51. Goldstein, D. *et al.* nab-Paclitaxel Plus Gemcitabine for Metastatic Pancreatic Cancer: Long-Term Survival From a Phase III Trial. *JNCI J. Natl. Cancer Inst.* **107**, dju413–dju413 (2015).

52. Von Hoff, D. D. *et al.* Increased Survival in Pancreatic Cancer with nab-Paclitaxel plus Gemcitabine. *N. Engl. J. Med.* **369**, 1691–1703 (2013).

53. Javed, M. A. *et al.* Impact of intensified chemotherapy in metastatic pancreatic ductal adenocarcinoma (PDAC) in clinical routine in Europe. *Pancreatology* **19**, 97–104 (2019).

54. Neoptolemos, J. P. *et al.* Therapeutic developments in pancreatic cancer: Current and future perspectives. *Nat. Rev. Gastroenterol. Hepatol.* **15**, 333–348 (2018).

55. Lee, R. C., Feinbaum, R. L. & Ambros, V. The C. elegans heterochronic gene lin-4 encodes small RNAs with antisense complementarity to lin-14. *Cell* (1993). doi:10.1016/0092-8674(93)90529-Y

56. Winter, J., Jung, S., Keller, S., Gregory, R. I. & Diederichs, S. Many roads to maturity: MicroRNA biogenesis pathways and their regulation. *Nat. Cell Biol.* **11**, 228–234 (2009).

57. Krol, J., Loedige, I. & Filipowicz, W. The widespread regulation of microRNA biogenesis, function and decay. *Nat. Rev. Genet.* **11**, 597–610 (2010).

58. Siomi, H. & Siomi, M. C. Posttranscriptional Regulation of MicroRNA Biogenesis in Animals. *Mol. Cell* **38**, 323–332 (2010).

59. Ha, M. & Kim, V. N. Regulation of microRNA biogenesis. *Nat. Rev. Mol. Cell Biol.* **15**, 509–524 (2014).

60. Creugny, A., Fender, A. & Pfeffer, S. Regulation of primary microRNA processing. *FEBS Lett.* **592**, 1980–1996 (2018).

61. Treiber, T., Treiber, N. & Meister, G. Regulation of

microRNA biogenesis and its crosstalk with other cellular pathways. *Nat. Rev. Mol. Cell Biol.* **20**, 5–20 (2019).

62. Saito, T. & Sætrom, P. MicroRNAs - targeting and target prediction. *N. Biotechnol.* **27**, 243–249 (2010).

63. Bartel, D. P. MicroRNAs: Target Recognition and Regulatory Functions. *Cell* **136**, 215–233 (2009).

64. Pasquinelli, A. E. MicroRNAs and their targets: Recognition, regulation and an emerging reciprocal relationship. *Nat. Rev. Genet.* **13**, 271–282 (2012).

65. Seok, H., Ham, J., Jang, E. S. & Chi, S. W. MicroRNA target recognition: Insights from transcriptome-wide non-canonical interactions. *Mol. Cells* **39**, 375–381 (2016).

66. Duchaine, T. F. & Fabian, M. R. Mechanistic insights into microrna-mediated gene silencing. *Cold Spring Harb. Perspect. Biol.* **11**, 1–22 (2019).

67. Matoulkova, E., Michalova, E., Vojtesek, B. & Hrstka, R. The role of the 3′ untranslated region in post-transcriptional regulation of protein expression in mammalian cells. *RNA Biol.* **9**, 563–576 (2012).

68. Huntzinger, E. & Izaurralde, E. Gene silencing by

microRNAs: Contributions of translational repression and mRNA decay. *Nat. Rev. Genet.* **12**, 99–110 (2011).

69. Jonas, S. & Izaurralde, E. Towards a molecular understanding of microRNA-mediated gene silencing. *Nat. Rev. Genet.* **16**, 421–433 (2015).

70. Calin, G. A. *et al.* Frequent deletions and down-regulation of micro-RNA genes miR15 and miR16 at 13q14 in chronic lymphocytic leukemia. *Proc. Natl. Acad. Sci. U. S. A.* **99**, 15524–15529 (2002).

71. Cho, W. C. S. OncomiRs: The discovery and progress of microRNAs in cancers. *Mol. Cancer* **6**, 1–7 (2007).

72. Lujambio, A. & Lowe, S. W. The microcosmos of cancer. *Nature* **482**, 347–355 (2012).

73. Peng, Y. & Croce, C. M. The role of microRNAs in human cancer. *Signal Transduct. Target. Ther.* **1**, (2016).

74. O'Donnell, K. A., Wentzel, E. A., Zeller, K. I., Dang, C. V. & Mendell, J. T. c-Myc-regulated microRNAs modulate E2F1 expression. *Nature* **435**, 839–843 (2005).

75. Chang, T. C. *et al.* Widespread microRNA repression by Myc contributes to tumorigenesis. *Nat. Genet.* **40**, 43–50

(2008).

76. Calin, G. A. *et al.* Human microRNA genes are frequently located at fragile sites and genomic regions involved in cancers. *Proc. Natl. Acad. Sci. U. S. A.* **101**, 2999–3004 (2004).

77. Volinia, S. *et al.* A microRNA expression signature of human solid tumors defines cancer gene targets. *Proc. Natl. Acad. Sci. U. S. A.* **103**, 2257–2261 (2006).

78. Zhang, L. *et al.* microRNAs exhibit high frequency genomic alterations in human cancer. *Proc. Natl. Acad. Sci. U. S. A.* **103**, 9136–9141 (2006).

79. Szafranska, A. E. *et al.* MicroRNA expression alterations are linked to tumorigenesis and non-neoplastic processes in pancreatic ductal adenocarcinoma. *Oncogene* **26**, 4442–4452 (2007).

80. Vila-Navarro, E. *et al.* MicroRNAs for Detection of Pancreatic Neoplasia. *Ann. Surg.* **265**, 1226–1234 (2017).

81. Müller, S. *et al.* Next-generation sequencing reveals novel differentially regulated mRNAs, lncRNAs, miRNAs, sdRNAs and a piRNA in pancreatic cancer. *Mol. Cancer* (2015). doi:10.1186/s12943-015-0358-5

82. Hernandez, Y. G. MicroRNA in pancreatic ductal adenocarcinoma and its precursor lesions. *World J. Gastrointest. Oncol.* **8**, 18 (2016).

83. Kwon, J. J., Factora, T. D., Dey, S. & Kota, J. A Systematic Review of miR-29 in Cancer. *Mol. Ther. - Oncolytics* **12**, 173–194 (2019).

84. Kwon, J. J. *et al.* Pathophysiological role of microRNA-29 in pancreatic cancer stroma. *Sci. Rep.* **5**, 1–15 (2015).

85. Huang, L. *et al.* MicroRNA-29c Increases the Chemosensitivity of Pancreatic Cancer Cells by Inhibiting USP22 Mediated Autophagy. *Cell. Physiol. Biochem.* **47**, 747–758 (2018).

86. Jiang, J. *et al.* Reduction of miR-29c enhances pancreatic cancer cell migration and stem cell-like phenotype. *Oncotarget* **6**, 2767–2778 (2015).

87. Zhang, X. *et al.* Induction of the cellular miR-29c by influenza virus inhibits the innate immune response through protection of A20 mRNA. *Biochem. Biophys. Res. Commun.* **450**, 755–761 (2014).

88. Matsuzaki, J. & Suzuki, H. Role of MicroRNAs-221/222 in Digestive Systems. *J. Clin. Med.* **4**, 1566–1577 (2015).

89. Greither, T. *et al.* Elevated expression of microRNAs 155, 203, 210 and 222 in pancreatic tumors is associated with poorer survival. *Int. J. Cancer* **126**, 73–80 (2010).

90. Song, J. *et al.* Potential value of miR-221/222 as diagnostic, prognostic, and therapeutic biomarkers for diseases. *Frontiers in Immunology* (2017). doi:10.3389/fimmu.2017.00056

91. Jung, J. *et al.* Simultaneous inhibition of multiple oncogenic miRNAs by a multi-potent microRNA sponge. *Oncotarget* **6**, 20370–87 (2015).

92. Xu, Q. *et al.* MiR-221/222 induces pancreatic cancer progression through the regulation of matrix metalloproteinases. *Oncotarget* **6**, 14153–14164 (2015).

93. Zhao, H., Chen, M., Tellgren-Roth, C. & Pettersson, U. Fluctuating expression of microRNAs in adenovirus infected cells. *Virology* (2015). doi:10.1016/j.virol.2015.01.033

94. Hodzic, J., Sie, D., Vermeulen, A. & Van Beusechem, V. W. Functional Screening Identifies Human miRNAs that Modulate Adenovirus Propagation in Prostate Cancer Cells. *Hum. Gene Ther.* **28**, 766–780 (2017).

95. Bleijs, M., Wetering, M., Clevers, H. & Drost, J. Xenograft

and organoid model systems in cancer research. *EMBO J.* **38**, 1–11 (2019).

96. Lancaster, M. A. & Huch, M. Disease modelling in human organoids. *DMM Dis. Model. Mech.* **12**, (2019).

97. Lancaster, M. A. & Knoblich, J. A. Organogenesisin a dish: Modeling development and disease using organoid technologies. *Science (80-.).* **345**, (2014).

98. Sato, T. *et al.* Single Lgr5 stem cells build crypt-villus structures in vitro without a mesenchymal niche. *Nature* **459**, 262–265 (2009).

99. Huch, M. & Koo, B. K. Modeling mouse and human development using organoid cultures. *Dev.* **142**, 3113–3125 (2015).

100. Broutier, L. *et al.* Human primary liver cancer-derived organoid cultures for disease modeling and drug screening. *Nat. Med.* **23**, 1424–1435 (2017).

101. Boj, S. F. *et al.* Organoid Models of Human and Mouse Ductal Pancreatic Cancer. *Cell* **160**, 324–338 (2015).

102. Sato, T. *et al.* Paneth cells constitute the niche for Lgr5 stem

cells in intestinal crypts. *Nature* **469**, 415–418 (2011).

103. Granat, L. M. *et al.* The promises and challenges of patient-derived tumor organoids in drug development and precision oncology. *Anim. Model. Exp. Med.* **2**, 150–161 (2019).

104. Drost, J. & Clevers, H. Organoids in cancer research. *Nat. Rev. Cancer* **18**, 407–418 (2018).

105. Kersten, K., Visser, K. E., Miltenburg, M. H. & Jonkers, J. Genetically engineered mouse models in oncology research and cancer medicine. *EMBO Mol. Med.* **9**, 137–153 (2017).

106. Hidalgo, M. *et al.* Patient-derived Xenograft models: An emerging platform for translational cancer research. *Cancer Discov.* **4**, 998–1013 (2014).

107. Gendoo, D. M. A. *et al.* Whole genomes define concordance of matched primary, xenograft, and organoid models of pancreas cancer. *PLoS Comput. Biol.* **15**, 1–30 (2019).

108. Tuveson, D. & Clevers, H. Cancer modeling meets human organoid technology. *Science* (2019). doi:10.1126/science.aaw6985

109. Matano, M. *et al.* Modeling colorectal cancer using CRISPR-

Cas9-mediated engineering of human intestinal organoids. *Nat. Med.* **21**, 256–262 (2015).

110. Liu, X. *et al.* Modeling Wnt signaling by CRISPR-Cas9 genome editing recapitulates neoplasia in human Barrett epithelial organoids. *Cancer Lett.* **436**, 109–118 (2018).

111. Drost, J. *et al.* Use of CRISPR-modified human stem cell organoids to study the origin of mutational signatures in cancer. *Science (80-.).* **358**, 234–238 (2017).

112. Seino, T. *et al.* Human Pancreatic Tumor Organoids Reveal Loss of Stem Cell Niche Factor Dependence during Disease Progression. *Cell Stem Cell* **22**, 454-467.e6 (2018).

113. Roerink, S. F. *et al.* Intra-tumour diversification in colorectal cancer at the single-cell level. *Nature* **556**, 437–462 (2018).

114. Tiriac, H. *et al.* Successful creation of pancreatic cancer organoids by means of EUS-guided fine-needle biopsy sampling for personalized cancer treatment. *Gastrointest. Endosc.* **87**, 1474–1480 (2018).

115. Tiriac, H. *et al.* Organoid profiling identifies common responders to chemotherapy in pancreatic cancer. *Cancer Discov.* **8**, 1112–1129 (2018).

116. Huang, L. *et al.* Ductal pancreatic cancer modeling and drug screening using human pluripotent stem cell- and patient-derived tumor organoids. *Nat. Med.* **21**, 1364–71 (2015).

117. Vlachogiannis, G. *et al.* gastrointestinal cancers. **926**, 920–926 (2018).

118. Ooft, S. N. *et al.* Patient-derived organoids can predict response to chemotherapy in metastatic colorectal cancer patients. *Sci. Transl. Med.* **11**, 1–10 (2019).

119. Huch, M. *et al.* Unlimited in vitro expansion of adult bi-potent pancreas progenitors through the Lgr5/R-spondin axis. *EMBO J.* **32**, 2708–2721 (2013).

120. Leung, C., Tan, S. H. & Barker, N. Recent Advances in Lgr5+ Stem Cell Research. *Trends Cell Biol.* **28**, 380–391 (2018).

121. Clevers, H. Modeling Development and Disease with Organoids. *Cell* **165**, 1586–1597 (2016).

122. Romero-Calvo, I. *et al.* Human organoids share structural and genetic features with primary pancreatic adenocarcinoma tumors. *Mol. Cancer Res.* **17**, 70–83 (2019).

123. Boj, S. F. *et al.* Organoid Models of Human and Mouse

Ductal Pancreatic Cancer. *Cell* **160**, 324–338 (2015).

124. Tsai, S. *et al.* Development of primary human pancreatic cancer organoids, matched stromal and immune cells and 3D tumor microenvironment models. *BMC Cancer* **18**, 335 (2018).

125. Alemany, R., Balagué, C. & Curiel, D. T. Replicative adenoviruses for cancer therapy. *Nat. Biotechnol.* **18**, 723–727 (2000).

126. Rahal, A. & Musher, B. Oncolytic viral therapy for pancreatic cancer. *J. Surg. Oncol.* **116**, 94–103 (2017).

127. Kelly, E. & Russell, S. J. History of oncolytic viruses: Genesis to genetic engineering. *Mol. Ther.* **15**, 651–659 (2007).

128. Martuza, R. L., Malick, A., Marker, J. M., Ruffner, K. I. & Coen, D. M. Experimental Therapy of Human Glioma by Means of. *Science (80-.).* **252**, 854–856 (1991).

129. Maroun, J. *et al.* Designing and building oncolytic viruses. *Future Virol.* **12**, 193–213 (2017).

130. Fukuhara, H., Ino, Y. & Todo, T. Oncolytic virus therapy: A new era of cancer treatment at dawn. *Cancer Sci.* **107**, 1373–

1379 (2016).

131. Kelly, E. & Russell, S. J. History of oncolytic viruses: Genesis to genetic engineering. *Mol. Ther.* **15**, 651–659 (2007).

132. Harrington, K., Freeman, D. J., Kelly, B., Harper, J. & Soria, J. C. Optimizing oncolytic virotherapy in cancer treatment. *Nat. Rev. Drug Discov.* **18**, 689–706 (2019).

133. Russell, S. J. & Peng, K. W. Oncolytic Virotherapy: A Contest between Apples and Oranges. *Mol. Ther.* **25**, 1107–1116 (2017).

134. Russell, L. & Peng, K. W. The emerging role of oncolytic virus therapy against cancer. *Chinese Clinical Oncology* (2018). doi:10.21037/cco.2018.04.04

135. Chesney, J. *et al.* Phase IIIb safety results from an expanded-access protocol of talimogene laherparepvec for patients with unresected, stage IIIB-IVM1c melanoma. *Melanoma Res.* **28**, 44–51 (2018).

136. Raja, J., Ludwig, J. M., Gettinger, S. N., Schalper, K. A. & Kim, H. S. Oncolytic virus immunotherapy: future prospects for oncology. *J. Immunother. Cancer* **6**, 1–13 (2018).

137. Russell, S. J. & Peng, K. W. Oncolytic Virotherapy: A Contest between Apples and Oranges. *Mol. Ther.* **25**, 1107–1116 (2017).

138. Liu, B. L. *et al.* ICP34.5 deleted herpes simplex virus with enhanced oncolytic, immune stimulating, and anti-tumour properties. *Gene Ther.* **10**, 292–303 (2003).

139. Zheng, M., Huang, J., Tong, A. & Yang, H. Oncolytic viruses for cancer therapy: barriers and recent advances. *Mol. Ther. - Oncolytics* **15**, 234–247 (2019).

140. Rowe, W. P., Huebner, R. J., Gilmore, L. K., Parrott, R. H. & Ward, T. G. Isolation of a Cytopathogenic Agent from Human Adenoids Undergoing Spontaneous Degeneration in Tissue Culture. *Proc. Soc. Exp. Biol. Med.* (1953). doi:10.3181/00379727-84-20714

141. Goradel, N. H. *et al.* Oncolytic adenovirus: A tool for cancer therapy in combination with other therapeutic approaches. *J. Cell. Physiol.* **234**, 8636–8646 (2019).

142. Baker, A. T., Aguirre-Hernández, C., Halldén, G. & Parker, A. L. Designer oncolytic adenovirus: Coming of age. *Cancers* (2018). doi:10.3390/cancers10060201

143. Cody, J. J. & Douglas, J. T. Armed replicating adenoviruses

for cancer virotherapy. *Cancer Gene Therapy* (2009). doi:10.1038/cgt.2009.3

144. Lynch, J. P. & Kajon, A. E. Adenovirus: Epidemiology, Global Spread of Novel Serotypes, and Advances in Treatment and Prevention. *Semin. Respir. Crit. Care Med.* **37**, 586–602 (2016).

145. Russell, W. C. Adenoviruses: Update on structure and function. *J. Gen. Virol.* **90**, 1–20 (2009).

146. Charman, M., Herrmann, C. & Weitzman, M. D. Viral and Cellular Interactions During Adenovirus DNA Replication. *FEBS Lett.* **593**, 1873-3468.13695 (2019).

147. Seth, P. & D, P. *Adenoviruses : Basic Biology to Gene Therapy I NTELLIGENCE U NIT 15 Adenoviruses : Basic Biology to Gene Therapy*. *Human Gene Therapy*

148. Ea, A. *et al.* crossm Hacking the Cell : Network Intrusion and Exploitation by MANIPULATION OF CELLULAR PROTEIN INTERACTION NETWORKS BY VIRAL. 1–18 (2018).

149. Hidalgo, P., Ip, W. H., Dobner, T. & Gonzalez, R. A. The biology of the adenovirus E1B 55K protein. *FEBS Lett.* **593**, 3504–3517 (2019).

150. Evans, J. D. & Hearing, P. Distinct Roles of the Adenovirus E4 ORF3 Protein in Viral DNA Replication and Inhibition of Genome Concatenation. *J. Virol.* **77**, 5295–5304 (2003).

151. Saha, B., Wong, C. M. & Parks, R. J. The adenovirus genome contributes to the structural stability of the virion. *Viruses* **6**, 3563–3583 (2014).

152. Nemerow, G. & Flint, J. Lessons learned from adenovirus (1970–2019). *FEBS Lett.* **593**, 3395–3418 (2019).

153. Stewart, P. L. *Adenovirus Structure*. *Adenoviral Vectors for Gene Therapy: Second Edition* (Elsevier Inc., 2016). doi:10.1016/B978-0-12-800276-6.00001-2

154. Nemerow, G. R., Stewart, P. L. & Reddy, V. S. Structure of human adenovirus. *Curr. Opin. Virol.* **2**, 115–121 (2012).

155. Mangel, W. F. & Martín, C. S. Structure, function and dynamics in adenovirus maturation. *Viruses* **6**, 4536–4570 (2014).

156. Liebert, M. A., Rux, J. J. & Burnett, R. M. JOHN J. RUX and ROGER M. BURNETT. *Hum. Gene Ther.* **1176**, 1167–1176 (2004).

157. Snijder, J. *et al.* Integrin and Defensin Modulate the

Mechanical Properties of Adenovirus. *J. Virol.* **87**, 2756–2766 (2013).

158. Alba, R., Bosch, A. & Chillon, M. Gutless adenovirus: Last-generation adenovirus for gene therapy. *Gene Ther.* (2005). doi:10.1038/sj.gt.3302612

159. Leopold, P. L. & Crystal, R. G. Intracellular trafficking of adenovirus: Many means to many ends. *Adv. Drug Deliv. Rev.* **59**, 810–821 (2007).

160. Nemerow, G. R., Pache, L., Reddy, V. & Stewart, P. L. Insights into adenovirus host cell interactions from structural studies. *Virology* **384**, 380–388 (2009).

161. Waye, M. M. Y. & Sing, C. W. Anti-viral drugs for human adenoviruses. *Pharmaceuticals* (2010). doi:10.3390/ph3103343

162. Bofill-De Ros, X., Rovira-Rigau, M. & Fillat, C. Implications of MicroRNAs in Oncolytic Virotherapy. *Front. Oncol.* **7**, 142 (2017).

163. Piedade, D. & Azevedo-Pereira, J. M. MicroRNAs as important players in host-adenovirus interactions. *Front. Microbiol.* **8**, 1–13 (2017).

164. Lu, Z. *et al.* High-throughput sequencing of MicroRNAs in adenovirus type 3 infected human laryngeal epithelial cells. *J. Biomed. Biotechnol.* **2010**, (2010).

165. Korn, W. M. *et al.* Expression of the coxsackievirus- and adenovirus receptor in gastrointestinal cancer correlates with tumor differentiation. *Cancer Gene Ther.* **13**, 792–797 (2006).

166. Stepanenko, A. A. & Chekhonin, V. P. Tropism and transduction of oncolytic adenovirus 5 vectors in cancer therapy: Focus on fiber chimerism and mosaicism, hexon and pIX. *Virus Res.* **257**, 40–51 (2018).

167. Uusi-Kerttula, H., Hulin-Curtis, S., Davies, J. & Parker, A. L. Oncolytic adenovirus: Strategies and insights for vector design and immuno-oncolytic applications. *Viruses* **7**, 5987–6020 (2015).

168. Rojas, J. J., Gimenez-Alejandre, M., Gil-Hoyos, R., Cascallo, M. & Alemany, R. Improved systemic antitumor therapy with oncolytic adenoviruses by replacing the fiber shaft HSG-binding domain with RGD. *Gene Ther.* **19**, 453–457 (2012).

169. Yamamoto, M. *et al.* Infectivity enhanced, cyclooxygenase-2 promoter-based conditionally replicative adenovirus for

pancreatic cancer. *Gastroenterology* **125**, 1203–1218 (2003).

170. Kim, E. *et al.* Development of a Conditional Replication Competent Adenovirus, Controlled by the Human Telomerase Promoter (hTERT). *Cancer Res. Treat.* (2003). doi:10.4143/crt.2003.35.3.191

171. Huch, M. *et al.* Urokinase-type plasminogen activator receptor transcriptionally controlled adenoviruses eradicate pancreatic tumors and liver metastasis in mouse models. *Neoplasia* **11**, 518–528 (2009).

172. Mato-Berciano, A. *et al.* A NOTCH-sensitive uPAR-regulated oncolytic adenovirus effectively suppresses pancreatic tumor growth and triggers synergistic anticancer effects with gemcitabine and nab-paclitaxel. *Oncotarget* **8**, 22700–22715 (2017).

173. Rojas, J. J. *et al.* Minimal RB-responsive E1A Promoter Modification to Attain Potency, Selectivity, and Transgene-arming Capacity in Oncolytic Adenoviruses. *Mol. Ther.* **18**, 1960–1971 (2010).

174. Kelly, E. J., Hadac, E. M., Greiner, S. & Russell, S. J. Engineering microRNA responsiveness to decrease virus pathogenicity. *Nat. Med.* **14**, 1278–1283 (2008).

175. Ros, X. B. De, Gironella, M. & Fillat, C. MiR-148a- And miR-216a-regulated Oncolytic Adenoviruses Targeting Pancreatic Tumors Attenuate Tissue Damage Without Perturbation of miRNA Activity. *Mol. Ther.* (2014). doi:10.1038/mt.2014.98

176. Bofill-De Ros, X., Villanueva, E. & Fillat, C. Late-phase miRNA-controlled oncolytic adenovirus for selective killing of cancer cells. *Oncotarget* **6**, 6179–6190 (2015).

177. Callegari, E. *et al.* Anti-Tumor Activity of a miR-199-dependent Oncolytic Adenovirus. *PLoS One* **8**, 1–16 (2013).

178. Huang, H. *et al.* Oncolytic adenovirus programmed by synthetic gene circuit for cancer immunotherapy. *Nat. Commun.* **10**, 1–15 (2019).

179. Villanueva, E. *et al.* Translational reprogramming in tumour cells can generate oncoselectivity in viral therapies. *Nat. Commun.* **8**, (2017).

180. Ganly, I. *et al.* A Phase I study of Onyx-015, an E1B attenuated adenovirus, administered intratumorally to patients with recurrent head and neck cancer. *Clin. Cancer Res.* **6**, 798–806 (2000).

181. Fueyo, J. *et al.* Erratum: A mutant oncolytic adenovirus targeting the Rb pathway produces anti-glioma effect in vivo

(Oncogene (2000) 19 (2-12)). *Oncogene* **19**, 5038 (2000).

182. Guedan, S. *et al.* Hyaluronidase expression by an oncolytic adenovirus enhances its intratumoral spread and suppresses tumor growth. *Mol. Ther.* **18**, 1275–1283 (2010).

183. Tedcastle, A., Illingworth, S., Brown, A., Seymour, L. W. & Fisher, K. D. Actin-resistant DNAse I expression from oncolytic adenovirus enadenotucirev enhances its intratumoral spread and reduces tumor growth. *Mol. Ther.* **24**, 796–804 (2016).

184. Mok, W., Boucher, Y. & Jain, R. K. Matrix metalloproteinases-1 and -8 improve the distribution and efficacy of an oncolytic virus. *Cancer Res.* **67**, 10664–10668 (2007).

185. Rodríguez-García, A. *et al.* Safety and efficacy of VCN-01, an oncolytic adenovirus combining fiber HSG-binding domain replacement with RGD and hyaluronidase expression. *Clin. Cancer Res.* **21**, 1406–1418 (2015).

186. Harrington, K., Freeman, D. J., Kelly, B., Harper, J. & Soria, J. C. Optimizing oncolytic virotherapy in cancer treatment. *Nat. Rev. Drug Discov.* **18**, 689–706 (2019).

187. Kuryk, L., Møller, A. S. W. & Jaderberg, M. Combination of

immunogenic oncolytic adenovirus ONCOS-102 with anti-PD-1 pembrolizumab exhibits synergistic antitumor effect in humanized A2058 melanoma huNOG mouse model. *Oncoimmunology* **8**, 1–11 (2019).

188. Twumasi-Boateng, K., Pettigrew, J. L., Kwok, Y. Y. E., Bell, J. C. & Nelson, B. H. Oncolytic viruses as engineering platforms for combination immunotherapy. *Nat. Rev. Cancer* **18**, 419–432 (2018).

189. De Sostoa, J. *et al.* Targeting the tumor stroma with an oncolytic adenovirus secreting a fibroblast activation protein-targeted bispecific T-cell engager. *J. Immunother. Cancer* **7**, 1–15 (2019).

190. Rovira-Rigau, M. *et al.* Bioselection Reveals miR-99b and miR-485 as Enhancers of Adenoviral Oncolysis in Pancreatic Cancer. *Mol. Ther.* **27**, 230–243 (2019).

191. Barta, T., Peskova, L. & Hampl, A. miRNAsong: a web-based tool for generation and testing of miRNA sponge constructs in silico. *Sci. Rep.* **6**, 36625 (2016).

192. Tay, F. C., Lim, J. K., Zhu, H., Hin, L. C. & Wang, S. Using artificial microRNA sponges to achieve microRNA loss-of-function in cancer cells. *Adv. Drug Deliv. Rev.* **81**, 117–127 (2015).

193. Jung, J. *et al.* Simultaneous inhibition of multiple oncogenic miRNAs by a multi-potent microRNA sponge. *Oncotarget* (2015). doi:10.18632/oncotarget.4827

194. Ebert, M. S., Neilson, J. R. & Sharp, P. A. MicroRNA sponges: Competitive inhibitors of small RNAs in mammalian cells. *Nat. Methods* (2007). doi:10.1038/nmeth1079

195. Oliveros, J. C. *et al.* Breaking-Cas-interactive design of guide RNAs for CRISPR-Cas experiments for ENSEMBL genomes. *Nucleic Acids Res.* (2016). doi:10.1093/nar/gkw407

196. Pérez-Torras, S. *et al.* Characterization of human pancreatic orthotopic tumor xenografts suitable for drug screening. *Cell. Oncol.* **34**, 511–521 (2011).

197. Sanjana, N. E., Shalem, O. & Zhang, F. Improved vectors and genome-wide libraries for CRISPR screening. *Nature Methods* (2014). doi:10.1038/nmeth.3047

198. Milone, M. C. & O'Doherty, U. Clinical use of lentiviral vectors. *Leukemia* (2018). doi:10.1038/s41375-018-0106-0

199. Broutier, L. *et al.* Culture and establishment of self-renewing human and mouse adult liver and pancreas 3D organoids and

their genetic manipulation. *Nat. Protoc.* **11**, 1724–43 (2016).

200. MacDonald, B. T. & He, X. Frizzled and LRp5/6 receptors for wnt/β-catenin signaling. *Cold Spring Harb. Perspect. Biol.* (2012). doi:10.1101/cshperspect.a007880

201. Staal, F. J. T., Burgering, B. M. T., Van De Wetering, M. & Clevers, H. C. Tcf-1-mediated transcription in T lymphocytes: Differential role for glycogen synthase kinase-3 in fibroblasts and T cells. *Int. Immunol.* (1999). doi:10.1093/intimm/11.3.317

202. Zhao, L., Wientjes, M. G. & Au, J. L.-S. Evaluation of Combination Chemotherapy. *Clin. Cancer Res.* (2004). doi:10.1158/1078-0432.CCR-04-1087

203. Alemany, R. & Curiel, D. T. CAR-binding ablation does not change biodistribution and toxicity of adenoviral vectors. *Gene Ther.* (2001). doi:10.1038/sj.gt.3301515

204. Rojas, J. J. *et al.* Minimal RB-responsive E1A promoter modification to attain potency, selectivity, and transgene-arming capacity in oncolytic adenoviruses. *Mol. Ther.* (2010). doi:10.1038/mt.2010.173

205. Stanton, R. J., McSharry, B. P., Armstrong, M., Tomasec, P. & Wilkinson, G. W. G. Re-engineering adenovirus vector

systems to enable high-throughput analyses of gene function. *Biotechniques* (2008). doi:10.2144/000112993

206. Puig-Saus, C., Gros, A., Alemany, R. & Cascalló, M. Adenovirus i-leader truncation bioselected against cancer-associated fibroblasts to overcome tumor stromal barriers. *Mol. Ther. Capitulo 1.pdf* (2012). doi:10.1038/mt.2011.159

207. Kleeff, J. *et al.* Pancreatic cancer. *Nat. Rev. Dis. Prim.* **2**, 1–23 (2016).

208. Eissa, I. R. *et al.* The current status and future prospects of oncolytic viruses in clinical trials against melanoma, glioma, pancreatic, and breast cancers. *Cancers* (2018). doi:10.3390/cancers10100356

209. Aberle, M. R. *et al.* Patient-derived organoid models help define personalized management of gastrointestinal cancer. *Br. J. Surg.* **105**, e48–e60 (2018).

210. Huch, M. *et al.* In vitro expansion of single Lgr5+ liver stem cells induced by Wnt-driven regeneration. *Nature* **494**, 247–250 (2013).

211. Wang, N. *et al.* Adenovirus-mediated efficient gene transfer into cultured three-dimensional organoids. *PLoS One* (2014). doi:10.1371/journal.pone.0093608

212. Toyoda, E. *et al.* Adenovirus vectors with chimeric type 5 and 35 fiber proteins exhibit enhanced transfection of human pancreatic cancer cells. *Int. J. Oncol.* (2008). doi:10.3892/ijo_00000103

213. Lu, J. *et al.* MicroRNA expression profiles classify human cancers. *Nature* (2005). doi:10.1038/nature03702

214. Garzon, R., Marcucci, G. & Croce, C. M. Targeting microRNAs in cancer: Rationale, strategies and challenges. *Nature Reviews Drug Discovery* (2010). doi:10.1038/nrd3179

215. Li, Z. *et al.* Tumor-Secreted Exosomal miR-222 Promotes Tumor Progression via Regulating P27 Expression and Re-Localization in Pancreatic Cancer. *Cell. Physiol. Biochem.* **51**, 610–629 (2018).

216. Frampton, A. E. *et al.* microRNAs with prognostic significance in pancreatic ductal adenocarcinoma: A meta-analysis. *Eur. J. Cancer* **51**, 1389–1404 (2015).

217. Rawat, M. *et al.* MicroRNA in pancreatic cancer: From biology to therapeutic potential. *Genes* (2019). doi:10.3390/genes10100752

218. Galardi, S. *et al.* miR-221 and miR-222 expression affects

the proliferation potential of human prostate carcinoma cell lines by targeting p27Kip1. *J. Biol. Chem.* **282**, 23716–24 (2007).

219. Vila-Navarro, E. *et al.* MicroRNAs for detection of pancreatic neoplasia: Biomarker discovery by next-generation sequencing and validation in 2 independent cohorts. *Ann. Surg.* **265**, 1226–1234 (2017).

220. Motwani, M., Pesiridis, S. & Fitzgerald, K. A. DNA sensing by the cGAS–STING pathway in health and disease. *Nature Reviews Genetics* (2019). doi:10.1038/s41576-019-0151-1

221. Tan, X., Sun, L., Chen, J. & Chen, Z. J. Detection of Microbial Infections Through Innate Immune Sensing of Nucleic Acids. *Annu. Rev. Microbiol.* (2018). doi:10.1146/annurev-micro-102215-095605

222. Wu, M.-Z. *et al.* miR-25/93 mediates hypoxia-induced immunosuppression by repressing cGAS. *Nat. Cell Biol.* **19**, 1286–1296 (2017).

223. Reyes, E. D. *et al.* Identifying Host Factors Associated with DNA Replicated During Virus Infection. *Mol. Cell. Proteomics* **16**, 2079–2097 (2017).

224. Bloomston, M. *et al.* MicroRNA expression patterns to

differentiate pancreatic adenocarcinoma from normal pancreas and chronic pancreatitis. *J. Am. Med. Assoc.* **297**, 1901–1908 (2007).

225. Zhang, Y. *et al.* Profiling of 95 MicroRNAs in pancreatic cancer cell lines and surgical specimens by real-time PCR analysis. *World J. Surg.* (2009). doi:10.1007/s00268-008-9833-0

226. Ebert, M. S. & Sharp, P. A. MicroRNA sponges: Progress and possibilities. *Rna* **16**, 2043–2050 (2010).

227. Tay, F. C., Lim, J. K., Zhu, H., Hin, L. C. & Wang, S. Using artificial microRNA sponges to achieve microRNA loss-of-function in cancer cells. *Advanced Drug Delivery Reviews* (2015). doi:10.1016/j.addr.2014.05.010

228. Barta, T., Peskova, L. & Hampl, A. MiRNAsong: A web-based tool for generation and testing of miRNA sponge constructs in silico. *Sci. Rep.* (2016). doi:10.1038/srep36625

229. Isaac, C. *et al.* Characterization of the nucleolar gene product, treacle, in Treacher Collins syndrome. *Mol. Biol. Cell* **11**, 3061–3071 (2000).

230. Song, C., Hotz-Wagenblatt, A., Voit, R. & Grummt, I. SIRT7 and the DEAD-box helicase DDX21 cooperate to

resolve genomic R loops and safeguard genome stability. *Genes Dev.* (2017). doi:10.1101/gad.300624.117

231. Cao, J. *et al.* DDX21 promotes gastric cancer proliferation by regulating cell cycle. *Biochem. Biophys. Res. Commun.* **505**, 1189–1194 (2018).

232. Han, Y. & Wang, X. The emerging roles of KPNA2 in cancer. *Life Sci.* **241**, 117140 (2020).

233. Wodrich, H. *et al.* Adenovirus Core Protein pVII Is Translocated into the Nucleus by Multiple Import Receptor Pathways. *J. Virol.* **80**, 9608–9618 (2006).

234. Kwiatkowski, N. *et al.* Targeting transcription regulation in cancer with a covalent CDK7 inhibitor. *Nature* (2014). doi:10.1038/nature13393

235. Chipumuro, E. *et al.* CDK7 inhibition suppresses super-enhancer-linked oncogenic transcription in MYCN-driven cancer. *Cell* **159**, 1126–1139 (2014).

236. Lu, P. *et al.* THZ1 reveals CDK7-dependent transcriptional addictions in pancreatic cancer. *Oncogene* (2019). doi:10.1038/s41388-019-0701-1

237. Posternak, V. & Cole, M. D. Strategically targeting MYC in

cancer [version 1 ; referees : 2 approved] Referee Status : *F1000Research* **5**, 1–8 (2018).

238. Hwang, C.-I., Boj, S. F., Clevers, H. & Tuveson, D. A. Preclinical models of pancreatic ductal adenocarcinoma. *J. Pathol.* **238**, 197–204 (2016).

239. Kloker, L., Yurttas, C. & Lauer, U. Three-dimensional tumor cell cultures employed in virotherapy research. *Oncolytic Virotherapy* **Volume 7**, 79–93 (2018).

240. Baker, A. T., Aguirre-Hernández, C., Halldén, G. & Parker, A. L. Designer oncolytic adenovirus: Coming of age. *Cancers (Basel).* **10**, 1–39 (2018).

241. Beer, R. L., Parsons, M. J. & Rovira, M. Centroacinar cells: At the center of pancreas regeneration. *Dev. Biol.* **413**, 8–15 (2016).

242. Rovira, M. *et al.* Isolation and characterization of centroacinar/terminal ductal progenitor cells in adult mouse pancreas. *Proc. Natl. Acad. Sci. U. S. A.* **107**, 75–80 (2010).

243. Tiriac, H. *et al.* Successful creation of pancreatic cancer organoids by means of EUS-guided fine-needle biopsy sampling for personalized cancer treatment. *Gastrointest. Endosc.* **87**, 1474–1480 (2018).

244. Eriksson, E. *et al.* Shaping the tumor stroma and sparking immune activation by CD40 and 4-1BB signaling induced by an armed oncolytic virus. *Clin. Cancer Res.* **23**, 5846–5857 (2017).

245. Maliandi, M. V. *et al.* AduPARE1A and gemcitabine combined treatment trigger synergistic antitumor effects in pancreatic cancer through NF-KB mediated uPAR activation. *Mol. Cancer* **14**, 1–12 (2015).

246. Schwartz, P. B., Uboha, N. V. & Weber, S. M. Editorial About: "A Prospective, Open-Label, Multicenter Phase II Trial of Neoadjuvant Therapy Using Full-Dose Gemcitabine and S-1 Concurrent with Radiation for Resectable Pancreatic Ductal Adenocarcinoma". *Ann. Surg. Oncol.* **26**, 4175–4177 (2019).

247. Maddipati, R. & Stanger, B. Z. Pancreatic cancer metastases harbor evidence of polyclonality. *Cancer Discov.* **5**, 1086–1097 (2015).

248. Standing, C. Metastasis in Pancreatic Ductal Adenocarcinoma : (2020).

249. Turajlic, S. & Swanton, C. Metastasis as an evolutionary process. *Science (80-.).* **352**, 169–175 (2016).

250. Ganaie, A. A. *et al.* Characterization of Novel Murine and Human PDAC Cell Models: Identifying the Role of Intestine Specific Homeobox Gene ISX in Hypoxia and Disease Progression. *Transl. Oncol.* **12**, 1056–1071 (2019).

251. Yano, S. *et al.* OBP-401-GFP telomerase-dependent adenovirus illuminates and kills high-metastatic more effectively than low-metastatic triple-negative breast cancer in vitro. *Cancer Gene Ther.* **24**, 45–47 (2017).

252. Carnero, E., Sutherland, J. D. & Fortes, P. Adenovirus and miRNAs. *Biochimica et Biophysica Acta - Gene Regulatory Mechanisms* (2011). doi:10.1016/j.bbagrm.2011.05.004

253. Vila-Navarro, E. *et al.* MicroRNAs for detection of pancreatic neoplasia: Biomarker discovery by next-generation sequencing and validation in 2 independent cohorts. *Ann. Surg.* (2017). doi:10.1097/SLA.0000000000001809

254. Yonemori, K., Kurahara, H., Maemura, K. & Natsugoe, S. MicroRNA in pancreatic cancer. *J. Hum. Genet.* **62**, 33–40 (2017).

255. Chen, Y. *et al.* HCV-Induced miR-21 Contributes to Evasion of Host Immune System by Targeting MyD88 and IRAK1. *PLoS Pathog.* **9**, (2013).

256. Yang, C. H., Li, K., Pfeffer, S. R. & Pfeffer, L. M. The type I IFN-Induced miRNA, miR-21. *Pharmaceuticals* **8**, 836–847 (2015).

257. Zhao, Q. *et al.* miR-21 promotes EGF-induced pancreatic cancer cell proliferation by targeting Spry2. *Cell Death Dis.* (2018). doi:10.1038/s41419-018-1182-9

258. Imig, J. *et al.* MicroRNA profiling in Epstein-Barr virus-associated B-cell lymphoma. *Nucleic Acids Res.* **39**, 1880–1893 (2011).

259. Bandopadhyay, M. *et al.* Tumor suppressor micro RNA miR-145 and onco micro RNAs miR-21 and miR-222 expressions are differentially modulated by Hepatitis B virus X protein in malignant hepatocytes. *BMC Cancer* **14**, 1–12 (2014).

260. Pied, N. & Wodrich, H. Imaging the adenovirus infection cycle. *FEBS Lett.* **593**, 3419–3448 (2019).

261. Douglas, J. T. Adenoviral vectors for gene therapy. *Mol. Biotechnol.* (2007). doi:10.1007/s12033-007-0021-5

262. Richart, L. *et al.* BPTF is required for c-MYC transcriptional activity and in vivo tumorigenesis. *Nat. Commun.* **7**, (2016).

263. McRae, E. K. S. *et al.* Human DDX21 binds and unwinds

RNA guanine quadruplexes. *Nucleic Acids Res.* **45**, 6656–6668 (2017).

264. Hao, H. *et al.* Dissecting the role of DDX21 in regulating HCMV replication. *J. Virol.* (2019). doi:10.1128/jvi.01222-19

265. Naji, S. *et al.* Host cell interactome of HIV-1 Rev includes RNA helicases involved in multiple facets of virus production. *Mol. Cell. Proteomics* **11**, 1–14 (2012).

266. Sohn, S.-Y. & Hearing, P. Adenovirus Sequesters Phosphorylated STAT1 at Viral Replication Centers and Inhibits STAT Dephosphorylation. *J. Virol.* **85**, 7555–7562 (2011).

267. Look, D. C. *et al.* Direct suppression of Stat1 function during adenoviral infection. *Immunity* **9**, 871–880 (1998).

268. Li, W. *et al.* miR-29c plays a suppressive role in breast cancer by targeting the TIMP3/STAT1/FOXO1 pathway. *Clin. Epigenetics* **10**, 1–14 (2018).

269. Zou, Y. *et al.* miR-29c suppresses pancreatic cancer liver metastasis in an orthotopic implantation model in nude mice and affects survival in pancreatic cancer patients. *Carcinogenesis* **36**, 676–684 (2015)

8. Appendix

Appendix 8.1. Sequencing and sequence alignment of CRISR/Cas9 edited cells used in this study.

PANC-1-miR93 KO

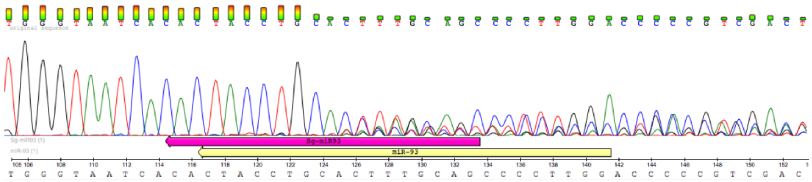

```
miR93-Ctrl          -CTGGGGGCTCCAAAGTGCTGTTCGTGCAGGTAG---TGTGATTACCCAACCTACTGCTG  56
PANC-1-miR93        CCGGGGGCTCGGGAAGTGCTAGCTCAGCAGTAGGTTGGGTAATCACACTACCTGCACTTT  60
                     * ****       ********       ****    *     ** ** ** * **** *    *

miR93-Ctrl          AGCTAGCACTTCCCGAGCCCCCGG      80
PANC-1-miR93        G----CAGCCCCTTGGACCCCCG-      79
                         *  *  *  ******
```

PANC-1-miR93 KO/1

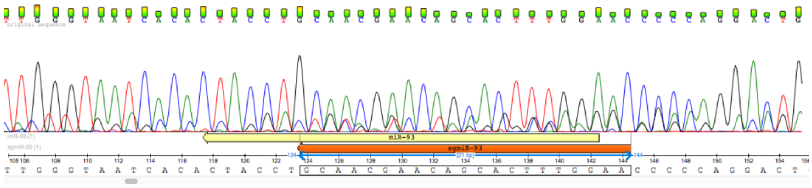

```
PANC-1-Ctrl         -CTGGGGGCTCCAAAGTGCTGTTCGTGCAGGTAGTGTGATTACCCAACCTACTGCTGAGC    59
PANC-1-miR-93-KO/1  CCGGGGGCTCGGGAAGTGCTAGCTCAGCAGTAGGTTGGGTAATCACACTACCTGCAACGA    60
                     * ****       ********       ****    **  * * * *  **    ****   *

PANC-1-Ctrl         TAGCACTTCCCGAGCCCCCGG    80
PANC-1-miR-93-KO/1  ACAGCACTTTGGAACCCCCAG    81
                        *   ** ***** *
```

PANC-1-miR93 KO/2

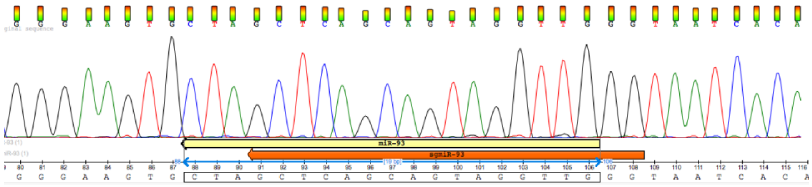

```
PANC-1-miR93-Ctrl   CTGGGGGCTCCAAAGTGCTGTTCGTGCAGG---TAGTGTGATTACCCAACCTACTGCTGA     57
PANC-1-miR93-KO/2   CGGGGGCTCGGGAAGTGCTAGCTCAGCAGTAGGTTGGGTAATCACACTACCTGCAATTTG     60
                    * ****       ********       ****    * * ** ** ** * **** *   *

PANC-1-miR93-Ctrl   GCTAGCACTTCCCGAGCCCCCGG  80
PANC-1-miR93-KO/2   TTTCCACCCCGCCTGACGTCC--  81
                      *    *   **   *  **
```

PANC-1-miR21 KO

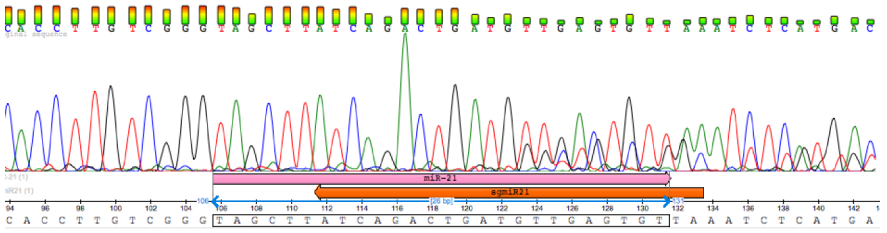


```
PANC-1-miR93-Ctrl       TGTCGGGTAGCTTATCAGACTGATGTTGACTGTTGAATCTCATGGCAACACCAGTCGATG     60
PANC-1-miR93KO          TGTCGGGTAGCTTATCAGACTGATGTTGAGTGTTAAATCTCATGACATTTTGGCTCCCAT     60
                        ****************************** **** ********* **       **

PANC-1-miR93-Ctrl       GGCTGTCTGACA--   72
PANC-1-miR93KO          CGCCTGACCGACGT   74
                         **
```

PANC-1-miR21 KO/1

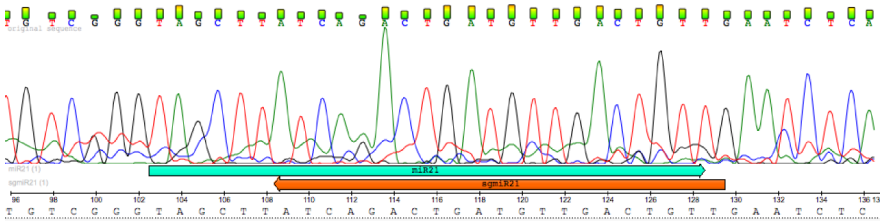


```
PANC-1-miR93-Ctrl       TGTCGGGTAGCTTATCAGACTGATGTTGACTGTTGAATCTCATGGCAACACCAGTCGATG     60
PANC-1-miR93KO/1        TGTCGGGTAGCTTATCAGACTGATGTTGACTGTTGAATCTCATGGGATGTCTGACATTTT     60
                        ********************************************* *   *       *

PANC-1-miR93-Ctrl       GGCTGTCTGACA---------    72
PANC-1-miR93KO/1        GCCATCTTTCGTCTGACCTTC    81
                        * *    *
```

PANC-1-miR21 KO/2

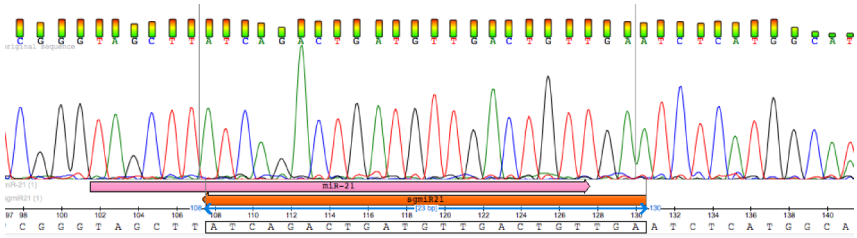


```
PANC-1-miR93-Ctrl       TGTCGGGTAGCTTATCAGACTGATGTTGACTGTTGAATCTCATGGCAACACCAGTCGATG     60
PANC-1-miR93KO/2        TGTCGGGTAGCTTATCAGACTGATGTTGACTGTTGAATCTCATGGCATGTCCAAAGGGCT     60
                        ************************************************   ***   *

PANC-1-miR93-Ctrl       GGCTGTCTGACA     72
PANC-1-miR93KO/2        GGCCGAA-----     67
                        *** *
```

PANC-1-miR222 KO

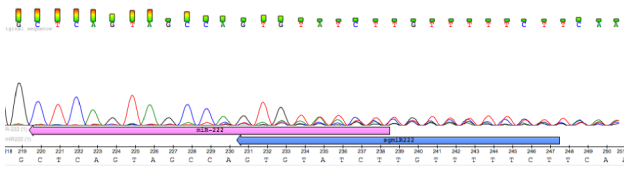

```
PANC-1-Ctrl          GCTGCTGGAAGGTGTAGGTACCCTCAATGGCTCAGTAGCCAGTGTAGATCCTGTCTTTCG      60
PANC-1-miR222-KO     GCTGCTGGAAGGTGTAGGTACCCTCAATGGCTCAGTAGCCAGTGTATCTTGTTTTTCTTC      60
                     ************************************************  * * * * *

PANC-1-Ctrl          TAATCAGCAGCTACATCTGGCTACTGGGTCTCTGATGGCATCTTCTAGCT        110
PANC-1-miR222-KO     AACACCTGC--CGCGGGGGGGGGGTGGGGGGGCCGACGGGGGTCTTCTTCCT     108
                      *  *          *    **      ***   * ** **  ******  **
```

PANC-1-miR761 KO

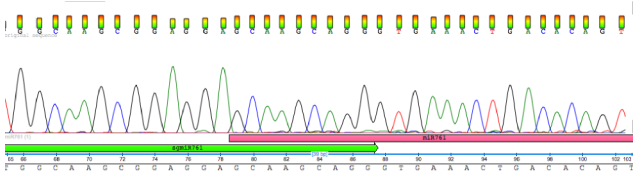

```
PANC-1-Ctrl          -GGAGGAGCAGCAGGGTGAAACTGACACAGTTCTGGTGAGTTTCACTTTGCTGCTCCTCC      59
PANC-1-miR761-KO     GGAGGAGCAAGCAGGGTGAAACTGACACAGTTCTGGTGAGTTTCACTTTGCTGCTCCTCC      60
                      *  *  ************************************************

PANC-1-Ctrl          - 59
PANC-1-miR761-KO     T 61
```

PANC-1-miR3714 KO

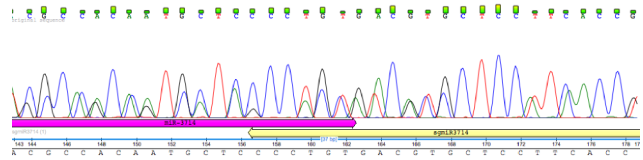

```
PANC-1-Ctrl          GAAGGCAGCAGTGCTCCCCTGTGACGTGCTCCATCACCGGGCAGGGAAGACACCGCTGCC      60
PANC-1-miR3714-KO    --ACGCCACAATGCTCCCCTGTGACGTGCTCCTTCACCGGGAATGCAACACACCCCTACC      58
                       * **  ** ********************** ******** * * ** ***** ** **

PANC-1-Ctrl          ACCTC    65
PANC-1-miR3714-KO    CCCTC    63
                      ****
```

PANC-1-miR221 KO

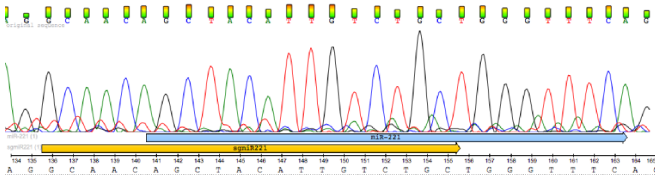

```
PANC-1-Ctrl          ---CCAATGGAGAACATGTTTCCAGGTAGCCTCAAACCCAGCAGACAATGTAGCTGTTGC      57
PANC-1-miR-221-KO    ACTTGCAAGCTGAACATCCAGGTCT-GGGGCATGAACCTGGCATACAATGTAGATTTCTG      59
                        * *  ******          * *   ****  *** ********* * *

PANC-1-Ctrl          CTAACGAACACAGAAATCTACATTGTATGCCAGGTTCATGCCCCA-GACCTGGATGTTCA      116
PANC-1-miR-221-KO    TGTTCGTTAGGCAACAGCTACATTGTCTGCTGGGTTTCAGGCTACCTGGAAACATGTTCT      119
                       **       * * ********* ***  ****   * *             ******

PANC-1-Ctrl          GCTTGCAAGT       126
PANC-1-miR-221-KO    CCATTGG---       126
                      * *
```

MIA PaCa-2-miR93 KO

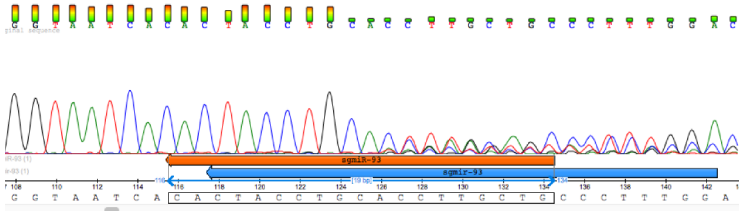


```
MIAPaCa-2-Ctrl          -CTGGGGGCTCCAAAGTGCTGTTCGTGCAGGT---AGTGTGATTACCCAACCTACTGCTG    56
MIAPaCa-2-miR93-KO      CCGGGGGCTCGGGAAGTGCTAGCTCAGCAGTAGGTTGGGTAATCACACTACCTGCACCTT    60
                         * ****      *******       ****      * ** ** ** * **** *  **

MIAPaCa-2-Ctrl          AGCTAGCACTTCCCCGAGCCCCCGG------- 80
MIAPaCa-2-miR93-KO      GCTGC----CCTTTGGACCCCCGTCGACTAAG 88
                             * *    ** ****
```

MIA PaCa-2 miR21 KO

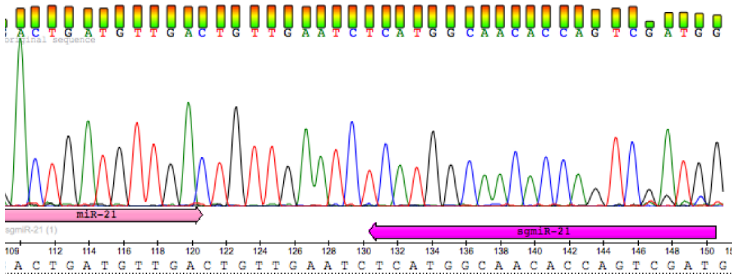


```
MIAPaCa-2-Ctrl          TGTCGGGTAGCTTATCAGACTGATGTTGACTGTTGAATCTCATGGCAACACCAGTCGATG    60
MIAPaCa-2-miR21-KO      TGTCGGGTAGCTTATCAGACTGATGTTGACTGTTGAATCTCATGGCAACACCAGTCGATG    60
                        ************************************************************

MIAPaCa-2-Ctrl          GGCTGTCTGACA    72
MIAPaCa-2-miR21-KO      GGCTGTCTGACA    72
                        ************
```

MIA PaCa-2 miR222 KO

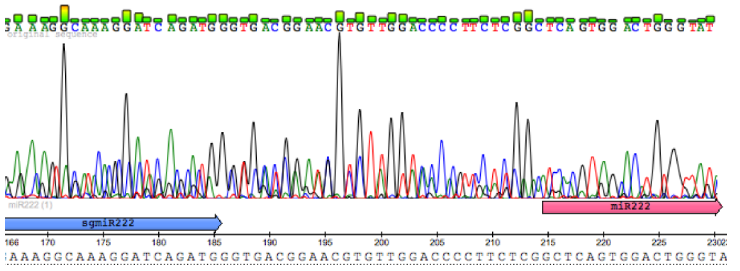


```
MIAPaCa-2-Ctrl          GCTGCTGGAAGGTGTAGGTACCCTCAATGGCTCAGTAGCCAGTGTAGATCCTGTCTTTCG    60
MIAPaCa-2-miR222-KO     GATGCTGAGGATGATGTCTTCTATGGTCTGCCGATGAGCCCC-------------TCCCG    47
                         * *****       *   * *  *     **  *  ****              *  **

MIAPaCa-2-Ctrl          TAATCAGCAGCTACATCTGGCTACTGGGTCTCTGATGGCATCTTCTAGCT----------    110
MIAPaCa-2-miR222-KO     AAAGGCAAAGGATCAGATGGGTGACGGAACGTGTTGGACCCCTTCTCGGCTCAGTGGACT    107
                         **      **   **  *** *   **  *      * *  ***** *

MIAPaCa-2-Ctrl          -----  110
MIAPaCa-2-miR222-KO     GGGTA  112
```

Appendix 8.2 Molecular targets of new miRNA candidates in c-GAS/STING pathway or in mechanisms of adenoviral biology

miRNA	c-GAS/STING Pathway	Adenoviral biology
miR-222	No targets among the genes analyzed	ERCC4 – PRKAB2-PRKAA2 – BPTF – DDX21 – KPNA2 – NOLC1 – TCOF1
miR-761	TTLL4 - PRKAA2 - PRKAG2 – PRKAB1	POLR1A – NAT10 – POU2F1 – MSH3
miR-3714	ENPP1 – ULK1 – ULK2 – PRKAA2	HEATR1 – NOLC1 – POLR1A – AP15 – NF1 - ATM
miR-4713	No targets among the genes analyzed	NOLC1 – POU2F1 – ERCC4

Appendix 8.3 Analysis of miR-222 molecular targets.

Genes target of miR-222 have been grouped for gene onthology and functions by the prediction software miRDB and PANTHER GO, which were used for the prediction. Only the top 25 - scored are listed. The pathways selected for further analysis have been highlighted.

Pathway	Expected hits	P-value
Nucleic Acid binding	**84.05**	**1.99E-16**
RNA binding	**36.95**	**1.30E-15**
Nucleus	**153.9**	**2.59E-15**
Organic cycling compound binding	**124.9**	**1.40E-14**
Cytosol	**111.6**	**1.37E-11**
Nuclear lumen	112.1	1.43E-11
Nucleoplasm	81.16	2.07E-10
Intracellular membrane-bounded organelle	**228.3**	**5.25E-9**
Intracellular organelle	261.3	2.38E-8
Protein binding	247.8	5.03E-8
Cadherin binding	7.27	1.52E-6
Macromolecule metabolic	192.6	3.61E-6

process		
Organelle organization	76.65	3.61E-6
Molecular function	340	1.44E-5
Cell cycle	**39.39**	**1.69E-5**
Negative Regulation of gene expression	39.94	1.69E-5
Nitrogen Compound metabolic process	205.7	2.06E-5
Enzyme binding	45.13	2.18E-5
Protein-containing complex	96.04	2.74E-5
Metabolic process	253.3	3.10E-5
Cell adhesion molecule binding	10.44	3.5E-5
Cellular metabolic process	221.4	4.64E-5
Gene expression	**114.9**	**5.55E-5**
Regulation of metabolic process	140.2	5.95E-5

Appendix 8.4 Scientific Publications

The results introduced in the section 4.1 of this thesis have been submitted for publication the journal EBioMedicine (currently under second review):

- *Patient-derived pancreatic tumor organoids identify therapeutic response to oncolytic adenoviruses*.
  G. Raimondi, A. Mato-Berciano, S. Pascual-Sabater, M. Rovira-Rigau, M. Cuatrecasas, C. Fondevila, S. Sánchez-Cabús, Harry Beghtel, S.F. Boj, H. Clevers, C. Fillat.

Additional scientific publications deriving from collaborations established during this PhD thesis are detailed as follow:

- *Germline mutations in FAF1 are associated with hereditary colorectal cancer.*
  L. Bonjoch, S. Franch-Expósito, P. Garre, J. Muñoz, C. Arnau-Collell, M. Díaz-Gay, A. Gratacós-Mulleras, **G. Raimondi**, C. Esteban-Jurado, Y. Soares de Lima, M. Cuatrecasas, T. Ocaña, A. Castells, C. Fillat, F. Balaguer, T. Caldés, L. Valle, S. Castellví-Bel. **Gastroenterology** (currently under second review).

- m*iR-93 is related to poor prognosis in pancreatic cancer and promotes tumor progression by modulating targets involved in microtubule dynamics.* E. Vila-Navarro, M.

Rovira-Rigau, E. Fernandez-Castañer, **G. Raimondi**, M. Vila-Casadesus, J.J. Lozano, P. Soubeyran, J. Iovanna, A. Castells, C. Fillat, M. Gironella. **Oncogenesis** (currently under second revision).

- *Bioselection reveals mir-99b and miR-485 as enhancers of adenoviral oncolysis in pancreatic cancer.*
  M. Rovira-Rigau, **G. Raimondi**, M.A. Marín, M. Gironella, R. Alemany, C. Fillat. **Molecular Therapy**, 2019.

- *Deciphering microRNA targets in pancreatic cancer using miRComb R package.*
  M. Vila-Casadesús, E. Vila-Navarro, **G. Raimondi**, C. Fillat, A. Castells, J.J. Lozano, M. Gironella. Oncotarget, 2018.

- *A NOTCH-sensitive uPAR-regulated oncolytic adenovirus effectively suppresses pancreatic tumor growth and triggers synergistic anticancer effects with gemcitabine and nab-paclitaxel.*
  Mato-Berciano, **G. Raimondi**, M.V. Maliandi, R. Alemany, L. Montoliu, C. Fillat. Oncotarget, 2017.

Molecular Therapy
Original Article

Bioselection Reveals miR-99b and miR-485 as Enhancers of Adenoviral Oncolysis in Pancreatic Cancer

Maria Rovira-Rigau,[1,2] Giulia Raimondi,[1,2] Miguel Ángel Marín,[1] Meritxell Gironella,[1,3] Ramon Alemany,[4] and Cristina Fillat[1,2,5]

[1]Institut d'Investigacions Biomèdiques August Pi i Sunyer (IDIBAPS), 08036 Barcelona, Spain; [2]Centro de Investigación Biomédica en Red de Enfermedades Raras (CIBERER), 08036 Barcelona, Spain; [3]Gastrointestinal & Pancreatic Oncology Group, Centro de Investigación Biomédica en Red de Enfermedades Hepáticas y Digestivas (CIBEREHD), 08036 Barcelona, Spain; [4]Institut Català d'Oncologia-IDIBELL, 08907 L'Hospitalet de Llobregat, Spain; [5]Facultat de Medicina i Ciències de la Salut. Universitat de Barcelona (UB), 08036 Barcelona, Spain

Oncolytic viruses are designed for cancer treatment. Cell-virus interactions are key determinants for successful viral replication. Therefore, the extensive reprogramming of gene expression that occurs in tumor cells might create a hurdle for viral propagation. We used a replication-based approach of a microRNA (miRNA) adenoviral library encoding up to 243 human miRNAs as a bioselection strategy to identify miRNAs that facilitate adenoviral oncolytic activity in pancreatic ductal adenocarcinoma. We identify two miRNAs, miR-99b and miR-485, that function as enhancers of adenoviral oncolysis by improving the intra- and extracellular yield of mature virions. An increased adenoviral activity is the consequence of enhanced E1A and late viral protein expression, which is probably mediated by the downregulation of the transcriptional repressors *ELF4*, *MDM2*, and *KLF8*, which we identify as miR-99b or miR-485 target genes. Arming the oncolytic adenovirus ICOVIR15 with miR-99b or miR-485 enhances its fitness and its antitumoral activity. Our results demonstrate the potential of this strategy to improve oncolytic adenovirus potency, and they highlight miR-99b and miR-485 as sensitizers of adenoviral replication.

INTRODUCTION

Viruses have evolved a number of strategies to hijack cellular resources, forcing them to synthesize new virions for a successful viral propagation.[1,2] These strategies have been acquired as a consequence of an adaptive process in specific cellular contexts. While the use of viruses in cancer treatments has long been studied,[3] tumor cells present a number of genetic alterations that elicit massive reprogramming of cellular gene expression, creating a novel context in which viruses have not adapted to replicate.[4] The inherent complexity of tumors makes the oncolytic viral activity highly dependent on the specific characteristics of tumor cells. In fact, the differential expression of certain genes in cancer cells can negatively impact viral replication.[5–7] Nevertheless, molecular mechanisms explaining viral replication heterogeneity in cancer cells remain to be fully appraised.[8]

MicroRNAs (miRNAs) are post-transcriptional negative regulators of gene expression that modulate a variety of cellular physiological processes. miRNAs also play important roles in host-virus interactions.[9] Viral infections can modulate the cellular miRNome with changes induced either by the virus, to promote a proviral environment, or by the antiviral cellular response, to limit the viral life cycle.[10–12] Although the mechanisms of miRNA-mediated regulation of viral infection have not been completely clarified, it is clear that host miRNAs can regulate viral infections.

In the context of tumorigenesis, many miRNAs with essential roles in cancer-associated pathways are dysregulated.[13] Participation of miRNAs has been demonstrated in central cancer processes, such as cell proliferation and death, cell differentiation, and maintenance of stem cell potency.[14] Aberrant expression of miRNAs has been well documented for pancreatic ductal adenocarcinoma (PDAC), and specific miRNA signatures have been associated with diagnosis, staging, progression, prognosis, and treatment response.[15,16] Hence, when viruses are used as oncolytic agents, they face an already perturbed miRNome in cancer cells. These miRNA profile changes may not necessarily favor viral replication and propagation within the tumor; indeed, the downregulation of certain miRNAs could induce the overexpression of viral-limiting factors.

Adenoviruses (Ads) are non-enveloped icosahedral viruses with double-stranded DNA genomes. The viral genome is sub-divided into regions termed early and late according to when transcription activation initiates. Early genes remodel the intracellular environment to prepare the cell for viral replication and activate the expression of other viral genes. Late genes primarily constitute viral structural proteins. Adenoviruses, and particularly adenovirus serotype 5 (Ad5), are

Received 23 April 2018; accepted 20 September 2018;
https://doi.org/10.1016/j.ymthe.2018.09.016.

Correspondence: Cristina Fillat, Institut d'Investigacions Biomèdiques August Pi i Sunyer (IDIBAPS), 08036 Barcelona, Spain.
E-mail: cfillat@clinic.ub.es

www.impactjournals.com/ oncotarget/ Oncotarget, 2018, Vol. 9, (No. 5), pp: 6499-6517

Research Paper

Deciphering microRNA targets in pancreatic cancer using miRComb R package

Maria Vila-Casadesús[1,2], Elena Vila-Navarro[1], Giulia Raimondi[3], Cristina Fillat[3], Antoni Castells[1], Juan José Lozano[1,2] and Meritxell Gironella[1]

[1]Gastrointestinal & Pancreatic Oncology Group, Centro de Investigación Biomédica en Red de Enfermedades Hepáticas y Digestivas (CIBEREHD), Hospital Clínic of Barcelona, Institut d'Investigacions Biomèdiques August Pi i Sunyer (IDIBAPS), Barcelona, Catalonia, Spain

[2]Bioinformatics Platform, CIBEREHD, Barcelona, Catalonia, Spain

[3]Gene Therapy and Cancer, Institut d'Investigacions Biomèdiques August Pi i Sunyer (IDIBAPS), Centro de Investigación Biomédica en Red de Enfermedades Raras (CIBERER), Universitat de Barcelona, Barcelona, Catalonia, Spain

Correspondence to: *Meritxell Gironella*, ***email:*** *meritxell.gironella@ciberehd.org*

Keywords: *microRNA; pancreatic cancer; target prediction; gene expression; CRISPR-Cas9*

Received: *August 09, 2017* ***Accepted:*** *January 02, 2018* ***Published:*** *January 08, 2018*

ABSTRACT

MiRNAs are small non-coding RNAs that post-transcriptionally regulate gene expression. They play important roles in cancer but little is known about the specific functions that each miRNA exerts in each type of cancer. More knowledge about their specific targets is needed to better understand the complexity of molecular networks taking part in cancer. In this study we report the miRNA-mRNA interactome occurring in pancreatic cancer by using a bioinformatic approach called miRComb, which combines tissue expression data with miRNA-target prediction databases (TargetScan, miRSVR and miRDB). MiRNome and transcriptome of 12 human pancreatic tissues (9 pancreatic ductal adenocarcinomas and 3 controls) were analyzed by next-generation sequencing and microarray, respectively. Analysis confirmed differential expression of both miRNAs and mRNAs in cancerous tissue versus control, and unveiled 17401 relevant miRNA-mRNA interactions likely to occur in pancreatic cancer. They were sorted according to the degree of negative correlation between miRNA and mRNA expression. Results highlighted the importance of miR-148a and miR-21 interactions among others. Two components of the Notch signaling pathway, ADAM17 and EP300, were confirmed as miR-148a targets in MiaPaca-2 pancreatic cancer cells overexpressing miR-148a. Moreover, a CRISPR-Cas9 cellular model was generated to knock-out the expression of miR-21 in PANC-1 cells. As expected, the expression of two miRComb miR-21 predicted targets, PDCD4 and BTG2, was significantly upregulated in these cells in comparison to control PANC-1.

INTRODUCTION

Pancreatic ductal adenocarcinoma (PDAC) is the fourth leading cause of cancer death in occidental countries and has the worst prognosis of all major malignancies with just a 6% five-year survival rate [1]. By the time of diagnosis, most patients present with locally advanced or metastatic disease that precludes curative resection and have a mean survival of less than 1 year [2, 3]. This fatal scenario is due, in part, to the high aggressiveness of the tumour and the lack of effective treatments. In order to overcome this dire problem, new and more efficient therapeutic targets are urgently needed. To achieve this goal is highly necessary to increase the knowledge about

www.impactjournals.com/ oncotarget/ Oncotarget, 2017, Vol. 8, (No. 14), pp: 22700-22715

Research Paper

A NOTCH-sensitive uPAR-regulated oncolytic adenovirus effectively suppresses pancreatic tumor growth and triggers synergistic anticancer effects with gemcitabine and nab-paclitaxel

Ana Mato-Berciano[1,2], Giulia Raimondi[1,2], Maria Victoria Maliandi[1,2], Ramon Alemany[3], Lluis Montoliu[2,4], Cristina Fillat[1,2]

[1]Institut d'Investigacions Biomèdiques August Pi i Sunyer (IDIBAPS), Barcelona, Spain

[2]Centro de Investigación Biomédica en Red de Enfermedades Raras (CIBERER), Barcelona, Spain

[3]Institut Català d'Oncologia-IDIBELL. L'Hospitalet de Llobregat, Barcelona, Spain

[4]Centro Nacional de Biotecnologia (CNB-CSIC), Madrid, Spain

Correspondence to: Cristina Fillat, **email:** lcfilat@ lin cub .es

Keywords: *pancreatic cancer, oncolytic adenovirus, cancer stem cells, gemcitabine, nab-paclitaxel*

Received: *February 08, 2016* ***Accepted:*** *January 23, 2017* ***Published:*** *February 07, 2017*

ABSTRACT

Notch signaling pathway is an embryonic program that becomes reactivated in pancreatic cancer and contributes to cancer stem cell (CSC) maintenance. We explored the concept of oncolytic adenoviral activity in response to Notch activation signaling, in the context of a chimeric promoter with uPAR regulatory sequences, as a strategy to drive its activity in neoplastic and CSC. We explored the advantages of a chemo-virotherapy approach based on synergistic combinations. Regulatory sequences recognized by the transcriptional factor CSL upstream a minimal uPAR promoter were engineered in adenoviral vectors and in the oncolytic adenovirus AdNuPARmE1A. Viral response to Notch signaling, and viral potency in cell lines and pancreatic cancer stem cells (PCSC) was tested. Preclinical toxicity and antitumor efficacy in xenografts and Patient-derived xenografts (PDX) mouse models was evaluated, as unimodal or in combination with gemcitabine+ nab-paclitaxel. Mechanistic studies were conducted to explore the synergism of combined therapies.

We demonstrate that CSL-binding site optimized-engineered sequences respond to Notch activation in AdNuPARmLuc and AdNuPARmE1A. AdNuPARmE1A showed strong lytic effects in pancreatic cancer cell lines and PCSC. AdNuPARmE1A displayed attenuated activity in normal tissues, but robust antitumor effects in xenograft and PDX models, leading to a reduced capacity of treated tumors to form tumorspheres. Chemo-virotherapy treatment enlarged therapeutic response in both tumor models. Synergistic effects of the combination resulted from viral sensitization of apoptotic cell death triggered by chemotherapy.

In summary we present a novel effective oncolytic adenovirus, AdNuPARmE1A that reduces PCSC and presents synergistic effects with gemcitabine and nab-paclitaxel, supporting further clinical development.

INTRODUCTION

Reactivation of embryonic programs is a common characteristic of human malignancies. In pancreatic cancer reactivation of Hedgehog, Wnt and Notch signaling pathways is well defind [1–4]. Notch signaling acts as a mediator of growth regulatory pathway and as a regulator of the balance between self-renewal and differentiation in the developing pancreas [5]. In pancreatic cancer Notch activity has been shown to synergize with K-ras, promoting PanIN initiation and progression, and to contribute to the maintenance of the pancreatic CSC population [6, 7]. The Notch pathway initiates when a cell expressing the appropriate ligand (jagged or delta)